STUDIES ON THE SYNTHESIS AND CHARACTERIZATION OF NANOCRYSTALLINE BORON CARBIDE

By

TRINADHA RAJA PILLADI
Enrolment No.: CHEM02200704018

Indira Gandhi Centre for Atomic Research
Kalpakkam, 603 102, Tamil Nadu, India

A thesis submitted to the
Board of Studies in Chemical Sciences
In partial fulfillment of requirements
For the Degree of

DOCTOR OF PHILOSOPHY

of

Homi Bhabha National Institute
Deemed University
Mumbai, India

AUGUST 2012

STUDIES ON THE SYNTHESIS AND CHARACTERIZATION OF NANOCRYSTALLINE BORON CARBIDE

A thesis submitted to the
Board of Studies in Chemical Sciences
In partial fulfillment of requirements
For the Degree of

DOCTOR OF PHILOSOPHY

of

Homi Bhabha National Institute

By

TRINADHA RAJA PILLADI
Enrolment No.: CHEM02200704018

Indira Gandhi Centre for Atomic Research
Kalpakkam 603 102, Tamil Nadu, India

Research Supervisor

Dr. S. Anthonysamy
Head, Materials Processing Chemistry Section
Materials Chemistry Division, Chemistry Group
Indira Gandhi Centre for Atomic Research
Kalpakkam 603 102, Tamil Nadu, India

AUGUST 2012

Homi Bhabha National Institute

Recommendations of the Viva Voce Board

As members of the Viva Voce Board, we certify that we have read the dissertation prepared by **Trinadha Raja Pilladi** entitled **"Studies on the synthesis and characterization of nanocrystalline boron carbide"** and recommend that it may be accepted as fulfilling the dissertation requirement for the Degree of Doctor of Philosophy.

Date: 17/4

Chairman-**Dr. P. R. Vasudeva Rao**

S. Anthonysamy **Date:** 17/4/13

Convener-**Dr. S. Anthonysamy**

G. S. Gupta **Date:** 17/04/13

External examiner- **Prof. Govind S. Gupta**

Date: 17.04.2013

Member 1-**Dr. V. Ganesan**

K. Nag **Date:** 17.04.2013

Member 2- **Dr. K. Nagarajan**

Final approval and acceptance of this dissertation is contingent upon the candidate's submission of the final copies of the dissertation to HBNI.

Date: 17/4/2013

Place: Indira Gandhi Centre for Atomic Research, Kalpakkam

CERTIFICATE

I hereby certify that I have read this dissertation prepared under my direction and recommend that it may be accepted as fulfilling the dissertation requirement.

S. Anthonysamy

S. Anthonysamy

(Research Supervisor)

Date: 23|8|2012

Place: Indira Gandhi Centre for Atomic Research, Kalpakkam

STATEMENT BY AUTHOR

This dissertation has been submitted towards partial fulfillment of requirements for an advanced degree at Homi Bhabha National Institute (HBNI) and is deposited in the library to be made available to borrowers under rules of the HBNI.

Brief quotations from this dissertation are allowable without special permission, provided that accurate acknowledgement of source is made. Requests for permission for extended quotation from or reproduction of this manuscript in whole or in part may be granted by the Competent Authority of HBNI when in his or her judgment the proposed use of the material is in the interests of scholarship. In all other instances, however, permission must be obtained from the author.

23/8/12
Trinadha Raja Pilladi

Kalpakkam
August 2012

DECLARATION

I, hereby declare that the investigation presented in the thesis entitled **"Studies on the synthesis and characterization of nanocrystalline boron carbide"** submitted to Homi Bhabha National Institute (HBNI), Mumbai, India, for the award of degree of Doctor of Philosophy in Chemical Sciences is the record of work carried out by me during the period from Sept 2007 to August 2012 under the guidance of Dr. S.Anthonysamy, Head, Materials Processing Chemistry Section, Materials Chemistry Division, Chemistry Group, Indira Gandhi centre for Atomic Research, Kalpakkam. This work is original and has not been submitted earlier as a whole or in part thereof for a degree/diploma at this or any other Institution/university.

23/8/12

Trinadha Raja Pilladi

Kalpakkam
August 2012

Dedicated to my grand father

Shri Arava Bhima Raju (late)

Acknowledgements

I wish to express my sincere gratitude to my research guide, Dr. S. Anthonysamy, Head, Materials processing Chemistry Section, Materials Chemistry Division for his teaching, invaluable guidance, patience and encouragement throughout my research period.

I am also thankful to Dr. K. Ananthasivan, Head, Advanced Fuel Studies Section, Fuel Chemistry Division for his inspiring guidance, constant encouragement and keen interest in my research work.

I would like to express my gratitude to the members of my doctoral committee, Dr. P. R. Vasudeva Rao, Dr. K. Nagarajan and Dr. V. Ganesan, for their valuable suggestions and encouragement.

I would like to thank Dr. M. Saibaba, Resource Management Group for providing me a pleasant accommodation at JRF enclave. I am also thankful to faculty members of HBNI for the course work that I was given.

I owe a special and sincere thanks to Dr. G. Panneerselvam, Mr. N. Ramanathan, Dr. R. Sudha, Mr. E. Prabhu, Mr. Thomas Paul, Smt. Usha Lakshmi and Mr. Raja Madavan for their valuable help and support in characterization of the various samples.

I take this opportunity to thank with great pleasure for strong support from the members of H-12 and Materials Processing Chemistry Section, Mr. R. K. Prabhu, Mr. S. Balakrishnan, Dr. Ashish Jain, Dr. Pankajavalli, Dr. Chandra Mouli, Mr. R. Ranganathan, Mr. Veerapandian, Mr. Kaliappan, Mr. V. Paramasivam, Mr. T. Ramoorthy, Ms. Ambika, Smt. Annie, Smt. Haseena, Mr. Gajendiran, Mr. Stanislas and other members of MPCS.

I thank my friends at IGCAR Mr. A. Sree Ramoorthy, Mr. T. Bapuji, Mr. D. Siva Kumar, Mr. G.V.S. Ashok Kumar, Mr. Jogeswar Rao, Mr. Swapan Kumar, Mr. Vishnu Vardan, Mr. Santha Ram and Mr. Kishore for their support through out my project work.

I was fortunate in having Mr. Rahul Pal as my colleague. I treasure all precious moments we shared and would really like to thank him for his support and help.

I am thankful and indebted to all the research scholars working in the centre for their help. To name few of them: V. Srihari, Bishnu Prasad, K. Lakshmoji, Vishnu, K. Srinivas, Ruth Nithila., Hari Babu, Saravana Kumar, Vargeese, Girish, Ashit Pattanaik, Bharath, Jagadeesh, Ravi, Ramana, Deepak & Kavya.

It is with an attitude of gratitude, I recall, a number of persons who lent me a helping hand in some way or the other through out my project work.

I am also indebted to my father Mohana Rao, Mother Ratna Vathi, my brother Pavan Kumar, sister-in-law Patralekha, Nikki, Sister Sridevi, brother-in-law Sridhar, my uncle Prabhakar, aunt Rajeswari, father in-law Narasimaha Murthy, mother-in-law Sudha Rani, Grand father Sarveswara Rao, Grand mother Satyavani, Vishnu, Teju, Sushanth, Sushmitha for their relentless support, encouragement and love. I would like to give credit and love to my wife Satya Swathi for support, affection and bearing me during the progress of this work.

Finally, I thank almighty for providing me opportunity to step into the world of science.

Kalpakkam Trinadha Raja Pilladi

CONTENTS

CHAPTER 1

Introduction

CHAPTER 2

Experimental

<u>CHAPTER 3</u>

Thermodynamic analysis of production of boron carbide through carbothermic reduction of boric oxide

CHAPTER 4

Synthesis and characterization of nanocrystalline boron carbide from gel precursors

CHAPTER 5

Studies on the thermal expansion of nanocrystalline boron carbide

CHAPTER 6

Development of an alternate method for the digestion of boron carbide for its chemical assay

CHAPTER 7

Summary and Conclusions

SYNOPSIS

Energy is the most fundamental requirement of every society or nation as it progresses through the ladder of development. The energy demand of the world is increasing every year due to population growth and increasing standard of living. The major energy sources of India are fossil fuels such as oil, coal and natural gas. Over 65% of power generated currently is contributed by thermal energy, which cuts down the precious coal reserves of the country and causes environmental problems. In order to transform India into a technologically and economically advanced nation an adequate growth in energy generation is necessary. To sustain the anticipated growth rate of Gross Domestic Product to catalyse the required industrial growth and to ensure improved standard of living, a nearly eight hundred percent increase in energy generation is projected as essential in the next four decades. This emphasizes the role of nuclear energy in India's plans for energy security. India has consciously proceeded to explore the possibility of tapping nuclear energy for the purpose of power generation. Considering the postulated energy demand by 2050 and taking stock of the availability of fuel resources in the country and internationally, it has been estimated by the Department of Atomic Energy that India would require an estimated contribution of at least 25% from nuclear energy.

India's domestic uranium reserve (~ 52,000 tons) is small and the country is dependent on uranium imports to fuel its nuclear power industry. On the other hand, thorium resources are large (~ 3, 19,000 tons). Keeping this fact in mind India is pursuing a three-stage nuclear powder program. In stage I - Pressurized heavy water reactor will use natural uranium (^{235}U–0.7%, fissile isotope and ^{238}U-99.3%, fertile isotope) as fuel to produce electricity and would produce ^{239}Pu as by-product through neutron capture reaction of ^{238}U. In the second stage of the nuclear program, fast breeder reactors will be producing energy by utilizing the ^{239}Pu produced in the first stage. At the same time these reactors will also be used for converting another naturally occurring fertile isotope ^{232}Th into fissile isotope ^{233}U. In the third stage of the nuclear program, ^{233}U produced from the second stage will be used as fuel for thermal breeder reactors. The three-stage nuclear program effectively utilizes the existing resources of uranium and thorium.

India has entered into the second stage of the nuclear programme successfully, with the design and construction of 500 MWe prototype fast breeder reactor (PFBR) at Kalpakkam. One of the major components in the PFBR is the control rod material. Due to high neutron absorption cross section of ^{10}B, boron in the form of boron carbide is used as the control rod and neutron shielding material in PFBR. In addition, its favourable physicochemical properties such as high melting point, high hardness, low density, good thermal conductivity, low thermal expansion coefficient and high chemical stability, make boron carbide an attractive candidate material for many industrial applications. Commercially boron carbide is synthesized by carbothermic reduction of boric oxide/boric acid. However, this method is energy inefficient and requires very high temperatures. The product obtained is in the form of nuggets and coarse-grained. Hence, this product is subsequently crushed and intensively milled to produce powder. The milled powder is inherently associated with contamination resulting from the grinding media and hence requires an acid leaching for purification. In addition, this process results in substantial loss of boron in the form of its oxides due to volatilization at high temperatures. Hence, the resultant final product, boron carbide, is often found to contain a significant amount of residual carbon. It is a challenge to synthesize boron carbide without free carbon residue for various industrial applications.

This thesis mainly deals with the research and development associated with the synthesis and characterization of nanocrystalline boron carbide at relatively lower temperatures. In addition, the thesis deals with the thermal expansion of boron carbide and development of a simple method for the digestion of boron carbide for its chemical assay.

Organization of the thesis

The thesis comprises of seven chapters that are listed below.

CHAPTER 1	: Introduction and literature review
CHAPTER 2	: Experimental
CHAPTER 3	: Thermodynamic analysis of the production of boron carbide through carbothermic reduction of boric oxide
CHAPTER 4	: Studies on the synthesis and characterization of nanocrystalline boron carbide from gel precursors
CHAPTER 5	: Studies on the thermal expansion of nanocrystalline and microcrystalline boron carbides
CHAPTER 6	: Studies on the development of a new method for the digestion of boron carbide for its chemical assay
CHAPTER 7	: Summary, conclusions and scope for future study

A brief overview of individual chapters is presented below.

Chapter 1

This chapter presents a general introduction to the importance of nuclear energy with particular emphasis to fast breeder reactors. Various components of nuclear reactors and types of reactors are then discussed. This is followed by a discussion on the control systems in nuclear reactors, various control rod materials and advantages of boron and boron carbide as control rod material. The chapter also discusses the advantages and disadvantages of various methods of synthesis of boron carbide reported in the literature. Importance of nanocrystalline materials, need of thermal expansion studies of materials and various methods for the determination of thermal expansion are also discussed. The need to develop an alternate method of digestion of boron carbide for its chemical assay is discussed. Finally the results of the present study are summarized and the scope for further study are highlighted.

Chapter 2

This chapter describes the experimental techniques and materials employed in the present investigation. The principles of chemical characterization (analysis of boron and carbon) and the details of powder and metallurgical characterization of materials (viz., bulk density, specific surface area analysis, FTIR, X-ray diffraction analysis, scanning electron microscopic analysis, transmission electron microscopic analysis, particle size distribution techniques etc.) that have been used in the present study are given.

Chapter 3

This chapter describes the thermodynamic analysis of the synthesis of boron carbide through carbothermic reduction of boric oxide. Commercially boron carbide is produced by the carbothermic reduction of either boric oxide or boric acid. In order to identify the optimum reduction temperature and the mole ratio of B_2O_3 to C, thermodynamic equilibrium calculations on the system B-O-C have been performed by using FactSage 6.2. The calculation of the equilibrium concentrations of various species has been performed over the temperature range 273–3573 K. All possible condensed phases and gaseous species have been taken into account. These calculations show that the carbothermic reduction of boric oxide is feasible at temperatures above 1830 K and the residual carbon in the final product can be reduced by suitably adjusting the mole ratio of carbon to boric oxide to a value slightly lower than that demanded by the stoichiometry of the reaction between B_2O_3 to C to give boron carbide. These results are consistent with the experimental observations reported in the literature. The influence of residual moisture present in argon carrier gas / purge gas on the yield of boron carbide during the carbothermic reduction of boric oxide has also been examined.

Chapter 4

This chapter deals with the development of energy efficient methods for the synthesis of nanocrystalline boron carbide based on the pyrolysis of suitable gel precursors. This is a novel technique for synthesizing boron carbide at relatively lower temperatures than those employed in commercial methods. Using this technique, nanocrystalline boron carbide was synthesized from various gel precursors. The chapter is divided into four different sub sections, namely, (i) synthesis and characterization of boron carbide from boric acid-citric acid gel precursor (ii) synthesis and characterization of boron carbide from boric oxide-citric acid gel precursor (iii) synthesis and characterization of boron carbide from boric acid-sucrose gel precursor and (iv) synthesis and characterization of boron carbide from boric oxide-sucrose gel precursor.

Chapter 5

This chapter presents the results of the thermal expansion of boron carbide. The lattice thermal expansion behaviour of nanocrystalline and microcrystalline boron carbides has been measured by the high-temperature X-ray diffraction technique in the temperature range 298–1773 K. The lattice parameters of both nano and microcrystalline boron carbides were found to increase with increase in temperature. The average thermal expansion coefficients in this temperature range for the nanocrystalline and the microcrystalline boron carbides were found to be 7.76×10^{-6} and 7.06×10^{-6} K^{-1} respectively. The difference observed in the thermal expansion behaviour is explained in this chapter.

Chapter 6

The development of an alternate method for the digestion of boron carbide for its chemical assay is described in this chapter. The boron carbide was digested using an acid mixture in a simple apparatus. Boron was subsequently determined by the conventional method of titration of mannitol-boric acid complex using the standard potassium hydroxide solution. Trace elements and isotopic ratio of $^{10}B/^{11}B$ were determined by using inductively coupled plasma mass spectrometer. The validity and accuracy of the digestion technique developed in this study was established by comparing the analytical results with those obtained by conventional "sodium carbonate fusion" method. The new digestion technique developed in this study facilitates relatively fast and accurate determination of total boron, its isotopic content and trace elements present in it.

Chapter 7

In this concluding chapter, the thesis is summed up by highlighting the main findings and the results of the present study. Finally the scope for future work has been presented.

List of Figures

List of Tables

Introduction

1.0 Introduction

This chapter presents a general introduction to the importance of nuclear energy with particular emphasis on fast breeder reactors. Various types of reactors and the components of nuclear reactors are discussed. This is followed by a discussion on control systems in nuclear reactors, various control rod materials and advantages of boron and boron carbide as control rod materials. The chapter also discusses various methods of synthesis of boron carbide reported in the literature. Importance of nanocrystalline boron carbide, need of thermal expansion studies and various methods for the determination of thermal expansion are also discussed. Finally various methods of digestion of boron carbide for its chemical assay are presented. The motivation and scope of the present study are also highlighted.

1.1 Energy and economy

Energy is the most fundamental requirement of every society or nation as it progresses through the ladder of development. The energy demand of the world is increasing every year due to population growth and increasing standard of living. Sustainable growth cannot be fully achieved without secure access to energy and electricity. There is a distinct and categorical correlation between the energy consumption and income of a nation—each reinforcing the other. A nation’s development index is linked to its per capita consumption of electricity [1, 2]. Per capita electricity consumption in developed countries is very high [3]. Developing countries such as India have very low per capita energy consumption which currently stands at 420 kWh per year as compared to USA (12190 kWh per year) and Japan (7290 kWh per year). In this regard, developing countries like India need to exploit all the available resources to produce energy to meet the ever-increasing demand of power and to bring the per capita energy consumption to reach that of the advanced countries within a few decades.

The major energy sources of India are fossil fuels such as oil, coal and natural gas. In the profile of energy sources in India, coal has a dominant position. Coal constitutes about 53% of India's primary energy resources followed by hydro (25%), gas (10%), renewables (8%) and nuclear (3%) [4]. Coal accounts for more than half of the country's energy consumption. The poor quality of Indian coal, coupled with lack of infrastructure to clean it, poses a major environmental threat. Although it is the world's third biggest coal producer after the United States and China, India's coal reserves at the current level of consumption could run out in forty years. As per the ministry of petroleum, Government of India, India has 1,437 billion cubic meters of confirmed natural gas reserves as of April 2010. Natural gas resources are likely to last for about thirty years at the present level of consumption. In India, resources of crude oil are meager. Almost 70 % of crude oil consumed is imported. The current reserves of crude oil are merely 786 Mt. These reserves including imports will last only for 1-2 decades at the present rate of consumption [5].

India has a share of 16 % in the world's population. The energy generation capacity needs to be increased to transform India into a technologically and economically advanced nation. India needs to increase its power production by eight hundred times in the next 30-40 years to achieve the anticipated Gross Domestic Product (GDP). India is aiming to reach at least a per capita energy consumption of about 2400 kWh/a (current world average) with 8% growth rate of GDP by 2031-32 [6]. In this context, the electricity generation capacity should be raised to about 778 GWe by 2031-32 [7]. This level of increased electricity generation capacity cannot be sustained for more than a few decades, even with full utilization of all existing resources such as exploitable domestic hydrocarbon, hydroelectric and non-conventional energy resources. The bulk import of fuel or energy is not an affordable proposition for India. In this context nuclear power will be called upon to play a crucial role in meeting the projected demand for electricity generation.

After thermal, hydro and renewable sources of electricity, nuclear power is the fourth largest source of electricity in India. Department of Atomic Energy aims to contribute 25% of electricity from nuclear power by considering the demand and the available energy resources in India by 2050. At present, there are 19 nuclear power reactors in operation with a gross capacity of 4560 MWe and 4 reactors with a capacity of 2720 MWe at an advanced stage of construction. Four indigenously-designed 700 MWe pressurized heavy water reactors (PHWRs) with a capacity of 2800 MWe have been launched, two reactors of 700 MWe at each of the existing sites, Kakrapar in Gujarat state and Rawatbhata in Rajasthan state [7].

India has a flourishing and largely indigenous nuclear power program and expects to have 20,000 MWe nuclear capacity on line by 2020 and 63,000 MWe by 2032 by setting up nuclear reactors based on both indigenous technologies of pressurized heavy water reactors (PHWRs), fast breeder reactors (FBRs) and large size light water reactors (LWRs).

1.2 India’s nuclear energy programme

The Indian nuclear programme was conceived based on unique sequential three-stages and associated technologies essentially to aim at optimum utilization of indigenous nuclear resources of modest uranium [6] and abundant thorium (~ 3, 19,000 tons) [7]. The first stage is based on PHWRs which use natural uranium (^{235}U–0.7%, fissile material and ^{238}U-99.3%, fertile material) as fuel to produce electricity. In this stage ^{239}Pu would be produced as by-product through neutron capture reaction of ^{238}U. In the second stage of the nuclear programme, fast breeder reactors will be producing energy by utilizing the ^{239}Pu produced in the first stage. At the same time these reactors will also be used for converting another naturally occurring fertile isotope Th^{232} into fissile isotope U^{233}. In the third stage, U^{233}-Th based reactors are proposed to be set up for utilizing the vast resources of thorium [8, 9].

1.3 Key components of nuclear reactors

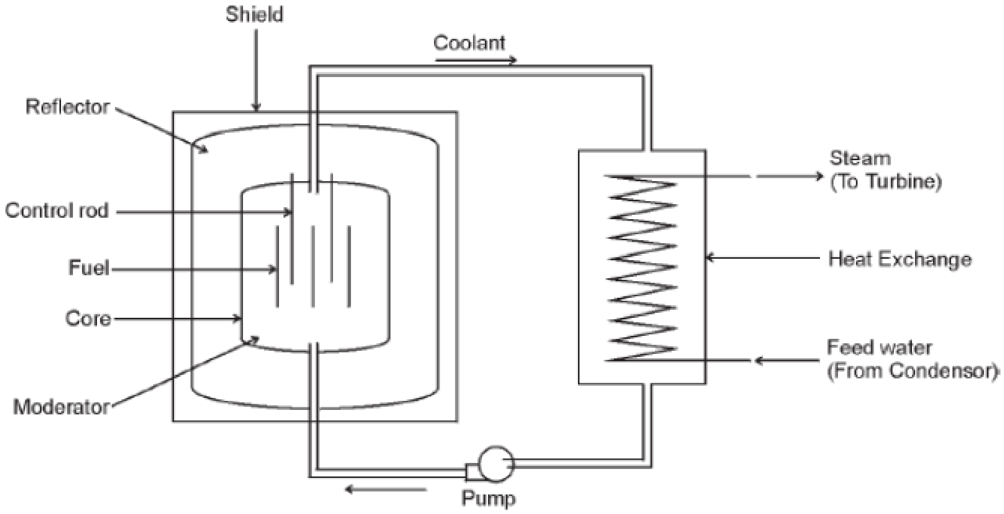

Fig. 1.1 Block diagram of a nuclear reactor

In general, a nuclear power reactor is not much different from a conventional power plant when it comes to generating electricity, except for the manner in which the heat is generated using nuclear chain reactions. A simple schematic of a typical nuclear reactor is shown in Fig. 1.1. The major components common to most types of nuclear power reactors are given below: [10]

Core: It is the heart of the reactor which consists of nuclear fuel [11]. Usually high-density pellets of UO_2, (U, Pu)O_2, (U, Pu)C, (U, Pu, Zr) alloy etc. sealed in a clad tube typically made of zirconium alloy, magnesium alloy or stainless steel etc., depending on the type of reactors form the fuel rods. The rods are arranged into fuel assemblies in the reactor core.

Moderator: Moderators are used only for thermal reactors but not for fast reactors. The moderator slows down the neutrons released from fission so that the probability of absorption of neutron by the fissile nuclide is increased. Commonly used moderators include light water, heavy water and graphite in various thermal reactors.

Control rods: Nuclear fission is a source of tremendous energy that could be either used for destructive purposes such as nuclear weapons or for constructive purposes such as production of electrical energy through a nuclear reactor. The nuclear chain reaction that produce tremendous amount of energy needs to be controlled in a predictable manner. It is here that the control rod comes into picture and form an important part of a nuclear reactor. Control rods containing neutron absorbing materials are used to control these nuclear chain reactions in a predictable way.

Coolant: Heat energy is generated in a nuclear reactor core due to nuclear fission reaction. This heat needs to be transported to the boiler where steam is raised to run a conventional turbine. A coolant plays an important role in a nuclear power plant and serves the dual purpose of removing the heat from the reactor as well as transferring it to the electricity generation circuit either directly or indirectly depending on the type of nuclear reactor being used for the purpose. Generally water or a liquid metal such as liquid sodium is used as a coolant in a nuclear reactor.

The Shielding Component: A nuclear reaction is a source of intense radiation apart from the heat generated in the exothermic process. Because of the harmful effects of radiation, shielding is required to prevent it from leaving the reactor. Concrete and steel are very good at absorbing radiation and they are equally strong as well, hence used in forming the shielding material.

1.4 Various types of nuclear reactors

Nuclear reactors are often classified in various ways based on the neutron kinetic energy, the purpose of the reactor and the kind of reactor fuel or coolant. The task of making a choice among the many possibilities is rendered difficult by the fact that every system that has been proposed has some advantages and some disadvantages. Further discussion here is focused mainly on power reactors. The power reactors are divided into the following categories [12]:

1. Light water moderated reactors (LWRs). This category includes both pressurized water reactors (PWR) and boiling water reactors (BWR) which are cooled and moderated by light water.
2. Heavy water moderated reactors (HWR). These reactors are generally moderated and cooled by heavy water.
3. Gas cooled reactors (GCR).
4. RBMK type (Russian: Reaktor Bolshoy Moshchnosti Kanalniy meaning High Power Channel type Reactor) (Graphite Moderated, Boiling Water) reactors.

The above reactors are thermal reactors.

5. Fast breeder reactors

6. Advanced nuclear reactors – These reactors may be of any of the above types incorporating advanced concepts.

1.5 Fast Breeder Reactors

A nuclear breeder reactor produces more fuel than it consumes. Breeding is possible only in case of fast reactors where chain reaction in the fast reactor is sustained by fast neutrons. Hence, these are called Fast Breeder Reactors (FBRs). The neutron energy and fission cross sections (probability to undergo nuclear fission) of the fissile material are inversely related. To compensate for the small cross sections in fast energy regions, highly enriched fuel (enriched in fissile isotope) is used in the core from criticality consideration. Blankets of thorium or natural uranium are used to capture the neutrons leaking from the core and thus produce fissile material ^{233}U or ^{239}Pu. The blanket also acts as a reflector of neutrons and thus reduces the critical mass. The fast reactors use liquid sodium as the coolant as it has highly favourable nuclear, physical and chemical properties. For example, sodium does not moderate neutrons. It has low melting point, which makes it easy to maintain in liquid form. Sodium has a very good heat transfer characteristics.

The first stage consisting of pressurized Heavy Water Reactors (PHWR) has reached a state of commercial maturity. India has mastered the technology of design and construction of PHWRs and built over 15 PHWRs of varying capacities. India has embarked in the second stage of FBRs and has commercially launched 500MWe Prototype Fast Breeder Reactor (PFBR) at Kalpakkam.

1.6 Control system in a nuclear reactor

Control rods containing neutron absorbing materials are used to control the nuclear chain reactions in a predictable way [13]. The power level of nuclear reactors is controlled by adjustment of the neutron flux. In any reactor, high power levels correspond to high neutron fluxes and low power levels to low neutron fluxes. The operation and control of a nuclear reactor is performed by monitoring and adjusting the neutron flux in the reactor. The neutron flux is defined in terms of 'effective multiplication factor' (K_{eff}). It is defined as the ratio of the number of fissions in any one generation to the number of fissions in the immediately preceding generation for a reactor of finite size. For a sustained chain reaction the 'k_{eff}' should be at least unity. A reactor is considered as critical when $k_{eff} = 1$, supercritical when $k_{eff} > 1$ and subcritical when $k_{eff} < 1$. The fractional departure of a system from criticality is defined as reactivity (Reactivity $=k_{excess} / k_{eff}$) where k_{excess} is the excess multiplication factor and is a measure of the departure of the system from criticality [14]. Due to decrease in the fissile nuclear fuel content and increase in the amount of fission products, some of which may absorb the neutrons, the reactivity of the reactor decreases with operation time. In order to avoid reactor to go subcritical, reactivity is always maintained greater than unity. This is possible by employing the following methods: addition/removal of (i) nuclear fuel in the core (ii) moderator in the core for thermal reactors (iii) reflector around the core and (iv) neutron absorbers in the core [15]. These methods can be applied either individually or collectively to control a nuclear fission reactor. The practical control method that has hitherto been widely used is the insertion or withdrawal of neutron absorber or control materials due to its convenience and simplicity [16].

Control rod materials absorb the excess neutrons and keep the reactor always in critical stage. Neutron absorption cross section (σ_c)[1] of control rod materials determine the rate of neutron absorption reaction. It is the property of the nucleus and defined for neutron of particular energy. It is expressed in terms of cm^2. Since absolute values of cross sections are very small, the unit barn (1 barn = 10^{-24} cm^2) is used. Neutron absorption cross section decreases with increasing neutron energy.

The quantity $N \times \sigma_c$ is equivalent to the cross section of the material per cm^3 for an absorption reaction when the material contains 'N' nuclei / cm^3. This is called macroscopic cross section and is the quantity used for evaluating absorber materials. The macroscopic cross section is: $\Sigma = N\ \sigma_c$ (cm^{-1}). It has the dimension of reciprocal of length. The inverse of 'Σ' is the mean free path (λ) which a neutron would probably travel through a material before undergoing an absorption reaction.

1.7 Control system of PFBR

The PFBR's systems are designed with defence-in-depth approach having redundancy, diversity and independence. The safety measures provided are two independent, fast acting and diverse reactor shutdown systems, two decay heat removal systems, a core catcher and reactor containment building. Each shutdown system consists of sensors, logic circuits, drive mechanisms and neutron absorber rods having boron carbide pellets [17]. There are two types of independent fast acting diverse shut down systems in PFBR for control and shut down of the reactor in case of any abnormal event. They are: (i) control and safety rod (CSR) and (ii) diverse safety rod (DSR). The respective drive mechanisms are control and safety rod drive mechanism (CSRDM) and diverse safety rod drive mechanism (DSRDM). CSRDM and DSRDM are housed in

---

[1] It is defined as the probability of occurance of a neutron absorption reaction

control plug which is a part of top shield of the reactor and are in-line with the respective absorber rods in the core.

The functions of CSRDM [18] are to facilitate:

1. Start-up and controlled shut down of reactor and to control reactor power by raising and lowering of CSR.

2. To shut down the reactor by lowering of CSR into the reactor core in abnormal conditions (due to slow transients)

3. To scram the reactor in abnormal condition (due to fast transients) by rapid insertion of CSR into the core.

The functions of DSRDM are to:

1. Provide the required shut down margin along with CSRs to take care of the fuel handling errors.

2. Maintain the reactor under cold shutdown state independent of CSR after a reactor scram even when one of the DSRs is stuck.

3. Scram the reactor in abnormal conditions (due to fast transients) by a rapid insertion of DSR into the reactor core.

1.8 Characteristics of neutron absorbers/control rod materials

In order to perform their functions, control materials have to meet the following requirements:

1. A neutron absorber should have high neutron absorption cross section. A minimum value of 100 barns for thermal reactors and 1 barn for fast reactors are essential for a material to act as a neutron absorber [19, 20].

2. It should have the desirable mechanical, thermal and physical properties.

3. It should have high wear and corrosion resistance.

4. It should have high thermal and irradiation stability.

5. It should be chemically compatible with the clad and the coolant.

6. It should be inexpensive.

1.9 Various Control rod materials

Chemical elements such as silver, indium, cadmium, boron, cobalt, hafnium, dysprosium, gadolinium, samarium, erbium and europium with a sufficiently high cross section for neutrons or their alloys and compounds (high-boron steel, silver-indium-cadmium alloy, boron carbide, zirconium diboride, titanium diboride, hafnium diboride, gadolinium titanate, and dysprosium titanate) are used as control rod materials. Table 1.1 shows the neutronic properties of various control materials [20]. The choice of materials is influenced by the energy of neutrons in the reactor, their resistance to neutron-induced swelling and the required mechanical and lifetime properties. The control rods may be in the form of, for example, stainless steel tubes filled with suitable neutron absorber in the form of high-density pellets. The swelling of the control rod material due to neutron flux/irradiation can cause deformation of the rod, leading to its premature replacement. The burn up of the absorbing isotopes is another lifetime limiting factor.

Hafnium is a hard, shiny and ductile metal. Naturally occurring hafnium has a microscopic thermal neutron absorption cross section of 105 barn. It absorbs the thermal and epithermal neutrons. Hafnium has excellent physical, mechanical and neutronic properties. It has good mechanical strength, can be easily fabricated and is resistant to corrosion in hot water. Hafnium can be alloyed with small amounts of other elements;

Table 1.1. Nuclear properties of elements envisaged as neutron absorbers. Reproduced from ref. [20].

Element	**Atomic mass (amu)**	**Isotopic abundance (atom fraction)**	**Microscopic cross section (barns)**	**Macroscopic cross section (cm^{-1})**
B	10.82		755 ± 2	104.00
	10.00	0.198	3813	
Ag	107.88		63 ± 1	3.63
	107.00	0.5135	31 ± 2	…
	109.00	0.4865	87 ± 7	…
Co	59.00	1.00	37.0 ± 1.5	3.37
Cd	112.41	…..	2450 ± 50	118.00
	113.00	0.1226	20000 ± 300	…
In	114.82	….	196 ± 5	7.30
	113.00	0.0423	58 ± 13	…
	115.00	0.9577	207 ± 21	…
Sm	150.35	……	5600 ± 200	166.00
	147.00	0.1507	87 ± 60	…
	149.00	0.1384	40800 ± 900	…
	152.00	0.2363	224 ± 7	…
Eu	152.00	…..	4300 ± 100	92.50
	151.00	0.4777	7700 ± 80	…
	153.00	0.5223	450 ± 20	…
	154.00	…...	1500 ± 100	…
Gd	157.26	…..	46000 ± 2000	1390.00
	155.00	0.1473	61000 ± 5000	…
	157.00	0.1568	240000 ± 12000	…
Dy	162..51	…..	950 ± 50	35.00
	164.00	0.2818	2600 ± 300	…
Hf	178.58	…...	105 ± 5	4.81
	174.00	0.0018	1500 ± 1000	…
	176.00	0.0515	15 ± 15	
	177.00	0.1839	380 ± 30	
	178.00	0.2708	75 ± 10	
	180.00	0.3544	14 ± 5	

e.g. tin and oxygen to increase tensile and creep strength, iron, chromium and niobium for corrosion resistance and molybdenum for wear resistance, hardness, and machineability. Some such alloys are designated as Hafaloy, Hafaloy-M, Hafaloy-N, and Hafaloy-NM. Hence it is a good candidate for reactors using water for both moderation and cooling.

Cadmium has a thermal absorption cross section of about 2400 barns. Its use as a control rod material is limited due to its relatively low melting point (594 K) and lack of strength. Its neutron absorption cross section decreases rapidly at energies above 0.18 eV. In order to improve its mechanical strength, thermal conductivity, surface hardness and corrosion resistance, an alloy of silver with 5% cadmium and 15% Indium has been used as control rod material for PHWRs.

Among the rare earth elements europium (Eu), erbium (Er), gadolinium (Gd), samarium (sm), dysprosium (Dy) and lutetium (Lu) in the form of oxides have been selected as control rod materials for thermal reactors. These elements have relatively high thermal neutron absorption cross section in the epithermal region. Dysprosium titanate is a new control rod material currently undergoing evaluation for pressurized water reactors. It is a promising replacement for Ag-In-Cd alloys because of its high melting point. In addition it does not react with cladding materials, easy to fabricate, does not produce radioactive waste and does not swell.

The two most abundant isotopes of boron are ^{10}B and ^{11}B. Natural boron consists of ~19.8 at% of ^{10}B and ~ 80.2 at% of ^{11}B. These two isotopes are chemically identical but possess different nuclear properties. The absorption cross section of ^{11}B isotope is very low (σ_c<< 0.01 barns, for fast neutrons), hence it is non-reactive from a nuclear standpoint. The neutron absorbing properties of boron are due to the high neutron absorption cross section of ^{10}B isotope. Due to this, boron in the form of boron carbide, boron-alloyed steels, alloys of boron and aluminium (BORAL) etc. are used as control rod material in various nuclear rectors. In addition, the wide absorption spectrum of boron makes it suitable as a neutron shield material [4].

1.10 Boron and its compounds as control rod material

Boron and its compounds such as boric acid, boron carbide, rare-earth and refractory metal borides find extensive applications in the nuclear industry as neutron sensors, neutron shielding material, control/shutoff rods and in nuclear material storage. The neutron absorption of natural boron is sufficiently high (752 barn) in the low neutron energy range to make it an excellent candidate for use in thermal reactors. The variation of neutron absorption cross section of boron with neutron energy is shown in Fig. 1.2 a and b.

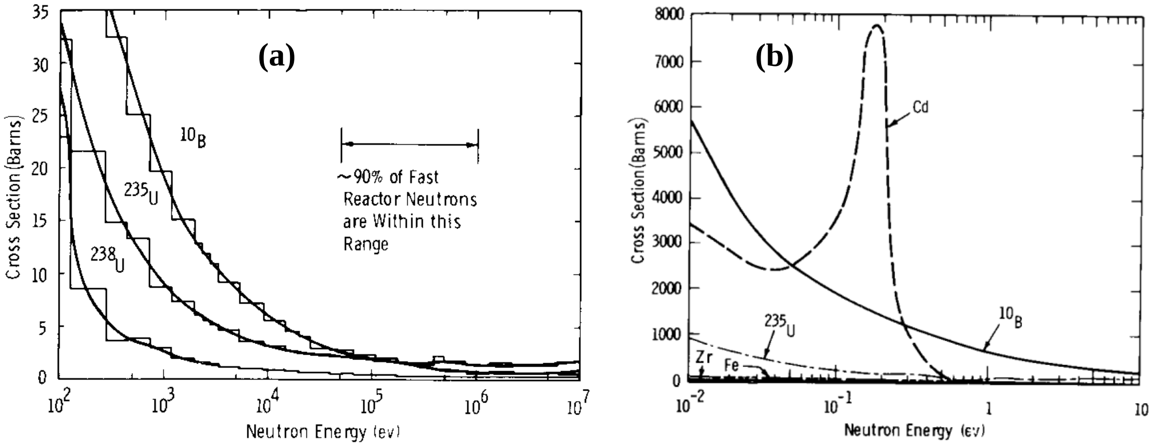

Fig. 1.2 Neutron absorption cross section at (a) high energies and (b) low energies Reproduced from ref. [14].

At higher neutron energies, the neutron absorption cross section of most other elements becomes very small, often abruptly as in the case of cadmium, whereas that of

^{10}B decreases monotonically with energy and the absorption cross section is sufficiently high at 1 barn for 1 MeV energy neutrons. Boron and its compounds such as B_4C are the most effective neutron absorbers in most types of reactors particularly in fast reactors. Absolute values of neutron absorption cross-section of B along the entire energy spectrum are of sufficient magnitude to make it very effective in the intermediate as well as fast energy range also. In addition to a high absorption cross section, boron has another advantage over other potential neutron absorber materials. The reaction products, helium and lithium, are formed as stable, non-radioactive isotopes. As they do not emit nuclear radiation, decay heating problems during reactor shutdowns and transfer of depleted control rods are minimal [16-18].

Among all the compounds of boron, boron carbide is the most effective material for use in nuclear reactors because of its favourable physico-chemical properties.

1.11 Boron carbide

Boron carbide (B_4C) which was discovered about 150 years ago made a tremendous impact on science and technology. It is one of the hardest materials known (also known as black diamond), ranking third behind the diamond and cubic boron nitride [21]. However, at temperatures above 1373 K, it is the hardest material [20]. It is the hardest material produced in tonnage quantities. B_4C was originally discovered in mid 19th century around 1858 [22] as a by-product in the production of metal borides. Joly in 1883 [23] and Mossian in 1894 synthesized B_4C in a purer form [23, 25] and identified boron-carbon compounds of different composition such as B_3C and B_6C. Boron carbide was studied in detail after 1930 and the first phase diagram was published in 1934 [4]. Stoichiometric formula B_4C was assigned in 1934 for boron carbide [23-25]. After that many other diverse formulae were proposed by Russian authors. These have not been confirmed yet but today a homogeneity range from $B_{4.0}C$ to $B_{10.4}C$ has been established [23, 26]. A high B/C molar ratio, as high as $B_{51}C$, is also reported in the literature [27].

Boron carbide is a suitable material for many high performance applications due to its attractive combination of properties such as high hardness, low density, high melting point, high elastic modulus, chemical inertness to acids, high neutron absorption cross-section, excellent thermoelectric properties, etc. Important physical properties are listed in Table 1.2 [28-40].

Table 1.2 Physical properties of boron carbide

Property	**Unit**	**Value**
Melting Point	K	2723
Boiling point	K	3770
Hardness (Knoop, 100g)	kg/mm^2	2900 - 3580
Elastic modulus	GPa	448
Neutron absorption cross section	Barns	3850
Density (273 K)	Kg/m^3	2520
Expansion coefficient (298-1213 K)	K^{-1}	4.5×10^{-6}
Electrical conductivity	Ωm^{-1}	140
Thermal conductivity (298 K)	W/(m−K)	29-67
Young’s modulus	GPa	450 - 470
Shear modulus	GPa	180
Poisson’s ratio	-	0.21
Fracture toughness	$MPa.m^{1/2}$	2.9 - 3.7

1.12 B-C phase diagram

Several phase diagrams have been proposed for the system B-C. The first B-C equilibrium diagram was published by Meerson and Samsonov [41]. New versions of this diagram have been established by Elliott [42] and other workers [43-44]. The boron-carbon binary system includes carbon- rich BC_2 and boron-rich $B_{12}C$, in addition to the two compounds $B_{13}C_2$ and $B_{12}C_3$ (B_4C) both with a large homogeneity range. A large number of phases of boron carbide have been reported viz., B_6C, B_2C_2, BC, B_3C,B_7C, $B_{12}C$, $B_{50}C_2$, $B_{12}C_3/B_4C$ and $B_{13}C_2$ [41]. The phase diagram by Elliott [42] which is widely recognized by most of the authors is shown in Fig. 1.3. Boron carbide (B_4C) exists in a wide homogeneity phase range (8.8-20 at% C). The compounds melts congruently at ~2723 K.

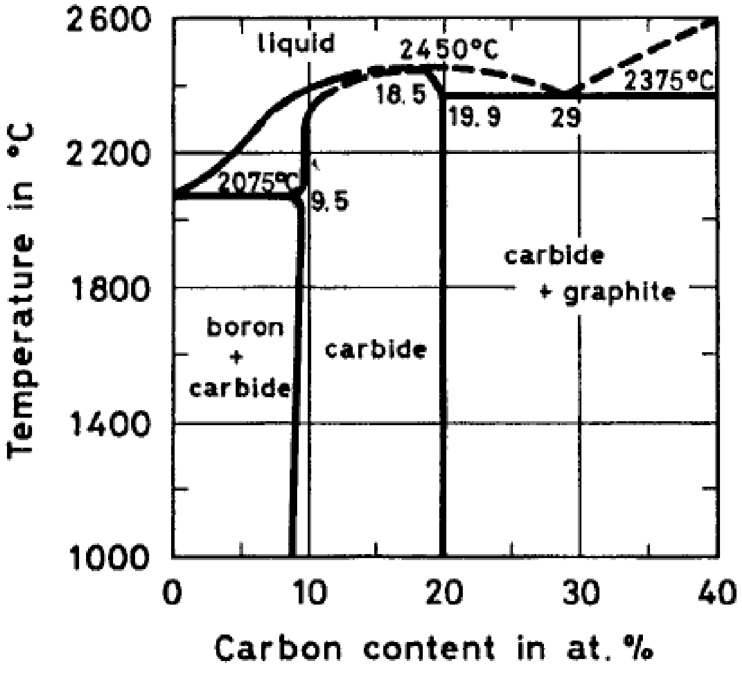

Fig. 1.3 Phase diagram of the system B-C by Elliott [2]

1.13 Boron carbide crystal structure

The most widely accepted crystal structure of boron carbide is rhombohedral, consisting of 12-atom icosahedra located at the corners of the unit cell. The rhombohedral structure of boron carbide consists of 12 icosahedral clusters of atoms linked by direct covalent bonds and through 3-atom inter-icosahedral chains along the longest diagonal of the rhombohedron. The boron-rich icosahedral structures reside at the vertices of a rhombohedron as shown in Fig. 1.4a [45-49]. Four sites are available for a total of 15 B and C atoms in the crystal arrangement. Thus, the B and C atoms can easily substitute for each other within both the icosahedra and the intericosahedral chains. This fact is the main reason for the large homogeneity range of boron carbide [48-49]. The most widely accepted structural model for B_4C with 20 at% C has $B_{11}C$ icosahedra with C-B-C intericosahedral chains. On the other hand, the phase $B_{13}C_2$ contains the B_{12} icosahedra with linear C-B-C chains, i.e. (B_{12}) CBC [22, 26]. The detail bonding structure of boron carbide is shown in Fig. 1.4b. The two icosahedral units are linked by the rear carbon atoms of the upper C-B-C chain and the forward lying carbon atoms of the lower C-B-C chain [50].

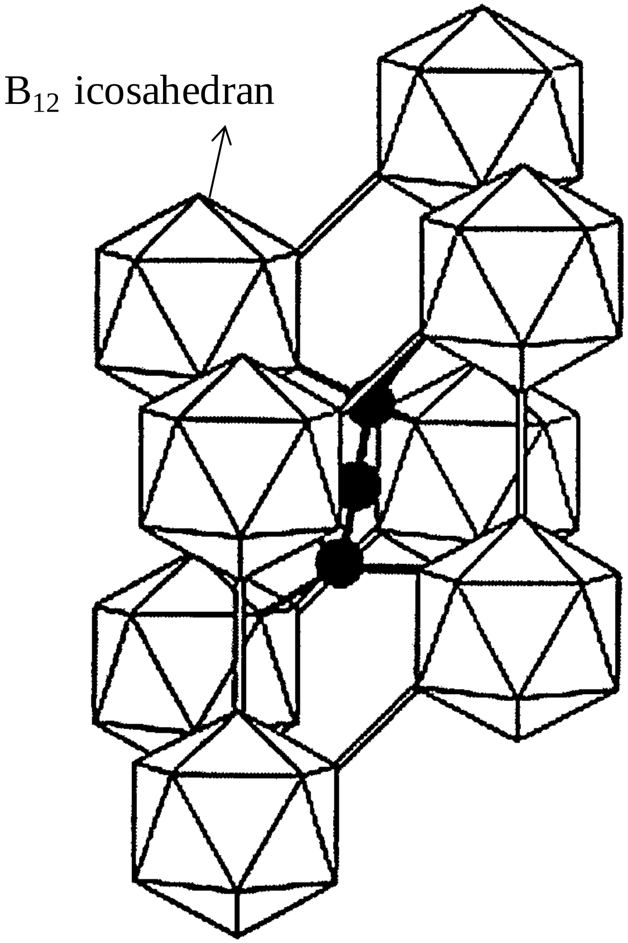

Fig.1.4a The rhombohedral crystal structure of boron carbide [25]

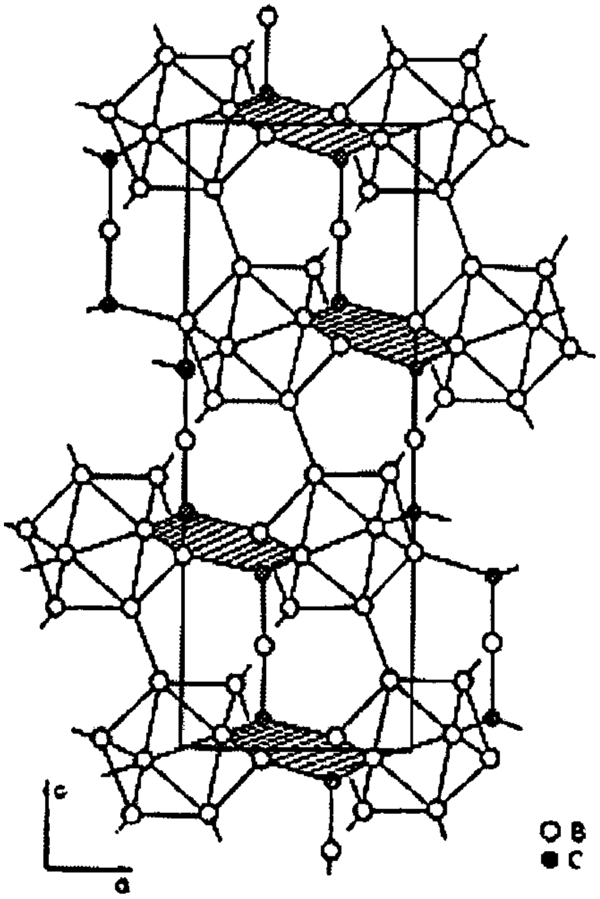

Fig.1.4b The B_4C_2 rings & bonding structure of boron carbide [25]

1.14 Applications of boron carbide

Boron carbide is used in the form of powder, sintered product as well as thin films. Its outstanding hardness makes it a suitable abrasive powder for lapping, polishing and water jet cutting of metals and ceramic materials [51]. Tools with boron carbide coating are used for cutting of various alloys such as brass, stainless steel, titanium alloys, aluminium alloys, cast iron etc. [23]. In sintered form, it is used as blasting nozzles, ceramic bearings and wire drawing dies due to its good wear resistance [52]. The combination of low density, high hardness and impact resistance makes it a suitable material as body and vehicle armour [53]. Modulus to density ratio of boron carbide is higher than that of most of the high temperature materials and hence it could be effectively used as a strengthening medium [54]. Thin films of boron carbide find application as protective coating in electronic industries [55-56].

Composite materials containing boron carbide with good thermal conductivity and thermal shock resistance are found suitable as first wall material of nuclear fusion reactors [57]. Boron carbide-based composites are potential inert matrix for actinide burning. Boron carbide is also used for the treatment of cancer by neutron capture therapy. As it is a p-type semiconductor, boron carbide is found to be a potential candidate material for electronic devices that can be operated at high temperatures [58]. Owing to its high Seebeck coefficient, boron carbide is an excellent thermoelectric material [59]. It finds new applications as thermocouple, diode and transistor devices as well [60]. Boron carbide is an important component for the production of refractory and other metal borides. The low density, high stiffness and low thermal expansion characteristics of B_4C make it attractive material for aerospace applications.

1.15 Synthesis of boron carbide

Boron carbide can be prepared from various starting materials viz., boric acid, boric oxide, borax, decaborane as well as by the direct combination of elemental boron and carbon [50]. Various methods were reported for the synthesis of boron carbide. These methods are:

(i) Carbothermic reduction

(ii) Magnesiothermic reduction

(iii) Synthesis from elements

(iv) Synthesis from polymer precursors

(v) Vapour phase reactions

(vi) Other methods.

1.15.1 Carbothermic reduction

Commercially boron carbide (B_4C) is produced by the carbothermic reduction of boric oxide/boric acid at high temperatures in a batch electric arc or resistance furnace [61]. The overall carbothermic reduction reaction of boric acid/boric oxide can be represented as follows:

$$4\, H_3BO_3\,(s) + 7\, C\,(s) \rightarrow B_4C\,(s) + 6\, CO\,(g) + 6\, H_2O\,(g) \qquad (1.1)$$

$$2\, B_2O_3\,(l) + 7\, C\,(s) \rightarrow B_4C\,(s) + 6\, CO\,(g) \qquad (1.2)$$

This reduction is thermodynamically feasible only above 1673 K [59]. The furnace temperature is usually maintained above 2273 K to enhance the rate of the overall carbothermic reduction. Three types of electric heating furnaces namely tubular, electric arc and Acheson type furnaces are used for the production of boron carbide [62]. An early patent by Scholl et al. [63] explains the production of boron carbide wherein the mixture of boric acid and petroleum coke is melted in an arc furnace followed by crushing the resultant product and mixing it with the same quantity of boric acid and remelting the mixture a second time. Scott [64] explained the design and operation of an electric arc furnace for the large scale production of boron carbide. Ridgway [65] reported the production of boron carbide using Acheson type furnaces, where a graphite rod was used as the heating element, surrounding which the reactants were charged. Rao et al. [66-67] have devised a method of measurement of core temperature in boron carbide manufacturing process as it was an important parameter in carbothermic reduction process.

Many researchers have investigated the process kinetics, influence of process parameters and conversion efficiency of carbothermic reduction. Porosity of the charge, type of carbon used for the reduction, the rate of heating and the final core temperature strongly influence the kinetics of the process and the quality of boron carbide powder. Subramanian et al. [68] have determined the onset temperature of formation of B_4C by the reduction of boric acid with petroleum coke in vacuum by thermogravimetric studies. Alizadeh et al. [69] have optimized the boric oxide to carbon ratio in order to reduce the free carbon content in boron carbide. They have reported that the yield could be improved by the addition of small quantity of NaCl to the reaction mixture. Tumanov [70] has reported the development of a continuous process for the production of boron carbide, by direct inductive heating of a charge made of boron oxide and carbon black. Weimer et al. [71] have designed a vertical apparatus for continuous production of boron carbide. Synthesis of nanosized boron carbide particles by carbothermic reduction process have also been reported in the literature. Herth et al. [72] have synthesized boron carbide particles of size 260 nm by the reduction of boric oxide vapours by carbon black at 1623 K. High-purity boron carbide nanowires were prepared from a mixed powder precursor containing boron, boron oxide and carbon black [73]. When the above said precursor was heated at 1923 K for 2 h under a flowing stream of argon, vapours of B_2O_3, B_2O_2 and CO react to form B_4C solid nanowires with a mean diameter of 50 nm and lengths of several hundreds of micrometres [73]. Large scale boron carbide nanowires of size 80–100 nm diameter and 5–10 mm in length have been synthesized using $B/B_2O_3/C$ powder precursor under argon flow at 1373 K [74]. Xu et al. [75] have synthesised nanostructures of boron carbide by heating boric oxide powder at 2223 K in a graphite crucible covered with a boron nitride disc.

Even though carbothermic reduction of boric oxide/boric acid results in a lower yield (due to loss of boron in the form of its oxides), this method is adopted as a commercial method mainly because of the simple equipment and cheap raw materials which make this route the most economical. This route is not only useful for production of boron carbide commercially but also for the production of nanocrystalline boron carbide. However, this process results in lower yield due to significant loss of boron in the form of oxides of boron during the reduction and subsequent process steps.

1.15.2 Magnesiothermic reduction

Magnesiothermic reduction of boric oxide in the presence of carbon [23, 26, 76] is an alternate commercial method for the production of boron carbide. The reaction is highly exothermic in nature. Since the vapour pressures of magnesium are high at temperatures above 1273 K, a cover gas such as argon or hydrogen is used to maintain the system pressure at a high value. The final product of the reaction is washed with HCl or H_2SO_4 to remove magnesium oxide, unreacted Mg from boron carbide [23]. This reduction technique yields very fine amorphous boron carbide powder, which is well suited for use in the fabrication of sintered products.

Gray [77] has reported a process for the production of boron carbide powders by magnesiothermic reduction of B_2O_3 or $Na_2B_4O_7$ in the presence of carbon at 1923–1973 K. Addition of metallic sulphate as catalyst has been found to reduce the reaction temperature to 973 K [78]. The heat of magnesiothermic reaction is sufficient enough for self propagating high temperature synthesis. Zhang et al. [79] and Khanra et al. [80] have studied the formation of ultra fine B_4C powder from the stoichiometric mixture of H_3BO_3, Mg and C by self-propagating high temperature synthesis (SHS). Mechanical alloying has also been utilised as a means of synthesising submicrometre B_4C particles by magnesiothermic reduction [81]. Jiang et al. [82] have synthesized boron carbide powder by combustion synthesis (CS) method directly from mixed powders of borax, magnesium and carbon. The synthesis of B_4C fibre–MgO composites by combustion of B_2O_3 + Mg + C_{fibre} samples in an argon filled chamber has been studied by Wang et al.[83]. Berchman et al. [84] have reported the synthesis of boron carbide powder by calciothermic reduction of borax ($Na_2B_4O_7$) or B_2O_3 in presence of carbon at 1273 K under argon cover.

Although boron carbide has been produced by magnesiothermic reduction, the high cost of magnesium will soon make this process obsolete for regular production. Boron carbide produced by this method was generally contaminated with magnesium borides [50].

1.15.3 Synthesis from elements

Synthesis of boron carbide from its elements is considered uneconomical due to high cost of elemental boron [85]. Although formation of boron carbide from its elements is thermodynamically feasible at room temperature, the heat of reaction (-39 kJ mol^{-1}) is not sufficient to carry out the reaction in a self-sustained fashion. Formation of boron carbide layer slows down further reaction. Slow diffusion of reacting species through this layer, necessitates high temperature and longer duration for complete conversion of the elements into the compound. For the synthesis of boron carbide from elements, boron and carbon are thoroughly mixed to form a uniform powder mixture, which is then pelletised and reacted at high temperatures (1773 K) in vacuum or under flowing inert atmosphere. The partially sintered pellet of boron carbide is then crushed and ground to get fine B_4C powder. To achieve a high-purity product of B_4C, high-purity elemental boron powder produced by fused salt electrolytic process is often used [86].

Mechanical alloying of B–C mixtures followed by heat treatment is one of the methods being investigated for the synthesis of boron carbide. Room temperature milling is carried out in planetary ball mills for prolonged duration to activate the powders and the alloyed mixture is then annealed to obtain boron carbide. Spark plasma synthesis is a new technique, in which a pulsed high D.C current is passed through the charge mixture contained in a cavity along with the application of uniaxial pressure [87]. In this process, the start and completion of formation has been noticed at 1273 and 1473 K respectively. Combination of mechanical alloying followed by spark plasma sintering has been studied by Hian et al. [88] to obtain 95% pure boron carbide. Shock wave technique has also been attempted for the synthesis of boron carbide from amorphous boron and graphite powder [89] using trimethylene trinitramine as detonator. The resultant product exhibited several different morphologies, such as filaments, distorted ellipsoid, plates and polyhedron and nano particles. Wei et al. [90] synthesized boron carbide nanorods by reacting the carbon nanotubes with boron carbide at 1423 K. Chen et al. [91] have prepared boron carbide nanoparticles by reacting multiwall carbon nanotubes with magnesium boride. Recently nanoparticles of boron carbide (200 nm) were prepared by direct reaction of amorphous boron and carbon at 1823 K [92].

1.15.4 Synthesis from gel precursors

A low-temperature synthesis of boron carbide by carbothermal reduction is possible by improving the dispersion of boric oxide and carbon components [93]. Carbothermal reduction using a condensed product as a precursor that is made up of boric acid/boric oxide and a polyol is attractive as a low-temperature method of preparation boron carbide [94]. The condensed product forms a B–O–C bond by the condensation reaction between boric acid and the polyol. The B–O–C bond forming reaction accelerates the dispersion of boron and carbon sources. Thus the temperature of synthesis is reduced owing to the enlarged surface-active area between the boric oxide and carbon components with superior reactivity [95]. Many polyols including glycerin [96-97], citric acid [98-101], sugar [102-103], and poly(vinyl alcohol) (PVA) [104-105] were hitherto used and crystalline boron carbide powder with micrometer-sized particles was synthesized at 1773-1673 K (temperatures lower than that for the general carbothermal reduction (2273 K)). Some of the boron loaded organic compounds such as carborane ($C_2B_nH_{n+2}$), triphenylborane, polyvinyl pentaborane and borazines on pyrolysis yield boron carbide [74]. Harris et al., [106] have described a process for making a free flowing boron carbide powder on heat treatment of boric acid and sugar solution in ethylene glycol at 1973 K for 7 h. Mondal et al. [104] and Yanase et al. [105] have described a low temperature synthesis route in which a polymeric precursor was synthesised by the reaction of boric acid and polyvinyl alcohol. This precursor on pyrolysis gave crystalline boron carbide. Sinha et al. [98], Hadian et al.[99], Khanra et al.[100] and Kasovic et al.[101] have reported processes in which a stable gel was formed from an aqueous solution of boric acid and citric acid. This gel was further processed to yield a precursor which on heating at temperatures above 1500 K produced B_4C. Economy et al. [107] have prepared boron carbide fibre by heating amine treated B_2O_3 fibre. In this process boric oxide fibers were heat treated with ammonia in the temperature range 623-873 K and further heated under a flowing stream of primary/secondary/tertiary amine in the temperature range of 873-1273 K followed by heating the resultant product in the temperature range 2273–2623 K in inert atmosphere to produce boron carbide fibers. Cihangir et al. [108] have synthesized B_4C and B_4C/SiC by the pyrolyssis of the precursors from boric acid, sugar and sodium metasilicate at 1673-1873 K. Masaki et al. have synthesized boron carbide from boric acid-mannitol and boric acid-glycerin gel precursors [95, 109]. Akihiro et al. have synthesized boron carbide microcrystals from saccharides such as glucose, cellulose and boric acid [103].

1.15.5 Vapour phase reactions

Several researchers have studied the synthesis of boron carbide by carrying out reaction between boron and carbon containing gaseous species [50, 110-114]. This method was mainly used for the formation of boron carbide coatings and for the synthesis of submicron boron carbide powders and whiskers. Boron halides viz., BCl_3, BBr_3, BI_3, boranes such as B_2H_6 and boric oxide were used as source of boron and gaseseous hydrocarbons such as CH_4, C_2H_4, C_2H_6, C_2H_2 and carbon tetra chloride (CCl_4) were employed as the source of carbon [50]. Bourdeau [110] in his patent has described a process for the production of boron carbide by reacting a halide of boron in vapour phase with hydrocarbon in the temperature range 1773–2723 K. Clifton et al. [111] have described a process for producing 0.05 to 0.25 μm boron carbide whiskers of by the reaction of B_2O_3 vapours with the hydrocarbon gas between 973 and 1873 K. James et al. [112] have patented a process for the production of boron carbide whiskers in which the use of catalytic elements to enhance the yield of the gas phase reaction was demonstrated. Ditter et al. [113] have described a process for the production of ultra-fine boron carbide powder with a surface area >100 m^2 g^{-1}. This process involves the gas phase reaction of acetylene with diborane. MacKinnon et al. [114] have reported that when boron trichloride was reacted with CH_4–H_2 mixture in argon plasma, boron carbides of variable B/C ratios were obtained as submicrometre powders. The product stoichiometry, however, depended on the composition of the reactant mixture.

Deposition of different types of boron carbide films ($B_{13}C_2$, B_4C, metastable phases, highly strained structures, etc.) by Chemical Vapour Deposition techniques has been extensively studied. The actual deposition was controlled by mass transfer and surface kinetics which affected the stoichiometry and properties of the boron carbide phases grown. Graphite, single crystal silicon, carbon fiber and boron were the substrate materials used for the synthesis of thin films [50]. The process was carried out in vacuum in the temperature range of 723 to 1723 K. Substrate temperature had strong influence on the process and the product quality. High substrate temperature resulted in poor adhesion whereas deposition rate was low at low temperatures. Amorphous boron carbide coating could be obtained at a low temperature of ~773 K whereas crystalline film was obtained at higher temperatures. Amorphous boron carbide coatings on SiC have been obtained by CVD from CH_4–BCl_3–H_2–Ar mixtures at low temperature (1173–1323 K) and reduced pressure (10 kPa) [23, 50].

1.15.6 Other methods

Shi et al. [115] have synthesized boron carbide in an autoclave at 723 K by coreduction of boron tribromide and carbon tetrachloride using sodium as reducing agent. Nanocrystalline boron carbide was synthesized by solvothermal reduction of carbon tetrachloride using lithium in presence of amorphous boron powder in an autoclave at 873 K [116]

Thin films of boron carbide can be prepared by ion beam synthesis. In this method boron carbide thin films can be grown by direct deposition of B^+ and C^- ions. In this process, parameters such as ion energy, ion flux ratio of different ion species and the substrate temperature, which can be independently controlled, could be advantageously used for obtaining the preferred composition and nature of the boron carbide film. Ronning et al. [117] have grown thin film of boron carbide (B_xC) by direct ion beam deposition on silicon using an ion energy of 100 eV at room temperature. Todorovic et al. [118] have observed the formation of amorphous boron carbide (B_xC) by bombardment of B^+ and B^{3+} ions on fullerene.

Several authors have prepared boron carbide whiskers by vapour-liquid-solid (VLS) growth mechanism. It involves the transport of boron and carbon gaseous species to a liquid catalyst metal viz., Fe, Ni, Co in which whisker constituents get dissolved.

When the liquid catalyst becomes supersaturated with boron and carbon, boron carbide whiskers precipitate out of the catalyst droplets. Carlsson et al. [119] have prepared boron carbide whiskers and platelets from boric oxide (boron source), carbon black (carbon source), sodium chloride and Co (catalyst) using VLS growth mechanism. Rao et al. [120] and Ma et al. [121] also have investigated the growth of boron carbide using the VLS growth mechanism.

Hong et al. [122] have fabricated boron carbide powder via the reaction of hexagonal boron nitride with carbon black at 2173 K for 5 h. Ahmet has reported the synthesis of boron carbide by aluminothermic reduction of boric oxide [123].

Natural boron contains 20 at% ^{10}B and 80 at% ^{11}B. The Indian Prototype Fast Breeder Reactor would employ high-density boron carbide pellets containing boron enriched in ^{10}B isotope to an extent of $\geq$ 65 at% as the control rod material. Conventional commercial methods such as carbothermic reduction or magnesiothermic reduction cannot be employed for the production of enriched boron carbide since the loss of highly precious and expensive enriched boron would be very high due to the vaporization of highly volatile oxides of boron during the carbothermic reduction process at very high temperatures (>2000K). The loss of boron in the form its oxides can be minimized only by reducing carbothermic reduction temperature. Hence, there is a need to develop alternate energy efficient methods for the synthesis of boron carbide at relatively lower temperatures than that employed in conventional methods.

In addition, preparation of high-density pellets/articles of boron carbide needs highly sinteractive boron carbide powders. Boron carbide obtained through conventional processes has to undergo a series of size reduction processes to obtain sinteractive powders. Such grinding operations are associated with contamination of the powder with the components of the grinding media and hence requires an elaborate acid leaching for purification. Highly sinteractive powders of boron carbide can be prepared by the pyrolysis of suitable gel precursors at relatively low temperatures. The boron carbide powder thus prepared would be nanocrystalline with high surface activity. In addition, the nanocrystalline materials can reduce the temperature of sintering substantially so that high-density boron carbide pellets can be prepared at relatively low temperatures.

1.16 Nanocrystalline materials

There is a rapid growth in the development of nanomaterials due to their potential applications in a wide variety of technological areas such as electronics, catalysis, ceramics, magnetic data storage, structural components etc. [124]. To meet the technological demands in these areas, the size of the materials should be reduced to nanometer scale. As the size reduces to nanometer range, the materials exhibit interesting mechanical and physical properties. Nanomaterials can be classified into nanoparticles and nanocrystalline materials. The former refers to ultra fine dispersive particles with diameters below 100 nm while the latter refers to polycrystalline bulk materials with grain sizes in the range of nanometers (less than 100 nm) [125]. These nanocrystalline materials exhibit unique, extraordinary physical properties relative to the corresponding properties present in bulk materials viz., increased mechanical strength, enhanced diffusivity, higher specific heat and electrical resistivity [126]. Since the grain sizes are small, a large volume fraction (>50%) of the atoms reside in grain boundaries. The interface or grain boundary structure plays an important role in determining the mechanical, physical properties of nanocrystalline materials [127]. One of the most critical characteristic of nanocrystalline materials is their very high surface to volume ratio i.e. large fractions of surface atoms. Thus, large fractions of surface atoms together with ultra fine size make nanocrystalline materials exhibit distinctly different properties from the bulk.

In order to understand and predict the behaviour of nanocrystalline materials, it is essential to have an accurate knowledge of their physical properties. In particular, knowledge on thermal expansion behaviour of materials is very useful for various industrial applications. Thermal expansion measurements are necessary in the temperature range of interest in order to address problems such as thermally induced stresses between dissimilar materials in contact. In this regard, the thermal expansion of nanocrystalline boron carbide is important in determining its performance in nuclear reactors as control rod material.

1.17 Thermal expansion studies

Temperature changes in materials cause dimensional changes so as to minimise the free energy of the system [128]. Lattice vibrations, free electron transitions, electric and magnetic dipole etc. contribute to the free energy. However, the largest contribution to the free energy, at moderate and high temperatures, is from the lattice vibrations. Hence the largest contribution to the thermal expansion is from lattice vibrations. There can be no thermal expansion if the atoms vibrate about their equilibrium positions symmetrically whatever be the amplitude. The thermal expansion of solid is a manifestation of the anharmonic nature of the lattice vibrations [129]. Due to the anharmonic component in the lattice vibrations, the interatomic separations increase with increase in temperature. These changes in the interatomic separations are reflected in the changes in the values of lattice parameters. Hence by measuring the lattice parameters as a function of temperature, the coefficient of thermal expansion (CTE) of crystalline materials can be obtained. The CTE of a material is defined as the fractional increase in length per unit increase in temperature and depends on the crystal structure and bonding and is directly proportional to the bond strength. Generally, for materials with covalent bonding the thermal expansion will be less than that in the case of ionic or metallic solids [130].

In addition, data on CTE are needed to derive heat capacity at constant volume (C_v) from the experimentally measured heat capacity at constant pressure (C_p) [131] and to derive thermal shock resistance of materials. Phase transformation of materials can also be derived form the measurement of coefficient of thermal expansion as a function of temperature [132].

1.17.1 Methods of measuring coefficient of thermal expansion

The methods of measurement of CTE are classified into the following two groups:

1. Bulk expansion measurements or macro methods (includes optical and electrical methods)
2. Lattice expansion measurements or micro methods (includes high temperature X-ray diffraction method)

These methods are briefly discussed below with special reference to measurements at high temperatures.

1.17.1.1 Bulk expansion measurements

1.17.1.1.1 Optical interferometry

The optical interferometer provides a highly sensitive means for measuring the thermal expansion of solids using the basic standard of the length. With optical interference techniques, displacement of the specimen ends is measured in terms of the number of wavelengths of monochromatic light. American Society for Testing and Materials (ASTM) Test Method E 289 (Ref 3) provides a standard method for the linear thermal expansion of rigid solids with interferometry that is applicable from 123 to 973 K. The accuracy of the measured length varies from 0.1 µm to 0.1 nm [133, 134].

In this method, the sample is placed between two quartz discs. The surfaces of these discs act as reflecting surfaces for monochromatic radiation from a helium light source. When the path difference between the two reflected rays is an integral multiple of wavelength, interference rings appear. When temperature increases, the upper disc will be pushed up. This alters the path difference between the two reflected rays and the interference fringes appear to move. The number of fringes, n, passing reference mark are measured and by using the following relationship the CTE is computed,

$$dl = n\lambda / (2l + (A/l)) \qquad (1.3)$$

where l = length of the sample

λ = wavelength of the radiation

dl = change in length and

A = correction factor to be added when the experiment is carried out in a medium other than vacuum.

This is an absolute technique, with good precision and accuracy. The application of laser beams has greatly enhanced its capability. A compatible vibration-free environment is needed for carrying out the experiments. If quartz is used as the reflecting disc, this device can be used for temperatures up to 1273 K, and with sapphire a maximum temperature of 2073 K can be attained.

1.17.1.1.2 Precision optical micrometry

In this technique, the thermal expansion is measured by observing the position of two index marks on a long specimen by means of two calibrated telemicroscopes mounted on an invar support. These microscopes are focused on the index marks, and can be made to follow their displacement when temperature is raised. The specimen is generally in the form of rods of length about 100 mm and diameter about 5-10 mm. Usually a graphite tube furnace, which operates up to a temperature of about 2573 K is used in this technique [135].

1.17.1.1.3 Push rod dilatometry

A dilatometer is a device which continuously records changes in linear dimensions of a specimen at elevated temperatures. Dilatometry is a very useful tool for material scientists to understand the expansion behaviour of materials. This technique is used to evaluate properties like (a) CTE (b) densification behaviour (c) binder burn out temperature (d) sintering onset temperature etc. In this technique, the difference in expansion between the sample material and a reference material is measured and hence called as ‘differential dilatometry’ [87]. Experimentally, the change of length between a quartz tube and the sample plus a quartz rod is measured. When the sample expands, the quartz rod is pushed up and the change of length is measured electronically. In order to make a length measurement, a precision-machined micrometer screw is driven downward until contact is made between the probe and push rod and a preset value of resistance is experienced at the contact point. After about 10 seconds, the screw is automatically retracted and the length is registered at the electronic counter.

1.17.1.2 Lattice thermal expansion measurements by high-temperature X-ray diffraction methods

The interatomic separations, which increase with increase in temperature due to the anharmonic component in lattice vibrations, are reflected in the lattice parameter. Hence, by measuring the lattice parameters as a function of temperature, the thermal expansion coefficient of solid materials can be obtained. In this technique, the reflection angles are accurately measured and from these data, the precise lattice parameters are computed. From the variation of lattice parameter with temperature, the coefficient of thermal expansion can be obtained on small powder samples. The presence of other phases does not affect the measurement.

1.18 Development of an alternate method for the digestion of boron carbide for its chemical assay

The physico-chemical properties of ceramics such as boron carbide produced through powder metallurgical route are influenced by the presence of impurities. Hence chemical assay of the raw materials as well as the finished products are very essential.

Chemical assay of boron carbide is important during the manufacture of products made from it for specific applications as these parameters strongly influence its physical as well as chemical properties. Thus it is of interest to develop analytical procedures for precise quantitative determination of boron, carbon and trace metal/non-metal impurities in boron carbide.

In the last two decades several analytical procedures have been developed for the determination of boron and trace elements in boron carbide. In order to carry out the chemical assay of boron carbide, the same has to be brought into solution. For this purpose, various methods of digestion of boron carbide in mineral acids using closed, pressurized vessels have been developed [136]. Heinrich et al. [137] have described the digestion of boron carbide in a mixture of nitric acid, hydrofluoric acid and sulfuric acid at 523 K for 12 h under pressure. Commercially available autoclave systems are being used for the high-pressure digestion of boron carbide in HNO_3 [138].

Presently, the amount of boron in boron carbide samples is estimated by using the sodium carbonate fusion technique [139]. In this method, boron carbide (about 100 mg) is fused with about 5 g of sodium carbonate in a platinum crucible at 1223 K. The resultant fused mass is then dissolved in hydrochloric acid. Boron present in this solution is estimated as borate by titrating it as mannitol-boric acid complex against standard sodium hydroxide solution [140]. The sodium carbonate fusion technique is time-consuming, requires expensive platinum crucibles and involves elaborate experimental system/procedure.

Watanabe has estimated boron in boron carbide by its stepwise pressure alkali/acid decomposition followed by titration of mannitol-boric acid complex [141]. Eventhough this is a relatively low temperature (temperature of digestion ~ 523 K for 16 h at high pressure) digestion method, the process is time-consuming. In addition, solutions obtained through the above mentioned digestion methods have to be necessarily diluted for the determination of trace elements present in it either by inductively coupled plasma optical emission spectrometry (ICP-OES) or by inductively coupled plasma mass spectrometry (ICP-MS) due to interference from sodium matrix. The dilution of the solution for the determination of trace elements either by ICP-MS or by ICP-OES brings down the detection limits to ppm from ppb level.

Zheng Wang et al. [142] have reported a method for the estimation of Al, Ca, Cr, Cu, Fe, Mg, Mn, Na, Ni, Si, Ti, V and Zr in high-purity boron carbide (B_4C) by using "slurry introduction axial viewed ICP-OES". Amberger et al. [138] have determined Ca, Co, Cr, Cu, Fe, Mn, Ni and Ti in boron carbide powders with different particle size distributions by means of "slurry sampling total reflection X-ray fluorescence spectrometry" (TXRF). Kantor et al. [136] have reported a direct optical emission spectrometric method for the determination of trace metals in boron carbide powders by employing direct current arc optical emission spectrometry (DC arc-OES). The head-end step in the determination of trace elements by these analytical methods require elaborate experimental arrangement**s**.

Thus it is of interest to develop a simple and fast method for the digestion of boron carbide for the quantitative determination of boron, carbon and trace metal/non-metal impurities in boron carbide.

1.19 Scope and objective of the work

Commercially boron carbide is synthesized by the carbothermic reduction of boric oxide/boric acid. However the yield of boron carbide is very low and the product is contaminated with significant quantity of 'free-carbon' as the second phase. In spite of these deficiencies, this route is adopted as a commercial method because it is a simple method and employs inexpensive raw materials. Production of boron carbide devoid of ‘free-carbon’ is rather difficult. In the present work, thermodynamic analysis of the carbothermic reduction of boric oxide to synthesize boron carbide was carried out using FactSage 6.2 to optimize the process parameters such as reduction temperature and boric oxide to carbon ratio to get boron carbide devoid of free-carbon.

High-density boron carbide pellets containing boron enriched in ^{10}B ($^{10}B \geq 65$ at%) will be used as the control rod material (neuron absorber) for the PFBR. Carbothermic reduction of boric oxide/boric acid is an energy inefficient process as it requires very high temperatures. In this process, a significant quantity of precious enriched boron is lost during the reduction and subsequent process steps. Carbothermic reduction of boric acid/boric oxide is not a suitable method for the synthesis of boron carbide containing enriched boron. In addition, the product obtained in this method is coarse grained and very high temperatures are required to get high-density boron carbide pellets. Hence, a relatively low-temperature method of synthesis of B_4C by carbothermal reduction was developed by improving the dispersion of B_2O_3 and carbon. Pyrolysis of a precursor that is made up of boron source (such as boric acid, boric oxide etc) and carbon source (such as a polyol, citric acid etc.) to yield a homogeneous mixture of boric oxide and carbon is an attractive low-temperature method of synthesis of B_4C. In the present work, energy efficient, relatively low temperature methods were developed for the synthesis of boron carbide from various gel precursors viz., boric acid-sucrose, boric acid-citric acid, boric oxide-sucrose and boric oxide-citric acid gel precursors.

Accurate values of thermal expansion are useful for various industrial applications of new materials. In this regard, the thermal expansion of nuclear fuels, neutron absorbers, and clad materials is important in determining their performance in the nuclear reactor. Thermal expansion of nanocrystalline boron carbide (prepared in this study) was measured over the temperature range 298 to 1773 K by employing High temperature X-ray diffraction technique and the results were compared with these obtained for microcrystalline boron carbide prepared through conventional carbothermic reduction method.

In order to carry out the chemical assay of boron carbide, the same has to be brought into solution. For this purpose, various methods of digestion of boron carbide in mineral acids using closed, pressurized vessels have been reported in the literature. However, these methods are time consuming and involve elaborate experimental system/procedure. In addition, expensive materials such as platinum crucibles are required for the digestion of boron carbide by the conventional methods. Thus it is of interest to develop an alternate simple procedure for the digestion of boron carbide. In this study, a new technique was developed for the digestion of boron carbide for its chemical assay. This new technique facilitates relatively fast digestion and accurate determination of total boron, its isotopic content of boron and trace elements present in boron carbide.

Experimental

2.0 Introduction

This chapter describes various experimental techniques employed in this study. In addition, information on various chemicals/materials used in this study are provided. The basic principles and procedures of chemical characterization (analysis of boron and carbon), physical characterization of powder samples, including bulk density, specific surface area analysis, Fourier transform infrared spectroscopy, X-ray diffraction analysis, scanning electron microscopic analysis, transmission electron microscopic analysis and particle size distribution are described.

2.1 Chemicals

Analytical grade boric acid (Purity ≥ 99%) procured from M/s. Paramount Chemicals, Chennai and boric oxide (Purity ≥ 99%) from M/s. Seventhilal & Mahasukhalal Co., Mumbai were used in this study. Citric acid (Purity ≥ 99%), sucrose (Purity ≥ 99%) nitric acid (15.6 N), sulphuric acid (36 N), p-nitrophenol and phenolphthalein indicator were obtained from M/s. Hi Pure Fine Chemicals, Chennai. Analytical grade potassium hydroxide, D-mannitol, sodium carbonate and hydrochloric acid were procured from M/s. Rankem Laboratory Chemicals Pvt. Ltd., Chennai. Microcrystalline boron carbide (Purity ≥ 99%) used for thermal expansion studies and digestion experiments was procured from M/s. Boron Carbide India Pvt. Ltd, Mumbai.

Analytical reagent grade nitric acid was further purified by sub-boiling distillation in a quartz apparatus. For the preparation of standard solutions for ICP-MS analyses, relevant specpure-grade metals or chemicals (M/s. Johnson Mattthey, USA) were used.

2.2 Design and fabrication of apparatus used in this study

2.2.1 Graphite boats and cylinders with lids

In order to pyrolyze the gel precursors developed in this study, suitable containers were developed. Since boric oxide reacts with alumina and quartz at temperatures above 800 K, they are not suitable as container materials. Hence, graphite was used as the container material in this study. Graphite boats and graphite cylinder with lids having a central hole of different diameters were used as containers for pyrolyzing the gel precursors. A schematic of graphite boat and cylinder with lids are shown in Figs. 2.1 and 2.2 respectively.

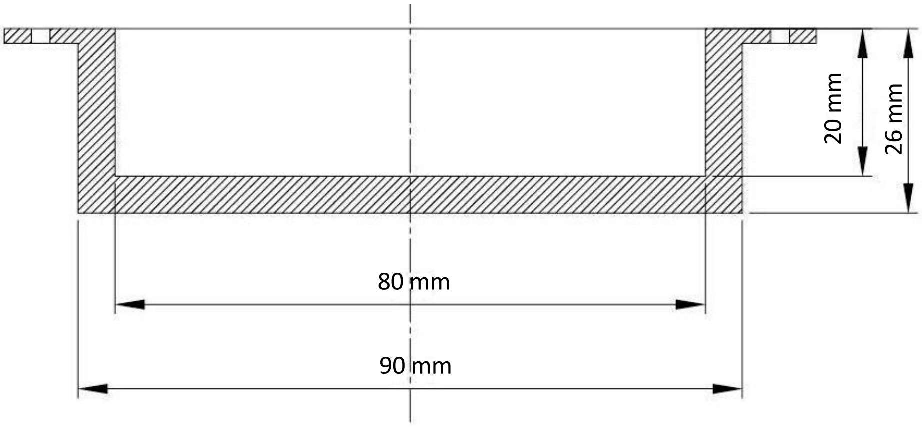

Fig. 2.1 A schematic of the graphite boat

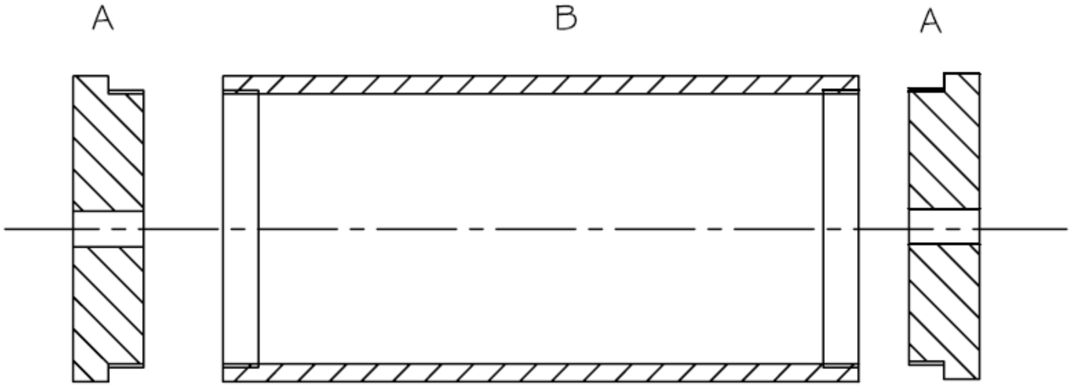

Fig. 2.2 A schematic of the graphite cylinder (B) with lids (A)

These graphite containers (boats and cylinders) were procured from M/s. Purelec Components, Pondicheery. The specifications of high-density graphite used for the fabrication of graphite boats and graphite cylinders with lids are given below.

1. Specific Gravity (g/cc): 1.85

2. Specific Resistance (μΩm): 11.0

3. Young's Modulus (GPa): 10.8

4. Flexural Strength (MPa): 49.0

5. Thermal Conductivity (W/mK): 116

2.2.2 Stainless steel vessel and reactor

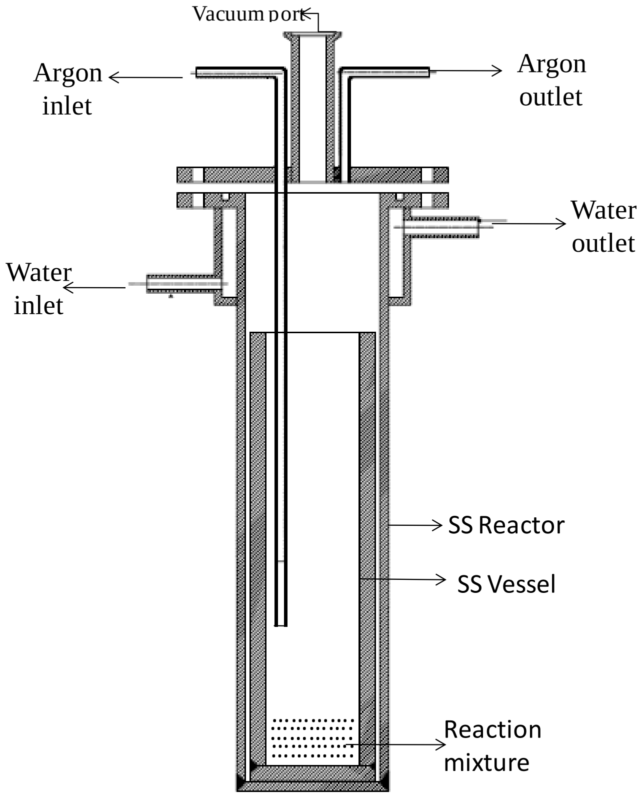

Fig. 2.3 A Schematic of SS vessel and SS reactor.

In order to prepare boron carbide from boric oxide-sucrose and boric oxide-citric acid gel precursors, a stainless steel vessel (seamless stainless steel pipe 316 type) of 65 ID×73 OD×200 mm long was used. The vessel containing the reactant mixture was then placed inside another stainless steel vessel (schedule 40 seamless tube) (stainless steel reactor) as shown in Fig. 2.3. This reactor is provided with an inlet and outlet for argon gas and a port for evacuation.

2.2.3 Quartz vessel for the digestion of boron carbide

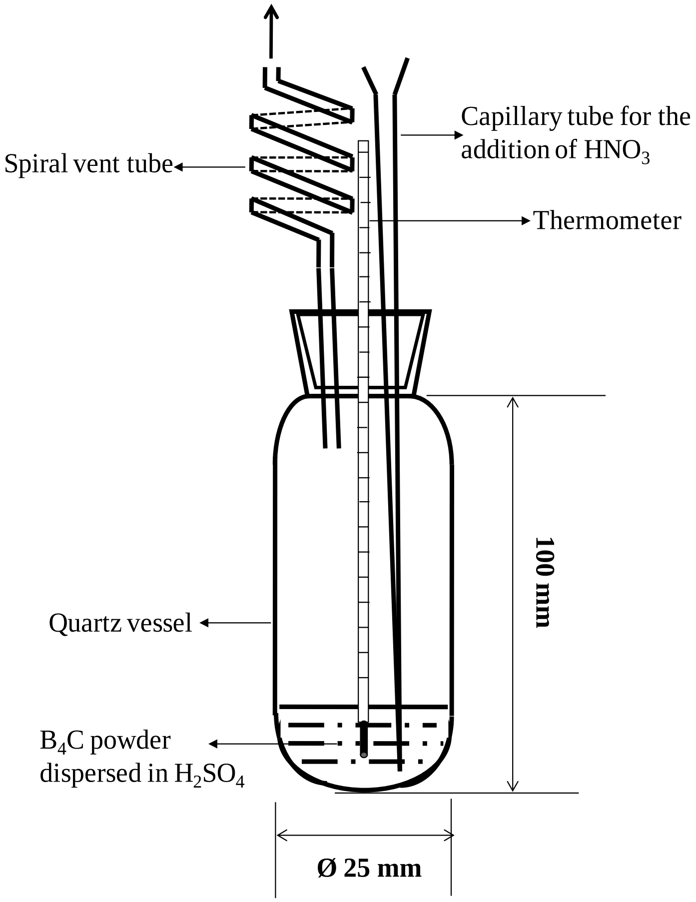

Fig. 2.4 A schematic of quartz vessel with spiral vent tube

A quartz vessel of 50 mL capacity was designed for the digestion of boron carbide. Fig. 2.4 shows a schematic of the quartz vessel. The bottom portion of the vessel is a 50 mL capacity round-bottom tube fitted with a female ground joint. The top portion is fitted with the corresponding male ground joint provided with two tubes. One of the two tubes has a small capillary end to facilitate addition of small amounts of HNO_3. This tube has sufficient length so that the capillary tip is well dipped in H_2SO_4 containing B_4C powder dispersed in it. The second one is a 8 mm (outer diameter) tube in the form of a coil with sufficient length protruding outside the vessel as shown in Fig. 2.4. This tube acts as a vent tube to reduce the sudden surge of pressure that could develop during the addition of HNO_3. It is also used for condensing vapours of nitric acid back into the vessel. In addition, the male ground joint has a provision for inserting a thermometer to measure the temperature of the solution during digestion.

2.3 Characterization techniques used in this study

2.3.1 Chemical characterization of boron carbide

2.3.1.1 Estimation of boron

Principle: In order to determine the total boron in boron carbide, sodium carbonate fusion technique was employed. During the fusion of boron carbide with sodium carbonate, borax is produced which is subsequently converted to boric acid by using excess mineral acid. The excess acid is then neutralized by KOH to a pH of 7 using p-nitrophenol as indicator. Since, boric acid, $B(OH)_3$ is a very weak monobasic acid and acts exclusively by hydroxyl ion acceptance rather than proton donation [143], its acidity is considerably enhanced by chelation with polyhydric alcohols (mannitol, glycerol).

$$B\,(OH)_3 + 2\,H_2O \leftrightarrow H_3O^+ + B\,(OH)_4^- \qquad pK_a=9.5 \tag{2.1}$$

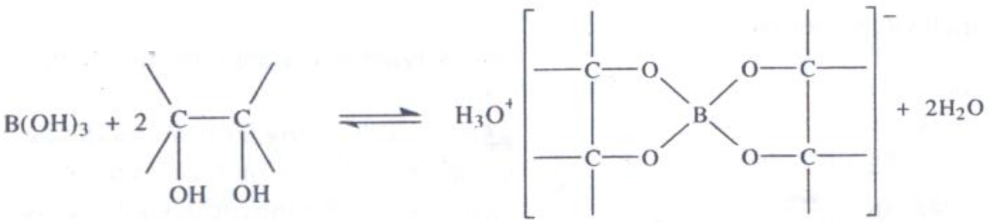

After adding mannitol, pK_a drops to 5.15, indicating an increase in the acid equilibrium constant by a factor of more than 10^4. Mannitol-boric acid complex is estimated by visual alkalimetry to a phenolphthalein end point using standard alkali (NaOH / KOH) [139, 144].

Procedure:

2.5 g of finely ground Na_2CO_3 was pressed into a platinum crucible and a small cavity was made at the centre into which an intimate mixture of 0.5 g of Na_2CO_3 and the pre-weighed boron carbide powder (~100 mg) was added. A further 2.5 g of Na_2CO_3 was spread over the mixture to cover it completely. The mixture was fused at 1223 K for 30 min in a muffle furnace. The melt was cooled and transferred to a Teflon beaker and dissolved in 30 mL of 1:3 HCl and further diluted with water. The contents of the beaker were heated gently to remove any traces of dissolved CO_2. The solution was made up to 100 mL and 20 mL aliquot of this solution was taken for titration. To this solution 5 drops of p-nitrophenol were added and 0.5 N KOH solution was added drop wise till the colourless solution became yellow in colour. Then 2.5 g of mannitol and a drop of phenolphthalein indicator were added and titrated against 0.1 N KOH which was pre standardized using standard potassium hydrogen phthalate solution.

The percentage of the boron was calculated using the following formula.

$$\% B = (A \times [KOH] \times V_{KOH} \times 100) / \text{weight of the sample (mg)} \qquad (2.2)$$

where A is the average gram atomic weight which depends on the isotopic composition of boron. For boron that is 65 at% enriched with ^{10}B, the value of 'A' is 10.37 and for natural boron with 20 at% ^{10}B, it is 10.81, [KOH] is the concentration of KOH, V_{KOH} is the volume of KOH consumed (in mL).

2.3.1.2 Estimation of carbon

The estimation of carbon involves the combustion of carbon present in the sample to CO_2, purification of gases evolved during combustion and detection of carbon dioxide by infrared detector [145]. A known amount of sample in the form of powder and tungsten as accelerator are taken in a ceramic crucible and subjected to combustion by induction heating under a flowing stream of high pure oxygen at temperatures above 1273 K. The gases evolved are passed through several chemical reagents (MnO_2 to trap oxides of nitrogen and sulphur, hot copper oxide to convert trace amounts of CO formed during the combustion to CO_2 and anhydrous magnesium perchlorate to remove water vapour). The purified CO_2 is detected by IR detector at a specific wavelength (2700 or 4300 nm).

The ceramic crucibles used as sample container were fired at 1073 K to avoid any contamination of carbon to the sample and to reduce the blank value. The apparatus was calibrated using NIST calcium carbonate standards for which carbon content is known accurately. A mixture of ~50 mg of sample and 1.5 g of tungsten flux was used for carbon estimation. An average of three estimates is reported as the % carbon by weight in the samples.

2.3.2 Physical Characterization

2.3.2.1 Bulk density of powders

The bulk density of powder is the weight of the powder divided by the volume it occupies, normally expressed as g/mL or kg/L. Bulk density of the powder provides information about the porosity present in the powder. It is influenced by the particle size, water content of the powder sample and temperature of measurement. The following procedure was adopted for the determination of bulk density. A small glass cup was used for bulk density determination. In order to determine the exact volume of the glass cup, it was filled with distilled water and weighed. The volume of the cup was determined from the weight and density of water at room temperature.

In order to determine the density of the sample, it was filled in the glass cup (volume ~10 mL), up to the rim using a spatula without shaking or tapping the glass cup. The excess powder was scraped off until it was flush with the rim of the cylinder. Excess powder was brushed off from the outer edge of the cylinder. The glass cup along with the powder was then weighed. With the known volume of the glass cup and weight of the powder, bulk density of the powder was calculated. The bulk density reported is the average value of 5 determinations.

2.3.2.2 Specific surface area of the powder

The Brunauer–Emmett-Teller (BET) equation [146], given below, is used to compute the amount of adsorbate required to form a monolayer,

$$\frac{1}{X\left[\frac{P^o}{P}-1\right]} = \frac{1}{X_m C} + \left[\frac{(C-1)}{X_m C}\right] \text{x} \ \frac{P}{P^o} \qquad (2.3)$$

where P = partial pressure of the adsorbate, P^o = the saturation equilibrium vapour pressure of the adsorbate at the temperature of the coolant bath, X = weight of the adsorbate at a given relative pressure (P/P^o), X_m = weight of the adsorbate required to cover the surface with one monolayer and C is a constant that is a function of the adsorbate-adsorbent interaction energy.

In the present study, the specific surface area of the powders was measured by using Monosorb MS-16 surface area analyzer supplied by M/s. Quantachrome Inc., USA. The equipment was calibrated with 1 mL of nitrogen gas.

In a typical experiment, 0.5-1 g of the sample was taken in a sample vial, which is essentially a "U" shaped tube made of glass, fitted with a quick disconnect assembly. The sample was heated in a stream of argon gas at 393 K for about 24 h, in order to remove moisture and adsorbed gases from the sample. Subsequently the sample vial was mounted on to the surface area analyzer. During the sample transfer, it was protected from exposure to atmosphere by means of a quick sealing coupling attached to the sample tube. A stream of a mixture of N_2 and He containing 0.3 mole fraction of nitrogen at 1 atmosphere pressure was passed over the sample at a flow rate of 20 sccm. The flow of N_2 and He were controlled by means of a "mass flow controller". The technique uses a thermal conductivity detector to measure the change in concentration of an adsorbate (N_2) /inert carrier gas (He) mixture as adsorption and desorption proceed. When integrated by the on-board electronics and compared to calibration, the detector provides the volume of gas adsorbed or desorbed.

The sample was cooled to the boiling point of liquid nitrogen, by immersing the sample vial, in the Dewar flask containing liquid nitrogen. The sample was then allowed to equilibrate with the gas mixture. The sample being at 77 K, nitrogen in the incoming gas mixture gets adsorbed on to the sample and this process was identified by the adsorption signal. After the completion of the adsorption the Dewar flask containing liquid nitrogen was withdrawn and hot air was blown on to the sample cell in order to desorb the nitrogen gas, which gives the desorption signal. Desorption signal was used to calculate the specific surface area of the sample.

2.3.2.3 Fourier Transform Infrared (FTIR) Spectroscopy

FTIR is used to identify both organic and inorganic substances and can be used for solids, liquids and gases. In addition to identifying unknown compounds, infrared spectroscopy can also determine the amount of an individual compound in a given substrate [147]. FTIR spectroscopic technique provides information on vibrational frequency. A vibration is IR-active if the dipole moment of molecule is changed during the vibration and is Raman-active if the polarizability is changed during the vibration. It is more difficult to obtain rotation and rotation-vibration spectra with high resolution in Raman than in FTIR spectroscopy. Both the techniques are employed for the analysis of amorphous samples when XRD no longer provides any information.

The basic components of an FTIR are shown schematically in Fig. 2.5. The infrared source emits a broad band of different wavelength of infrared radiation. The IR source used in the present study is silicon carbide. The IR radiation goes through an interferometer that modulates the infrared radiation. The modulated IR beam passes through the sample where it is absorbed to various extents at different wavelengths by the various molecules present. Finally the intensity of the IR beam is detected by a detector.

The detector signal is digitized and Fourier transformed by the computer to get the IR spectrum of the sample.

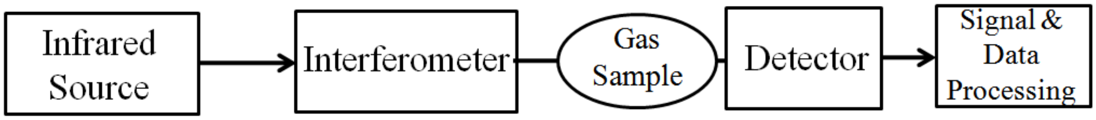

Fig. 2.5 The schematic of components of an FTIR

In the present study, The FTIR spectrum of the samples were acquired with an FTIR spectrometer, supplied by M/s. Bomem, Hartmann and Braun, Canada by using the pressed KBr pellet technique. A typical specimen for recording the IR was prepared by compacting a mixture of the sample and KBr in the weight ratio of 1:100. The spectrum was recorded in the frequency range 4000-500 cm^{-1}.

2.3.2.4 X-Ray Diffraction (XRD)

X-ray diffraction (XRD) technique is a versatile, non-destructive technique that reveals detailed information about the crystallographic structure of materials [148]. The basic components of an XRD instrument are X-ray source, detector and control unit. The X-rays, with a wavelength comparable to that of the lattice spacing, fall on the sample and interacts with the atoms in the lattice causing scattering in all directions. When the sample is crystalline and has a periodic arrangement of atomic planes, the X-rays scattered by each plane constructively interfere and results in interference maxima at particular angles. This happens when the path difference of the scattered X-rays from successive atomic planes forms an integral multiple of the wavelength (λ) of the X-ray. The condition for the formation of diffracted radiation is known as Bragg's law of diffraction and is expressed as

$$n\lambda = 2d \sin\theta \qquad (2.4)$$

Where λ is the wavelength of X-ray used (Cu K_α λ =1.54056 Å), θ is the diffraction angle, n is the order of diffraction and d is the lattice spacing.

In a diffraction pattern, the recorded intensity is usually plotted against the diffraction angle 2θ. Each peak in the diffractogram can be correlated to a plane in the crystal structure. The X-ray diffraction peaks were compared with Joint Commission on Powder Diffraction Software (JCPDS) data of various phases of boron carbide to yield information on overall crystal structure. Scherrer formula [149], given below, was employed for the computation of the average crystallite size,

$$L = 0.94\,\lambda / \{(\beta_e^2 - \beta_i^2)^{1/2} * \cos\theta)\} \qquad (2.5)$$

where L = crystallite size, λ = wave length of the X-ray used,

β_e = Experimental line broadening

β_i = instrumental broadening

θ = Bragg angle

Standard silicon was used for the estimation of the instrumental broadening. The X-ray powder patterns were obtained by using Philips X-pert X-ray diffractometer (Xpert MPD system obtained from Philips, The Netherlands), employing filtered Cu K_α radiation.

2.3.2.5 Measurement of Thermal expansion

2.3.2.5.1 High Temperature X-ray equipment

The high temperature attachment consists of a cylindrical brass chamber at the centre of which the sample is mounted. The cylinder is of double-walled construction and is closed at one end. This end is fixed to a vertical goniometer. The body of the chamber is provided with a long beryllium window for the incidence and emergence of the X-ray beam in the 2θ angular range of 0° to 180°. The powder sample is placed as a thin layer on a flat tantalum strip, which is connected to two electrodes. The sample-carrying strip is subjected to electrical resistance heating at programmed rates. For minimizing thermal losses from the sample, the surroundings of the sample are maintained at a high temperature by means of a "U" shaped heater. Cooling water is circulated through the annular space between the chamber walls. The electrodes are also water-cooled. Temperature measurement is carried out by using W-3% Re/ W-23% Re thermocouple spot welded at the back side of the sample carrier strip. The temperature of the sample was controlled within ±1 K by using a PID controller coupled to the sensing thermocouple. The diffraction studies were performed by using Cu Kα radiation in the Bragg-Brentano geometry, at a temperature interval of 100 K upto 1773 K. A heating rate of 1 K/min and a holding time of 1 h at each temperature of measurement were adopted. The specimen stage was flushed with high purity argon before the start of every experimental run and a vacuum level of about 10^{-5} mbar was maintained throughout the experiment. Typical operating conditions for recording XRD were: operating voltage 40 kV, current of 30 Amp for the X-ray tube, scan speed of 0.02 s^{-1} with a counting time of 6 s per step and an angular range (2θ) of 10-60 for the diffractometer.

2.3.2.5.2 Lattice parameter estimation

Boron carbide has a rhombohedral crystal structure (space group $R\bar{3}m$ (No.166)) indexed on hexagonal coordinates. It consists of twelve-atom icosahedral clusters linked by direct covalent bonds and through three-atom intericosahedral chains along the longest diagonal of the rhombohedron. In the hexagonal system, the lattice parameters, *a* and *c*, are related to the d-spacing by the following relation:

$$d_{hkl} = \left[\frac{4}{3a^2} \left(h^2 + hk + k^2 \right) + \frac{l^2}{c^2} \right]^{-\frac{1}{2}} \tag{2.6}$$

Two linear equations were set up by substituting the $d_{(h\ k\ l)}$ and the corresponding (h k l) values in the above equation. The lattice parameters a and c were computed by solving the two linear equations simultaneously. The procedure was repeated with d-spacings pertaining to different temperatures.

The most important advantage of this method is that the experiment can be carried out on small powder samples and the presence of other phases does not affect the measurement.

2.3.2.6 Scanning Electron Microscopy (SEM)

Principle: The development of electron microscope was driven primarily to improve the limited resolution of the optical microscope due to wavelength limit imposed by visible light [150]. The resolving power of a microscope is given by the following relationship

$$\rho = \frac{0.61\lambda}{\mu \sin \alpha} \tag{2.7}$$

where ‘ρ’ is the resolving power of the microscope, λ is the wavelength of the light, μ Sinα is the numerical aperture of the objective lens. ‘μ’ is index of refraction of medium between point source and lens, relative to free space. ‘α’ is half the angle of the cone of light from specimen plane accepted by the objective (half aperture angle in radians). For light microscope λ = 400 nm (for green light) and μ Sin α is limited to 1.6, hence the ‘ρ’ will be 150 nm. On the other hand if electron beam (λ = 0.001nm) is used in place of green light, the resolving power will be of the order of 1nm. Hence, the resolving power of an optical microscope can be increased by using the electron beam as the light source.

In scanning electron microscopy, the surface of the solid is scanned in a raster pattern with a beam of energetic electrons. This process is repeated until a desired area of the surface has been scanned. During this process a variety of signals are produced which are used to derive information such as topography, morphology, composition and crystallographic information.

In the present work, the microstructure analysis was carried out by using scanning electron microscope supplied by M/s. Philips, XL30, The Netherlands. In a typical experiment, samples were compacted into 8 mm diameter and 1 mm thickness pellets. Since samples were electrically non-conducting, they were coated with a gold–palladium alloy by using a sputter coater (M/s. VG Microtech, UK) before the SEM examination. These gold-palladium alloy coated pellets were placed on a graphite tape and was used for the morphological characterization

2.3.2.7 Transmission Electron Microscopy (TEM)

Principle: In transmission electron microscopy a focused beam of electrons is used instead of light to “see through” the specimen [151]. A beam of electrons is transmitted through an ultra thin specimen, interacting with the specimen as it passes through. In transmission electron microscopy one can switch between imaging the sample and viewing its diffraction pattern. This can exclusively be used for the determination of size and nature of the sample (crystalline or amorphous).

Procedure: Due to strong interaction between electrons and matter, the specimens have to be rather thin (< 100 nm) for transmission electron microscopy investigation. Thus, bulk materials have to be thinned to make them electron transparent. The boron carbide powder synthesized in this study was ultra-sonicated in methanol and one drop of the suspension was loaded on to carbon coated grids. This was dried under a lamp for over 8 hours and loaded into the specimen carousel of the JEOL 2000 EX II TEM operated at 200 kV.

2.3.2.8 Particle Size Distribution

Light scattering method was used in this study for the determination of particle size distribution [152]. The particle size analysis was carried out by using Mastersizer particle size analyzer supplied by M/s. Malvern Wocestershire, UK.

In a typical experiment about 1g of the sample powder was dispersed in distilled water using a sampling device. This suspension was circulated through the sample cell by means of a pump which is also an integral part of the equipment. The light that was passed through a suspension of particles in liquid was scattered and received by a detector array. The scattered light was due to the contribution of many particles. The signal was deconvoluted back into a particle size distribution. The de-convolution consisted of known scattering pattern of a number of size classes to deduce the contribution made by each class to the total pattern.

2.3.2.9 Inductively Coupled Plasma Mass Spectrometric analysis

Inductively Coupled Plasma Mass Spectrometry (ICP-MS) is an analytical technique used for elemental determination. It has many advantages over other elemental analysis techniques such as atomic absorption and optical emission spectrometry. Its detection limits for most elements are equal to or better than those obtained by Graphite Furnace Atomic Absorption Spectroscopy (GFAAS). It is possible to handle both simple and complex matrices with minimum matrix interferences due to the high-temperature of the ICP source. In addition, the ability to obtain isotopic information from ICP-MS makes it a superior technique than compared to other techniques.

In this technique, the sample is typically introduced into the ICP plasma as aerosols either by aspirating a liquid or dissolved solid sample into a nebulizer or using a laser to directly convert solid samples into aerosols. Once the sample aerosol is introduced into the ICP torch, it is completely desolvated and the elements in the aerosols are converted first into gaseous atoms and then ionized towards the end of the plasma. After the conversion of elements to ions, they are then brought into the mass spectrometer via the interface cones and are separated by mass to charge ratio.

In the present study, an Elan 250 inductively coupled plasma mass spectrometer supplied by SCIEX (Thornhill Ontario, Canada) was used. The instrumental operating conditions are given in Table 1.

Mass spectrometric measurements were made by peak jumping using the sequential scanning mode. Ion counts were measured and integrated at three points per mass peak. The measurement time was 0.1 s per point on the mass peak. The entire scanning process was repeated ten times for final integration.

Table 2.1 ICP-MS instrumental operating conditions

Coolant argon flow rate	12 $dm^3\ min^{-1}$
Auxiliary argon flow rate	1.4 $dm^3\ min^{-1}$
Injector argon flow rate	0.4 $dm^3\ min^{-1}$
Nebulizer pressure	38 psi (6892 Pa)
Sampling depth	23 mm
Resolution	
Low	1±0.1 amu
High	0.6+0.05 amu

Gallium was used as the internal standard for Al, Ni, Co and Fe, while rhodium was used for Mo, Cd and Pb. Generally the measurements were carried out in the low resolution mode (peak width at 10% of peak height is 1±0.1 amu), but for Mg, Fe and Al high-resolution mode (peak width at 10% of peak height is 0.6 ±0.05 amu) was employed.

ArC^+ is known to interfere spectrally in the determination of ^{52}Cr. Hence for the determination of Cr, only the isotope (^{53}Cr) free from such spectral interferences was employed for the analysis. Similarly ArO^+ interferes with ^{56}Fe. Hence ^{57}Fe was the isotope considered for the estimation of iron.

Thermodynamic analysis of synthesis of boron carbide through carbothermic reduction of boric oxide

3.0 Introduction

Several methods have been reported in the literature for the preparation of boron carbide [50]. However, on a commercial scale, it is synthesized by the carbothermic reduction of boric oxide. The overall carbothermic reduction of boric oxide is represented by Eq.1.2 (Chapter 1).

This reaction is highly endothermic and becomes thermodynamically feasible only at high temperatures where the entropy contribution is overwhelming and positive [64]. Synthesis of single phase boron carbide devoid of free-carbon as the second phase is rather difficult. This is due to the loss of volatile boron oxide species during the reduction process which alters the composition of the final product. Therefore, the final product contains considerable amount of free-carbon. This free-carbon as a second phase in boron carbide influences the physical and chemical properties. Thus it is of interest to choose appropriate conditions that include C to B_2O_3 mole ratio (CBMR) and temperature of reduction in order to synthesize a product devoid of free-carbon. In order to arrive at the conditions suitable for the carbothermic reduction, apriori, thermodynamic calculations of the system B-O-C pertaining to the carbothermic reduction were carried out. These calculations are useful in evolving the equilibrium compositions in the desired temperature range and allow the prediction of conditions such as temperature, pressure and composition of the system suitable for the synthesis of boron carbide devoid of free-carbon. Dacic et al. [153] have studied the thermodynamics of gas phase carbothermic reduction of boric oxide. In these calculations, they have studied the influence of feed composition, temperature and “gas phase dilution” on the product composition. However, these authors have not considered the presence of BO_2, B and B_2O in the equilibrium mixture.

In this work, detailed thermodynamic calculations have been carried out by using FactSage 6.2 in order to establish the phase equilibrium in the system B-O-C, choose the appropriate CBMR required to synthesize boron carbide devoid of free-carbon. A stability diagram pertaining to the system B-O-C has also been constructed in the temperature range 273-3073 K. Further, the effect of moisture present in the argon carrier gas on the yield of boron carbide has also been examined.

3.1 FactSage

Phase equilibrium calculations on the ternary system B-O-C have been carried out using FactSage thermochemical software and database. FactSage was introduced in 2001 and is a fusion of the FACT-Win/F*A*C*T and ChemSage/SOLGAMIX thermochemical packages, which were developed over 25 years ago [154]. The FactSage package consists of a series of information, database and calculation modules, which enable access to pure substances and solution databases. With the various modules, a wide variety of thermochemical calculations can be performed and tables, graphs and figures of interest to chemical and physical metallurgists, chemical engineers, inorganic chemists, geochemists, ceramists, electrochemists and environmentalists could be generated [154].

One can interact with the software and the databases in a variety of ways and calculate thermochemical equilibria in various forms. They consist of a Reaction module, Predom module, EpH module, Equilib module, Phase diagram and Figure modules.

The Reaction module calculates changes in extensive thermochemical properties (enthalpy, Gibbs energy, entropy etc.) for a single species, a mixture of species or for a chemical reaction. The species may be pure element, stoichiometric compound or ion (both plasma and aqueous ions).

With the Predom module, isothermal predominance area diagrams for one-, two-or three–metal systems can be calculated and plotted using data retrieved from the compound databases.

The EpH module is similar to the predom module and permits the generation of E_h vs. pH (Pourbaix) diagrams for one-, two- or three-metal systems using data retrieved from the compound databases, which also include data on infinitely dilute aqueous solutions.

The Equilib module is the Gibbs energy minimization workhorse of FactSage. It calculates the concentration of chemical species when specified elements or compounds react or partially react to reach a state of chemical equilibrium.

The phase diagram and figure modules is a generalized module which permits the calculation and plotting of unary, binary and ternary phase diagram sections, whereby the axes can be various combinations of temperature, pressure, volume, composition, activity, chemical potential etc. The resulting phase diagram is automatically plotted by the Figure module.

3.2 Computational procedure

The composition of the equilibrium phases during the carbothermic reduction of boric oxide was calculated by using the Equilib module of FactSage 6.2. The relative quantities of the constituents at equilibrium pertaining to mixtures with different CBMR were examined at different temperatures and at 0.98 bar pressure. The constituents, whose concentrations (number of moles / partial pressure) at equilibrium were less than 10^{-15}, were considered to be insignificant and hence these species were not included in the results presented. In the present calculations, the presence of 14 species enlisted in Table 3.1 were assumed.

Table 3.1 List of species considered for the calculations

species	Constituents
Condensed solid species	B_2O_3, C, B_4C, B
Condensed liquid species	B_2O_3, B_4C, B
Gaseous species	B_2O_3, B_2O_2, BO, B_2O, BO_2, CO, B

The relative amounts of the constituents of the system B-O-C depend on the CBMR. For more than 150 different values of CBMR (0.5-1.75), at 0.98 bar pressure and at the temperature in the range of 273 to 3573 K, the amount of different species in equilibrium were calculated. This procedure enabled the determination of boundaries between stable phase regions at equilibrium.

In general the carbothermic reduction of boric oxide is carried out under flowing argon carrier gas. This carrier gas might contain impurities such as moisture, oxygen, carbon dioxide etc. In order to study the effect of moisture present in the carrier gas on the yield of boron carbide and to arrive at a permissible level of moisture in the carrier gas, the thermodynamic equilibrium calculations were carried out for the mixture of C and B_2O_3 whose CBMR is 3.3.

3.3 Results and discussion

3.3.1 Carbothermic reduction of boric oxide

The variation in the equilibrium concentration of the condensed phases and the gaseous constituents in the temperature range 273–3573 K for different CBMR is presented in Figs. 3.1a-3.1j. Figs. 3.1a, 3.1c, 3.1e, 3.1g and 3.1i show the dependence of the concentration of the condensed constituents of the system B-O-C at equilibrium on the values of CBMR 3.5, 1.75, 1, 0.7 and 0.5 respectively at different temperatures. In these figures, the index aa^1 denote the melting transition of $B_2O_{3(s)}$, bb^1 represents the onset temperature of the carbothermic reduction of boric oxide, gg^1 shows the phase transition of $B_4C_{(s)}$ to $B_4C_{(l)}$ and ii^1 corresponds to the decomposition of $B_4C_{(l)}$ into its constituent elements (Eq. 3.1).

$$B_4C_{(l)} \rightarrow B_{(l)} + C_{(s)} \tag{3.1}$$

All these transitions and their indices are listed in Table 3.2. In Figs. 3.1c, 3.1e, 3.1g and 3.1i, dd^1 represents the conversion of $B_2O_{3\ (l)}$ to other oxides of boron (the plausible reactions are shown in Table 3.3). From Figs.3.1a, 3.1c, 3.1e, 3.1g and 3.1i, it is clear that upto 1830 K, boron carbide is not among the condensed phases under the conditions of CBMR and temperatures shown in these figures. $B_2O_{3(l)}$ and $C_{(s)}$ are the only stable condensed phases upto 1830 K. This indicates that under thermodynamic equilibrium conditions, the carbothermic reduction of $B_2O_{3(s)}$ is feasible only at temperatures above 1830 K. From Fig. 3.1a, it is evident that $B_4C_{(s)}$ is thermodynamically stable up to 2743 K. In the temperature range 2773-3002 K, $B_4C_{(l)}$ is the sole boron containing condensed phase. Above 3002 K, $B_4C_{(l)}$ decomposes into $B_{(l)}$ and $C_{(s)}$ (Eq. 3.1).

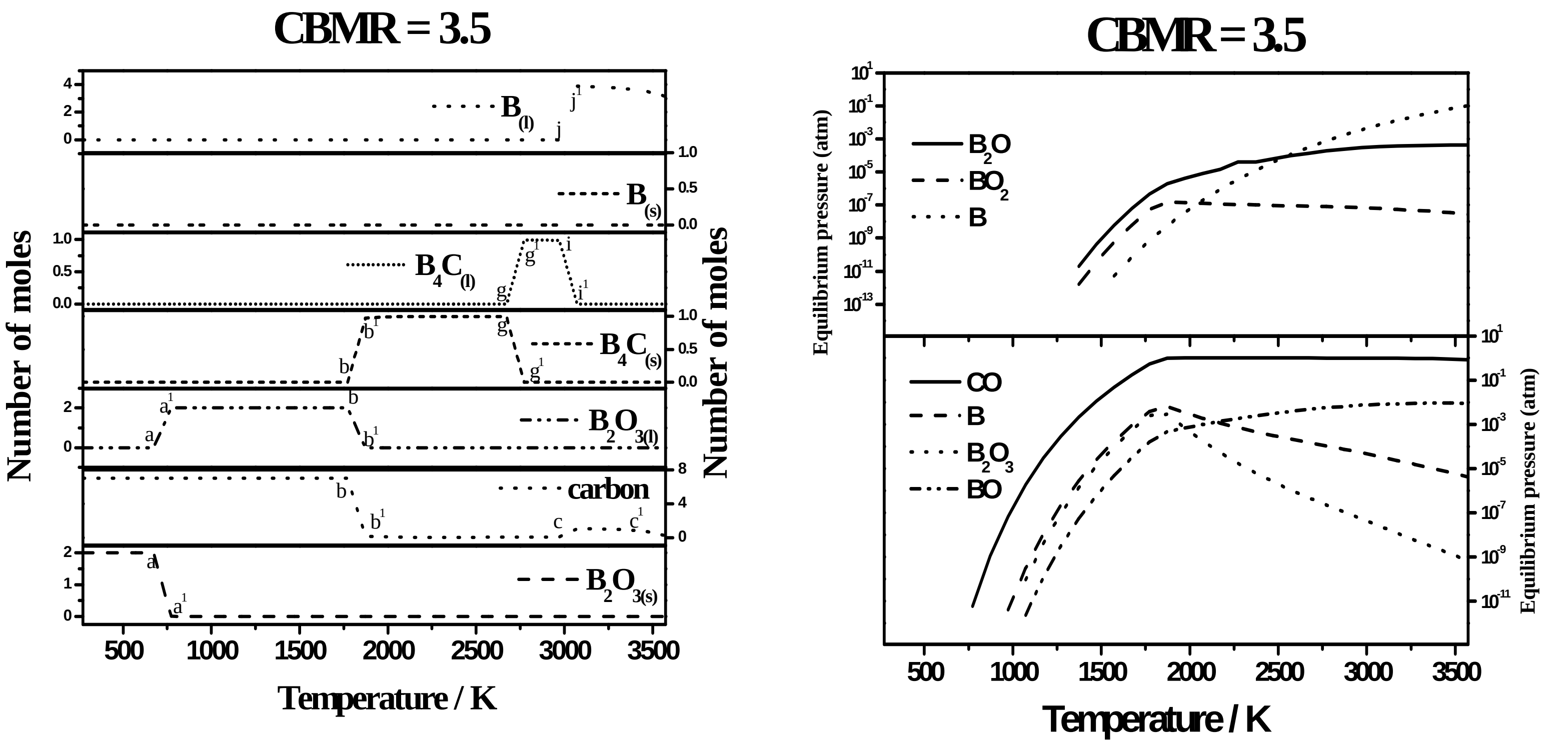

(a)

(b)

Fig. 3.1a & 3.1b: The equilibrium composition of condensed species and gaseous species over the temperature range 273–3573 K for CBMR of 3.5

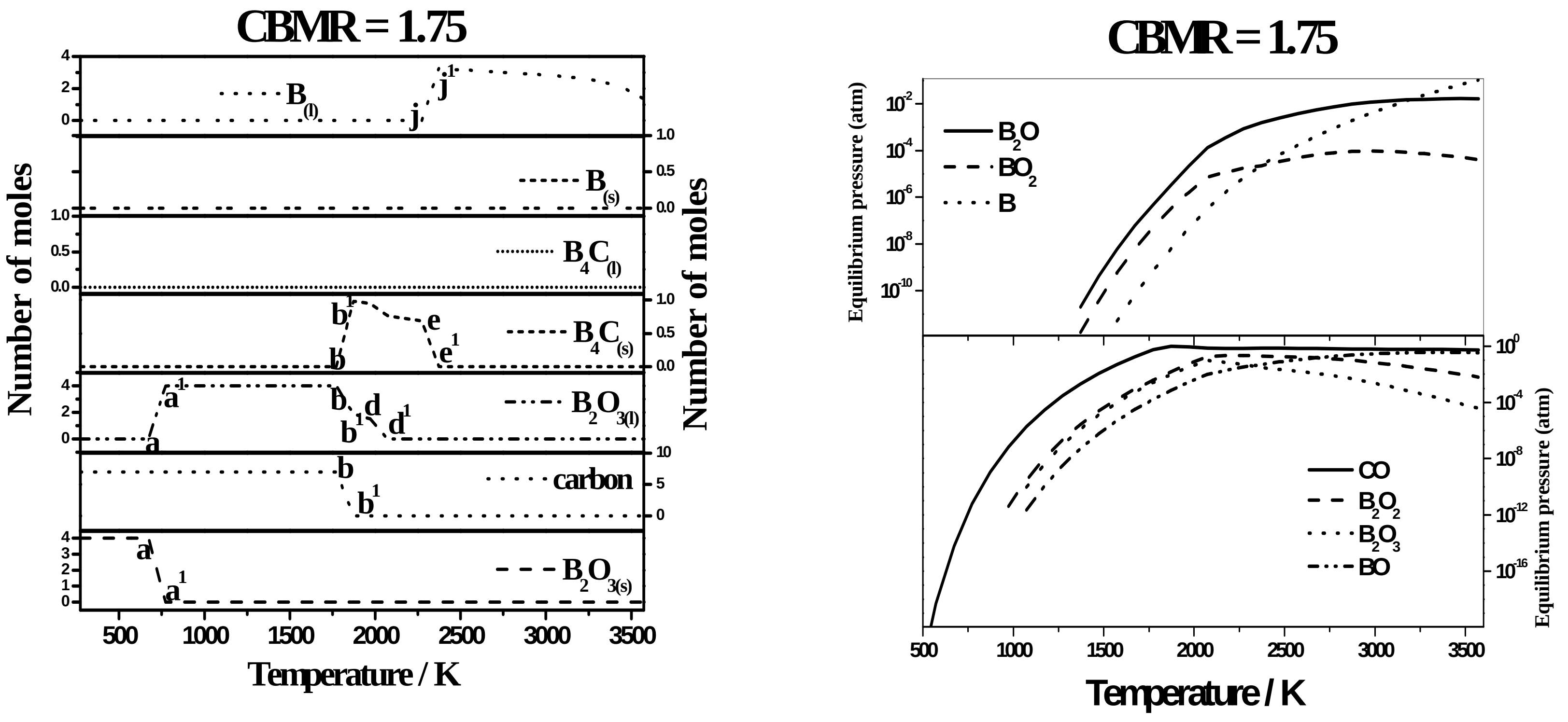

(c) (d)

Fig. 3.1c &3.1d: The equilibrium composition of condensed species and gaseous species over the temperature range 273–3573 K for CBMR of 1.75

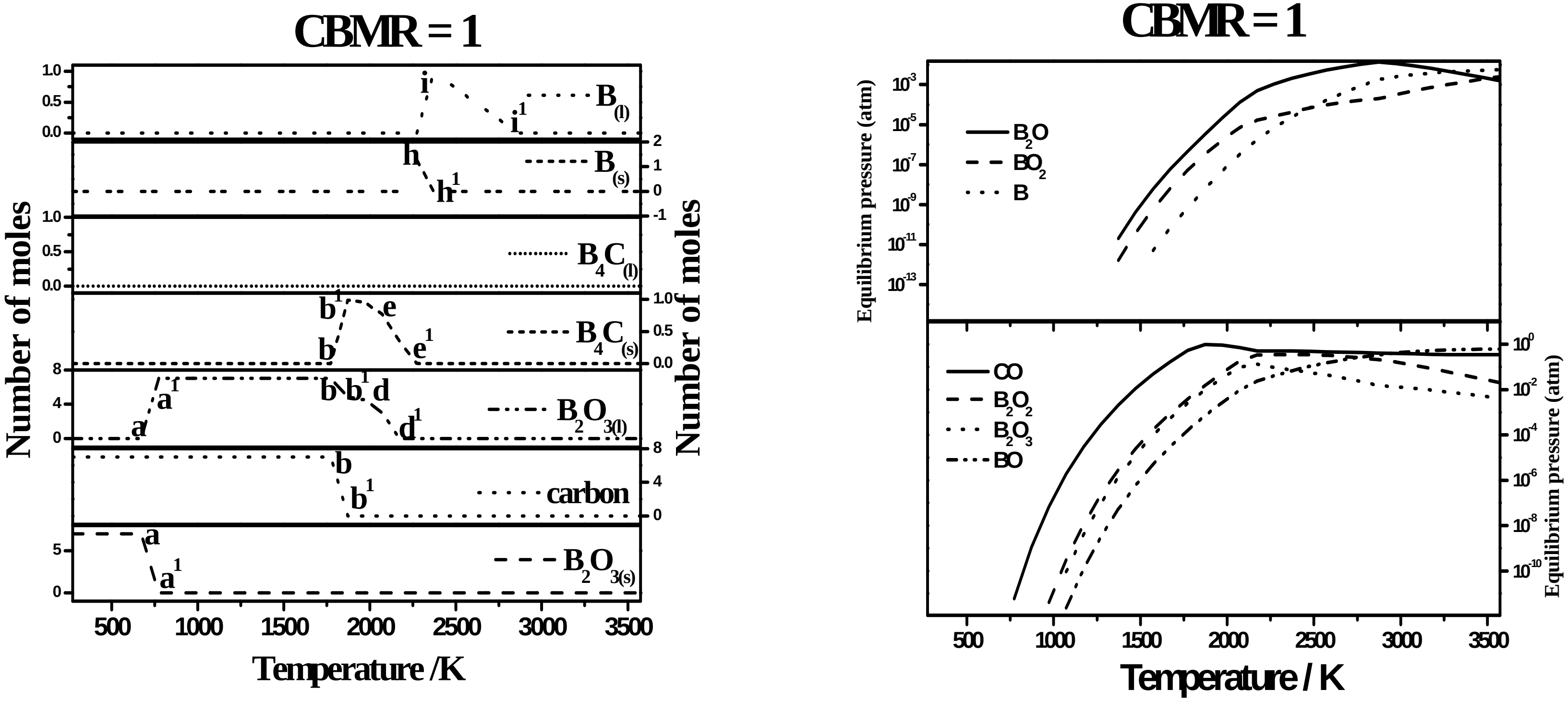

(e) (f)

Fig. 3.1e &3.1f: The equilibrium composition of condensed species and gaseous species over the temperature range 273–3573 K for CBMR of 1

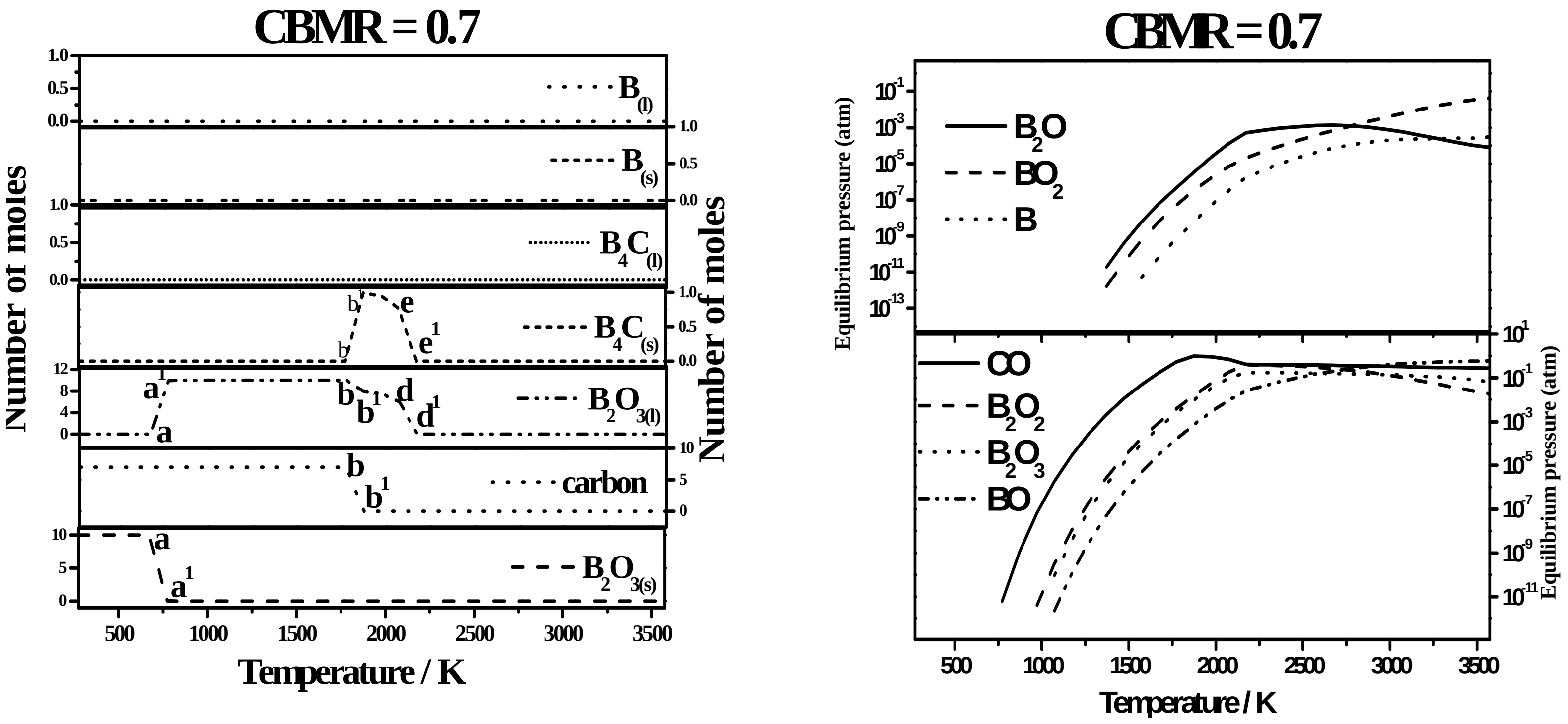

(g)

(h)

Fig. 3.1g &3.1h: The equilibrium composition of condensed species and gaseous species over the temperature range 273–3573 K for CBMR of 0.7

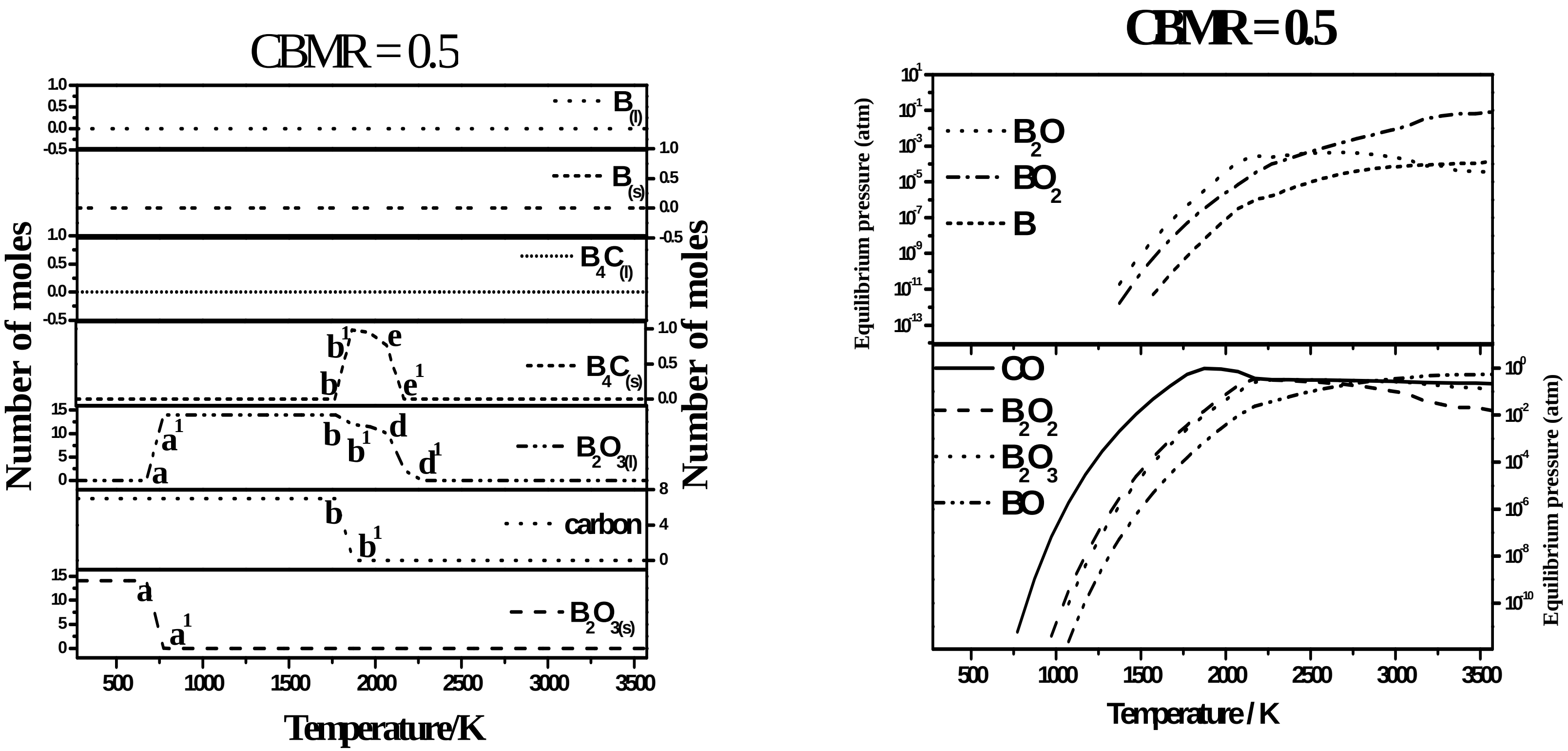

(i) (j)

Fig. 3.1i & 3.1j: The equilibrium composition of condensed species and gaseous species over the temperature range 273–3573 K for CBMR of 0.5

Table 3.2 Phase transitions observed during the carbothermic reduction

S.No	Notation	Phase change
1	aa[1]	Melting point of boric oxide
2	bb[1]	Onset temperature for the reaction or formation of boron carbide as per Eq. 1.2
3	cc[1]	Precipitation of carbon
4	dd[1]	Conversion of $B_2O_{3(l)}$ to gaseous boron oxides
5	ee1	Reaction between boric oxide and C
6	ff[1]	Reaction B_4C with boron oxides
7	gg[1]	Melting point of boron carbide
8	ii[1]	Melting point of $B_{(s)}$
9	jj[1]	Decomposition of B_4C to elemental boron

When the CBMR is ≥ 3.38, the final products of the carbothermic reduction carried out in the temperature range 1830-2743 K would contain both boron carbide and free-carbon phases. This free-carbon results due to the distribution of B among the following species; $B_2O_{3(g)}$, $B_2O_{2(g)}$, $BO_{2(g)}$, $B_2O_{(g)}$ and $B_{(g)}$ and their losses due to volatilization during the reduction process. From Figs. 1a, 1c, 1e, 1g and 1i, it is also observed that with decrease in the value of CBMR the temperature span over which $B_4C_{(s)}$ is the stable phase narrows down. This may either be due to the reaction of boric oxide with boron carbide to form other sub oxides of boron viz., BO_2, B_2O_2, BO or due to the decomposition of B_4C into its constituents or both. Reactions involving boron carbide and the oxides of boron and the inter conversions among the latter are shown in Table 3.3.

Figs. 3.1b, 3.1d, 3.1f, 3.1h and 3.1j depict the variation of the vapour pressures of the gaseous species formed during the carbothermic reduction of $B_2O_{3(s)}$ for CBMRs 3.5, 1.75, 1, 0.7 and 0.5 respectively, with temperature. The equilibrium concentration of these gaseous species would depend upon their relative stabilities. Upto about 1800 K, $B_2O_{3(g)}$ is the predominant species in the gas phase. However, its vapour pressure decreases beyond this temperature. This decrease may either be due to the decomposition of $B_2O_{3(g)}$ into

Table 3.3 Possible reactions of boron carbide with the oxides of boron and inter conversion among the oxides of boron

Equilibria	Description
A. Reactions involving the oxidation of B_4C	$B_4C_{(s)} +5\ B_2O_{3(l)} \rightarrow 7\ B_2O_{2(g)} + 5CO_{(g)}$
	$B_4C_{(s)} +5\ B_2O_{3(g)} \rightarrow 7\ B_2O_{2(g)} + 5\ CO_{(g)}$
	$B_4C_{(s)} +5\ B_2O_{3(l)} \rightarrow 14\ BO_{(g)} + CO_{(g)}$
	$B_4C_{(s)} + 5\ B_2O_{3(g)} \rightarrow 14\ BO_{(g)} + CO_{(g)}$
	$B_4C_{(s)} + B_2O_{3(l)} + 5O_2 \rightarrow 6\ BO_{2(g)} + CO_{(g)}$
	$B_4C_{(s)} + B_2O_{3(g)} + 5O_2 \rightarrow 6\ BO_{2(g)} + CO_{(g)}$
	$B_4C_{(s)} +1.5\ B_2O_{3(l)} \rightarrow 3.5\ B_2O_{(g)} + CO_{(g)}$
	$B_4C_{(s)} +1.5\ B_2O_{3(g)} \rightarrow 3.5\ B_2O_{(g)} + CO_{(g)}$
	$3B_4C_{(s)} + B_2O_{3(l)} \rightarrow 14\ B_{(g)} + 3\ CO_{(g)}$
	$B_4C_{(s)} + B_2O_{3(g)} \rightarrow 14\ B_{(g)} + CO_{(g)}$
	$B_4C_{(s)} +5\ B_2O_{3(l)} \rightarrow 14\ BO_{(g)} + CO_{(g)}$
	$B_4C_{(s)} +5\ B_2O_{3(g)} \rightarrow 14BO_{(g)} + CO_{(g)}$
	$B_4C_{(s)} +0.5\ B_2O_{2(g)} \rightarrow 5\ B_{(s)} + CO_{(g)}$
	$B_4C_{(s)} + BO_{(g)} \rightarrow 5\ B_{(s)} + CO_{(g)}$
	$B_4C_{(s)} + B_2O_{(g)} \rightarrow 6\ B_{(s)} + CO_{(g)}$
	$B_4C_{(s)} + 0.5\ BO_{2(g)} \rightarrow 4.5\ B_{(s)} + CO_{(g)}$
B. Reduction of the oxides of boron by carbon	$B_2O_{3(l)} + C_{(s)} \rightarrow B_2O_{2(g)} + CO_{(g)}$
	$B_2O_{3(g)} + C_{(s)} \rightarrow B_2O_{2(g)} + CO_{(g)}$
	$B_2O_{3(l)} + C_{(s)} \rightarrow 2\ BO_{(g)} + CO_{(g)}$
	$B_2O_{3(g)} + C_{(s)} \rightarrow 2\ BO_{(g)} + CO_{(g)}$
	$B_2O_{3(l)} + 3C_{(s)} \rightarrow 2\ B_{(g)} + 3CO_{(g)}$
	$B_2O_{3(g)} + 3C_{(s)} \rightarrow 2\ B_{(g)} + 3CO_{(g)}$
	$B_2O_{3(l)} + 2C_{(s)} \rightarrow B_2O_{(g)} + 2CO_{(g)}$
	$B_2O_{3(g)} + 2C_{(s)} \rightarrow B_2O_{(g)} + 2CO_{(g)}$
	$2\ B_2O_{3(l)} + 4C_{(s)} + 3\ O_{2(g)} \rightarrow 4BO_{2(g)} +4\ CO_{(g)}$
	$B_2O_{3(g)} + 2C_{(s)} + O_{2(g)} \rightarrow 2BO_{2(g)} + CO_{(g)}$

C. Gas phase equilibria involving the oxides of boron.	$B_2O_{2(g)} \rightarrow 2BO_{(g)}$
	$2\ B_2O_{2(g)} \rightarrow 2\ B_2O_{(g)} + O_{2(g)}$
	$B_2O_{2(g)} + O_{2(g)} \rightarrow 2\ BO_{2(g)}$
	$B_2O_{2(g)} \rightarrow 2\ B_{(g)} + O_{2(g)}$
	$2\ B_2O_{2(g)} + O_{2(g)} \rightarrow 2\ B_2O_{3(g)}$
	$2\ BO_{2(g)} \rightarrow B_2O_{(g)} + O_{2(g)}$
	$2\ BO_{2(g)} \rightarrow B_2O_{3(g)} + 0.5\ O_{2(g)}$
	$BO_{2(g)} \rightarrow BO_{(g)} + 0.5\ O_{2\ (g)}$
	$2\ BO_{2(g)} \rightarrow B_2O_{(g)} + 2\ O_{2(g)}$
	$BO_{2(g)} \rightarrow B_{(g)} + O_{2(g)}$
	$B_2O_{(g)} \rightarrow B_{(g)} + O_{2(g)}$
	$B_2O_{(g)} + O_{2(g)} \rightarrow B_2O_{3(g)}$
	$B_2O_{(g)} + 0.5\ O_{2(g)} \rightarrow B_2O_{2(g)}$
	$B_2O_{(g)} + 1.5\ O_{2(g)} \rightarrow 2BO_{2(g)}$
	$B_2O_{(g)} + 0.5\ O_{2(g)} \rightarrow 2BO_{(g)}$
	$2\ B_{(g)} + 1.5O_{2(g)} \rightarrow B_2O_{3(g)}$
	$2\ B_{(g)} + O_{2(g)} \rightarrow B_2O_{2(g)}$
	$2\ B_{(g)} + 0.5O_{2(g)} \rightarrow B_2O_{(g)}$
	$B_{(g)} + O_{2(g)} \rightarrow BO_{2(g)}$
	$B_{(g)} + 0.5\ O_{2(g)} \rightarrow BO_{(g)}$
	$2\ BO_{(g)} + 0.5\ O_{2(g)} \rightarrow B_2O_{3(g)}$
	$2\ BO_{(g)} \rightarrow B_2O_{2(g)}$
	$BO_{(g)} \rightarrow B_{(g)} + 0.5\ O_{2(g)}$
	$2\ BO_{(g)} \rightarrow B_2O_{(g)} + 0.5\ O_{2(g)}$
	$BO_{(g)} + 0.5\ O_{2(g)} \rightarrow BO_{2(g)}$

other oxides or due to its reaction with B_4C. A scheme showing the decomposition reactions of B_2O_3 are shown in Table 3.3. With an increase in the value of CBMR, it is observed from the results of this computation that over the entire temperature range the vapour pressure of carbon monoxide far exceeds those of the oxides of boron and the former becomes almost constant above 1830 K as could be seen from the plateau regions in Figs. 1b, 1d, 1f, 1h and 1j. The plateau region for $p_{CO(g)}$ corresponds to the carbothermic reduction of oxides of boron that lead to the formation of $CO_{(g)}$ as shown in Table 3.3. The plateau regions for p_{BO} and p_{BO2} gaseous species can be seen from the Figs 3.1b, 3.1d, 3.1f, 3.1h and 3.1j. These plateau regions are due to the relative stabilities of these species at a given temperature.

Fig. 3.2 shows the stability boundaries for various phases that are in equilibrium in terms of CBMR and temperature at 0.98 bar pressure. It is seen that the lowest temperature required for the carbothermic reduction of boric oxide to boron carbide is 1830 K. Under thermodynamic equilibrium conditions, boron carbide cannot be synthesized by the carbothermic reduction of boric oxide when CBMR is less than 0.69 and the temperature is above 2137 K. At temperatures below 2137 K, boron carbide coexists along with $B_2O_{3(l)}$ (as condensed phase) depending on the value of CBMR. As the temperature decreases from 2173 K, the value of CBMR must be increased so that $B_4C_{(s)}$ is in thermodynamic equilibrium with $B_2O_{3(l)}$ (represented as Region X in Fig. 3.2). $B_4C_{(s)}$ exists as a single phase over the values of CBMR and temperature represented by ‘Region Y’ in Fig. 3.2. It is seen that the temperature range over which the single phase $B_4C_{(s)}$ is stable, increases with increasing CBMR values. However, at relatively lower CBMR values (~0.69-1.75) and at temperatures in the range of 2137-2350 K elemental $B_{(s)}$ coexists along with $B_4C_{(s)}$ (Region Z in Fig. 3.2). At much higher values of CBMR (~1.25-3.38) and temperatures (>2350 K), $B_{(l)}$ coexists along with $B_4C_{(s)}$. The stability region over which $B_4C_{(s)}$ is the only stable condensed phase spans between the CBMR values of 0.69 and 3.38 and at temperatures above 1830 K.

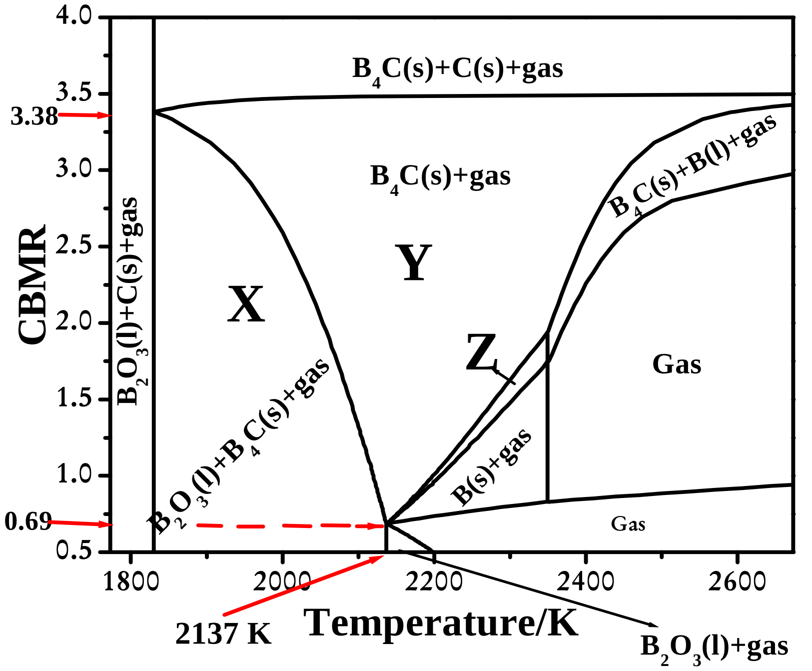

Fig. 3. 2 Stability diagram of B-O-C system at 0.98 bar pressure

Fig. 3.3 shows the stability boundaries for various phases that are in equilibrium in terms of CBMR and temperature at 0.098 bar pressure. From this figure it is seen that by the removal of gaseous species from the reaction mixture, the stability regions in the system B-O-C are shifted towards lower temperatures. Hence carbon-free boron carbide can be prepared by the carbothermic reduction of boric oxide at temperatures above 1623 K when the system pressure is 0.098 bar and CBMR values are in the range of 0.69-3.38.

Several authors have carried out experimental investigations on the carbothermic reduction of boric oxide (Table 3.4) [69, 155]. Jung et al. [155] have synthesized boron carbide by a modified carbothermic reduction of boric oxide. They have used a mixture of

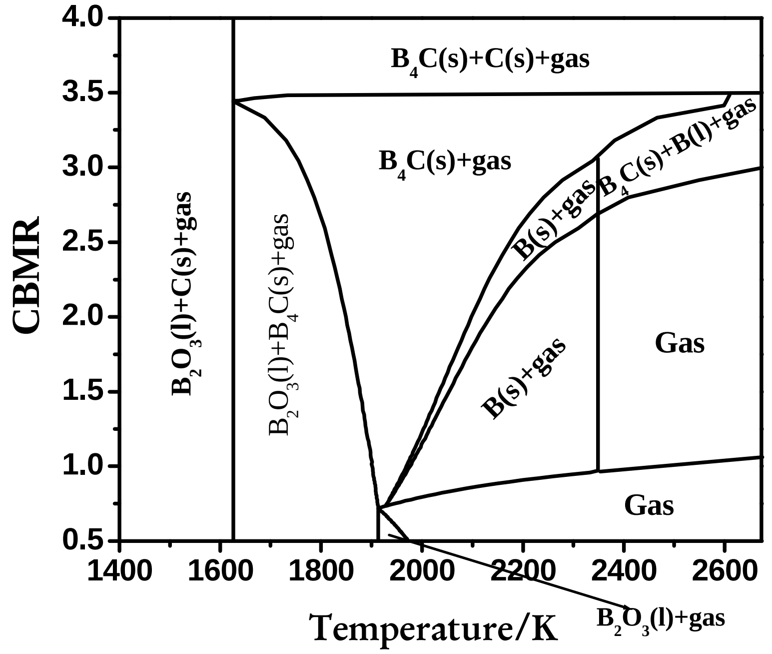

Fig. 3.3 Stability diagram of B-O-C system at 0.098 bar pressure

boric oxide and carbon with a value of CBMR less than that required for the stoichiometric equation (Eq. 1.2) (3.5). These results are consistent with the present calculations. However, Alizadeh et al. [69] have produced boron carbide powder by using boric oxide as the boron source and petroleum coke/“carbon active” as a reducing agent at 1743 K which is lower than the temperature predicted by the present thermodynamic calculations. However, the thermodynamic activity of carbon is higher than unity for the carbon sources (“carbon active”) used for the carbothermic reduction by Alizadeh et al [69]. These authors claimed that the “carbon active” which was with high surface area reacted with B_2O_3 at a relatively lower temperature to produce boron carbide. The optimum CBMRs required to obtain boron carbide free from carbon were reported to be 3.7 and 3.4 for petroleum coke and “carbon active” respectively. Present calculations also show that the stoichiometric value of CBMR (3.5) results in a biphasic mixture of boron carbide and carbon irrespective of the temperature of carbothermic reduction. The presence of free-carbon in boron carbide can be avoided in practice by using a reaction mixture of boric oxide and carbon with CBMR slightly less than 3.5 depending on the carbothermic reduction temperature (Figs. 3.2 and 3.3). The results of the present calculations are in agreement with the experimental results reported in the literature as can be seen from Table 3.4.

3.3.2 Effect of moisture on carbothermic reduction of boric oxide

The influence of moisture content in the flowing inert carrier gas (e.g. argon) on the equilibrium concentration of boron carbide produced during the carbothermic reduction of a mixture of boric oxide and carbon with CBMR=3.3 at various temperatures is depicted in Fig. 3.4. From this figure it is observed that with an increase in the moisture content in the cover gas, the equilibrium concentration of boron carbide decreases. The variation of the equilibrium concentration of various gas species (moisture content in the gas phase is one mole) with temperature is shown in Figs. 3.5a and b. At temperatures below 1273 K, the vapour pressures of hydrogen borates are higher than those of the oxides of boron (for example at 1073 K, p_{HBO2} is 1.83×10^{-5} atm and p_{BO2} is 1.79×10^{-15} atm).

Consequently the loss of boron (due to vapourization of hydrogen borates) is higher when the carrier gas contains significant quantity of moisture than the loss of boron (due to the vapourization of oxides of boron) when the carrier gas is free from moisture. Hence, the reaction mixture becomes deficient in boric oxide, which in turn reduces the yield of boron carbide, when moisture is present as the impurity in the carrier gas.

Table 3.4 Details of experimental studies on carbothermic reduction of boric oxide

S. No	Reactants	Reaction parameters	Remarks	Optimum CBMR for zero free carbon	Reference
1	B_2O_3(s)+C(s)	1800^{0}C, 20–300 min, Ar		<3.5	[155]
2	B_2O_3+Petroleum Coke	1470^{0}C; 100^{0} min^{-1}, 1–5 h, Ar	Stoichiometric composition as per Eq. 1.2 leads to significant residual carbon in the final product (B_4C).	<3.3	[69]
	B_2O_3+"carbon active"	1470^{0}C; 100^{0} min^{-1}, 1–5 h, Ar		<3.7	
3	B_2O_3 + carbon	Above 1830 K	CBMR < 3.5 irrespective of temperature	3.4	Present calculations

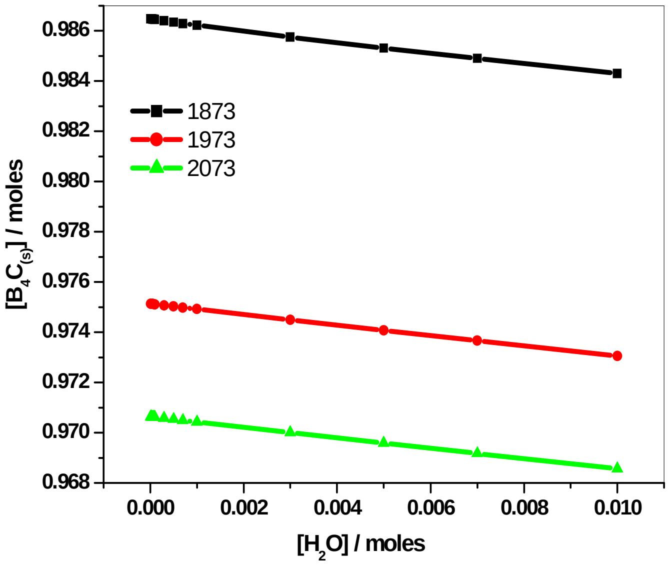

Fig. 3.4 Variation of equilibrium concentration of boron carbide with number of moles of water in the carrier gas (CBMR =3.3 at different temperatures)

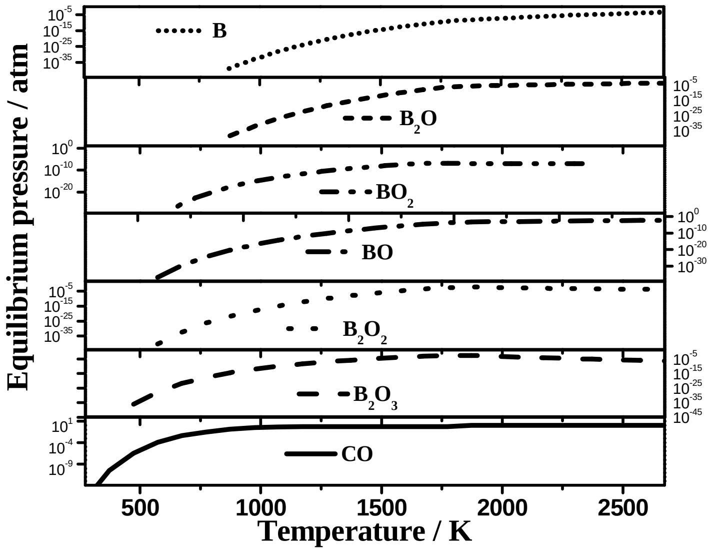

(a)

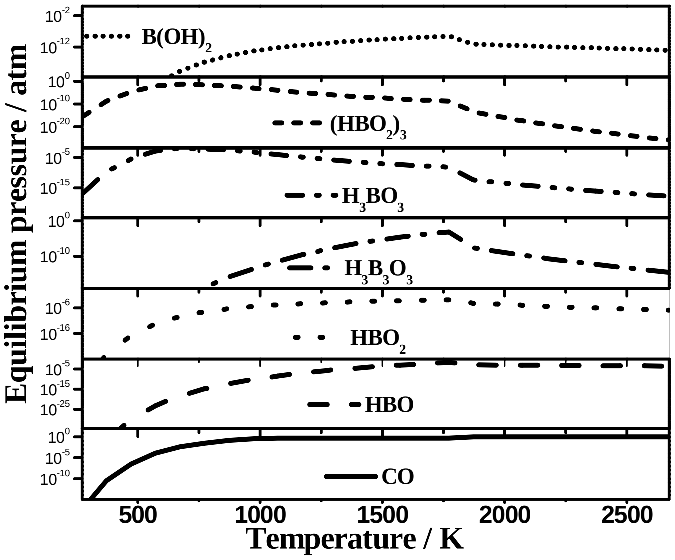

(b)

Fig. 3.5 Variation of equilibrium vapour pressure of the (a) oxides of boron and (b) hydrogen borates with temperature for stoichiometric CBMR =3.3

However, this decrease in equilibrium concentration of boron carbide is relatively insignificant. Hence, commercial grade argon (containing < 10 ppm of moisture) can be used to carry out the carbothermic reduction.

3.4 Conclusions

Thermodynamic equilibrium calculations on the carbothermic reduction of boric oxide have been carried out using FactSage 6.2. The stability boundaries pertaining to B_2O_3 $_{(l)}$, $B_4C_{(s)}$, $B_4C_{(l)}$, $B_{(s)}$, $B_{(l)}$ and $C_{(s)}$ have been evaluated as a function of temperature and CBMR. The results of these calculations identified the most favourable conditions of temperature and CBMR for the synthesis of carbon-free boron carbide through carbothermic reduction of boric oxide.

Synthesis and characterization of nanocrystalline boron carbide from gel precursors

4.0 Introduction

Commercially boron carbide is synthesized by carbothermic reduction of boric oxide/boric acid [156]. However, this method cannot be employed for the synthesis of boron carbide containing isotopically enriched boron since the loss of highly precious and expensive enriched boron in the form of its oxides during the reduction is high which renders this process uneconomical. As an alternative to this high-temperature reaction technique, there is a great interest in the development of gel precursors to produce sinteractive boron carbide powder at relatively lower temperatures [93]. Table 4.1 shows the studies reported in the literature on the synthesis of boron carbide using gel precursors.

In the present study, nonaqueous gel precursors have been developed for the first time for the synthesis of boron carbide.

4.1 Synthesis of boron carbide from boric acid-sucrose xergo gel

4.1.1 Experimental

In a typical experiment, 9 g of sucrose was taken in a combustion bowl and melted using a silicone oil bath at 440 ± 5 K. To this melt, 11.3 g of boric acid was added slowly to obtain a homogeneous gel. Upon heating this gel at 440 ± 5 K, a black-coloured dry xerogel (XSG) was obtained. This product was placed in a high-density graphite boat and pyrolyzed using a kanthal wire-wound resistance furnace (horizontal) under flowing ultra high-pure (UHP) argon (purity 99.993%, oxygen <2 ppm, total impurities <30 ppm) at 1273 K for 2 h. The black mass thus obtained was designated as XSG1000 (Fig. 4.1).

Table 4.1 Summary of studies reported in the literature on the synthesis of boron carbide from gel precursors

S.No	Gel Precursor	Processing Temperature, K	Holding time, h	Atmosphere	Ref.
1	Reaction product of H_3BO_3 and citric acid	1623	2	Vacuum	[98]
2	Reaction product of H_3BO_3 and citric acid	1773	2.5	Vacuum	[99]
3	Reaction product of H_3BO_3 and citric acid	1723	5	Argon	[101]
4	Solution of H_3BO_3, sugar and ethylene glycol	1973	5	H_2	[50]
5	Solution of H_3BO_3 and glycerin	1523	5	Argon	[95]
6	Reaction product of H_3BO_3 and mannitol	1573	0.5-20	Argon	[109]

Fig. 4.1 Photograph of typical XSG1000

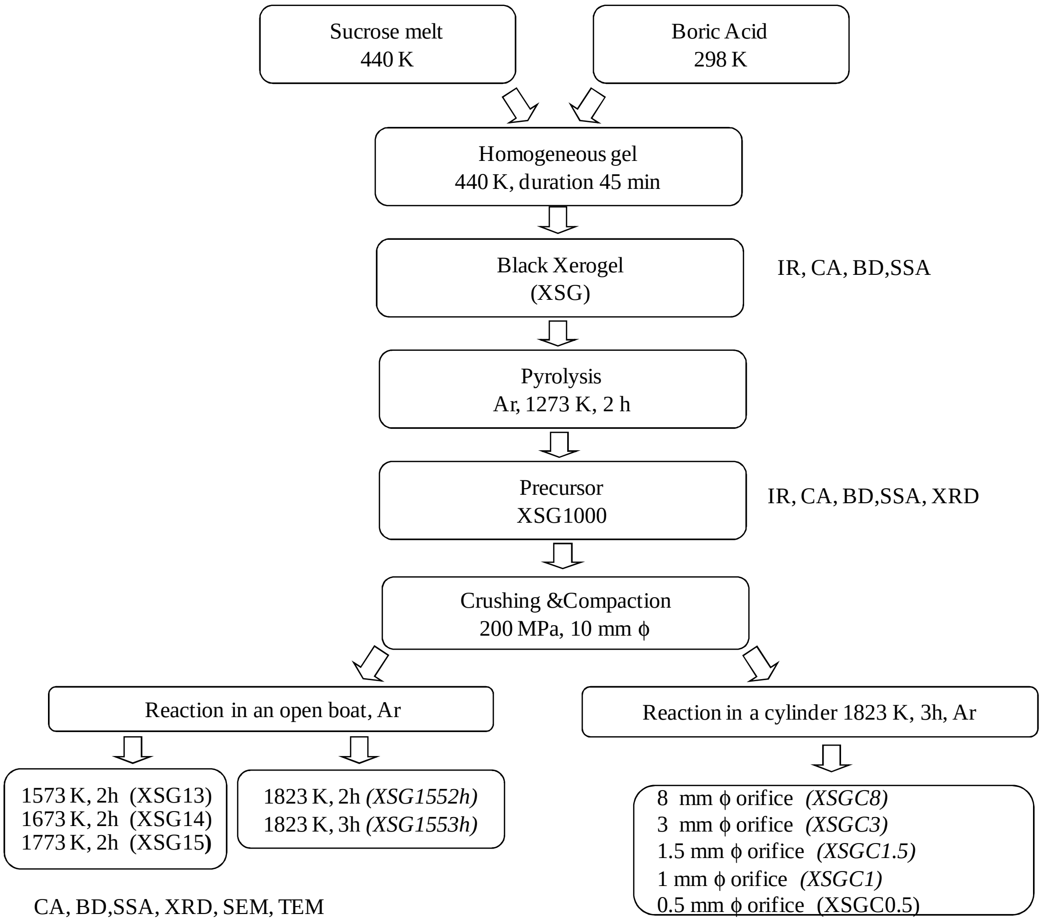

Fig. 4.2 The scheme of preparation of boron carbide from boric acid-sucrose xerogel

This XSG1000 was crushed and compacted into pellets of 16 mm diameter by using a uniaxial hydraulic press. These pellets were placed in a high-density graphite boat (Fig. 2.1) and heated using a molybdenum wire-wound furnace at 1573, 1673 and 1773 K for 2 h (resultant products are designated as XSG13, XSG14 and XSG15 respectively) and at 1823 K for 2 and 3 h (resultant products are designated as XSG1552h and XSG1553h respectively) at a heating rate of 0.15 K s^{-1}. In an another independent experiment, the pellets of XSG1000 were placed in a specially designed high-density graphite cylinder provided with lids on both sides (Fig. 2.2) and heated at 1823 K for 3 h at a heating rate of 0.15 K s^{-1}. Lids having a central hole with different diameters viz., 8, 3, 1.5, 1, and 0.5

mm were used in different experiments and the resultant products were designated as XSGC8, XSGC3, XSGC1.5, XSGC1 and XSGC0.5 respectively. The scheme of the preparation is shown in Fig. 4.2.

The xerogels and the precursors were characterized by using Fourier transform infrared spectroscopy. The constituent phases were identified by using X-ray diffraction while their elemental composition was established with the help of chemical assay. The microstructure of boron carbide synthesized in this study was examined with the help of scanning electron microscopy (SEM) and transmission electron microscopy (TEM).

4.1.2 Results and Discussion

4.1.2.1 IR analysis

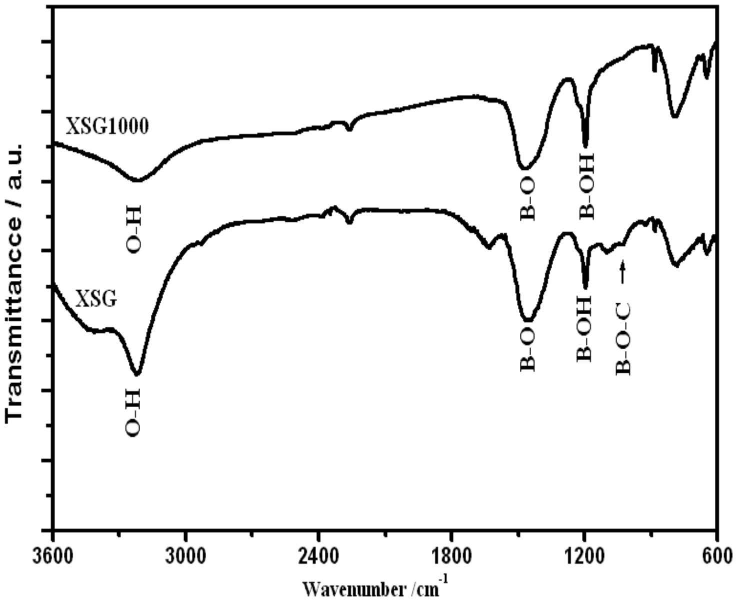

Fig. 4.3 IR Spectra of XSG and XSG1000

The FTIR spectra of XSG and XSG1000 are shown in Fig. 4.3. Boric acid and sucrose form a complex during gelation as evidenced by the band at 1015 cm^{-1} in the IR spectrum of XSG. This feature could be assigned to the B–O–C stretch [104, 105]. The absence of this feature in the IR spectrum pertaining to XSG1000 suggests its destruction during pyrolysis. In the IR spectra of both XSG and XSG1000, the broad band between 2900 and 3500 cm^{-1} could be assigned to the stretching of O–H pertaining to the moisture adsorbed on the surface of these samples. The band at 1450 cm^{-1} could be attributed to the B–O stretching and that at 1190 cm^{-1} to the B–O–H stretching. These results suggest that a complex is formed between boric acid and sucrose, which subsequently undergoes pyrolysis resulting in a precursor that yields boron carbide on further decomposition.

4.1.2.2 Chemical analysis

Boric acid and sucrose were taken in the molar ratio of 1:0.145 since this mixture could yield B_2O_3 and carbon required for the formation of B_4C in the subsequent step shown in Eq. 1.2 (Chapter 1). The overall reaction between boric acid and sucrose could be represented by Eq. 4.1.

$$48H_3BO_3 + 7C_{12}H_{22}O_{11} \rightarrow 12B_4C + 72CO + 149H_2O \tag{4.1}$$

Table 4.2 shows typical chemical composition of XSG, XSG1000, XSG1552h and XSG1553h. According to Eq. 1.2 (Chapter 1), the number of moles of boron and carbon in the final reaction mixture should bear the stoichiometric weight ratio 1:1.9 to facilitate the complete conversion of B_2O_3 and C into B_4C. However, the chemical analysis indicates that the gel XSG is carbon deficient (B:C is 1:1.36). However, in the pyrolyzed product XSG1000, the boron to carbon weight ratio was found to be 1:1.7 which is close to the desired value mentioned above. It is interesting to note that Yanse et al. [105] have reported significant loss of boron due to volatilization at temperatures above 1273 K and recommended the use of a carbon-deficient starting mixture (C/B weight ratio 1.8) than demanded by Eq. 1.2 (Chapter 1) for the synthesis of boron carbide.

Table 4.2 Chemical analyses of XSG, XSG1000, XSG1552h and XSG1553h

Sample	Boron (wt %)	Carbon (wt %)	Phases present
XSG	13.3	18.2	-
XSG1000	18.5	30.7	B_2O_3
XSG1552h	49.2	35.3	B_4C, B_2O_3, carbon
XSG1553h	59.1	40.5	B_4C, carbon

In the gel-based processes, the yield cannot be improved unless the loss of boron is avoided during the crucial carbothermic reduction step. In order to achieve the above objective a special sample container was designed out of high-density graphite. By suitably tailoring the design of this sample cell, CO was effectively removed from the reaction site while the oxides of boron (mostly B_2O_3) were retained within the reaction zone. The molecular masses of the various gaseous species vary in the following order $B_2O_3 > B_2O_2 > BO_2 > B_2O > CO$. Thus their root mean square velocities and rates of effusion from the reaction site through an orifice would follow the reverse order. Thus CO would effuse out faster compared to the oxides of boron through the orifice in the sample container. However, arriving at an optimum value for the diameter of the orifice in this sample container had to be achieved through careful experimentation. The results obtained after heat treating the precursor XSG1000 at 1823 K for 3 h under flowing argon in the graphite cylinder with lids having different orifices are depicted in Table 4.3 and Fig. 4.4. The results show that the diameter of the orifice had a bearing on the composition of the final product. The amount of B and C in the product has a dependence on the diameter of the orifice. The rate of effusion through an orifice has an inverse dependence on the area of the orifice (or the square of its radius). Thus it is reasonable to conclude that the loss of vapour species during the reduction is controlled probably by an effusion mechanism. An orifice with a diameter of 0.5 mm proved to be the most suitable for it yielded a product with boron to carbon ratio closest to the desirable value.

The use of graphite as the container material helped to promote the reaction of the boron containing moieties emanating from the precursor with the walls of the graphite cylinder with lids. Progressive deterioration of the container and the loss of its weight upon repeated usage testified this premise. The design of a closed container and its orifice thus turn out to be critical in controlling both the yield and composition of the final product. This is a novel feature reported for the first time.

The yield of boron carbide was found to be 48% when the precursor XSG1000 was heated at 1823 K for 3 h in a graphite cylinder with lids having an orifice diameter of 0.5 mm and the free carbon in the final product (XSGC0.5) was reduced to about 6 wt%.

Table 4.3 Chemical analyses of the boron carbide obtained after heat treating XSG1000 at 1823 K for 3 h in a graphite cylinder with lids

Sample	**Boron (wt %)**	**Carbon (wt %)**	**Phases present**	**SSA (m^2g^{-1})**	**B D (gcm^{-3})**	**XCS (nm)**
XSGC8	59.5	39	B_4C, carbon	15.72	0.29	66
XSGC3	65.1	34.5	B_4C, carbon	15.94	0.48	74
XSGC1.5	72.9	26.8	B_4C, carbon	17.21	0.61	58
XSGC1	75.5	24.3	B_4C, carbon	29.5	0.71	52
XSGC0.5	75.8	23.9	B_4C, carbon	30.5	0.74	52

SSA: specific surface area, XCS: X-ray crystallite size, B.D: bulk density

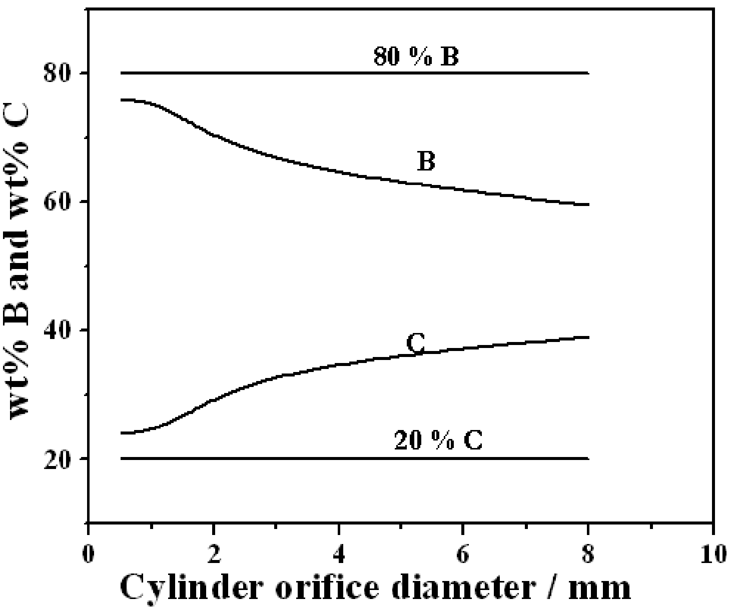

Fig. 4.4 Variation of amount of boron and carbon in the reaction product with the diameter of the cylinder orifice when precursor XSG1000 was heat treated at 1823 K for 3 h

4.1.2.3 XRD analysis

The XRD patterns of XSG1000 and the products obtained after subjecting it to heat treatment at different temperatures and durations are shown in Fig. 4.5. The XRD patterns pertaining to the pyrolysed gels XSG1000, XSG13, XSG14 (Fig. 4.5a, 4.5b and 4.5c respectively) revealed the presence of only B_2O_3 phase and the absence of B_4C. The carbon present in those samples pyrolyzed at temperatures below 1773 K was X-ray amorphous. Hence the formation of boron carbide is not feasible at temperatures below 1773 K. The XRD patterns (Fig. 4.5d and 4.5e) of XSG15 and XSG1552h indicate the presence of B_2O_3 and graphite in addition to boron carbide. The presence of B_2O_3 and carbon along with B_4C in XSG1552h (Fig. 4.5e) indicate that the reaction did not proceed to completion.

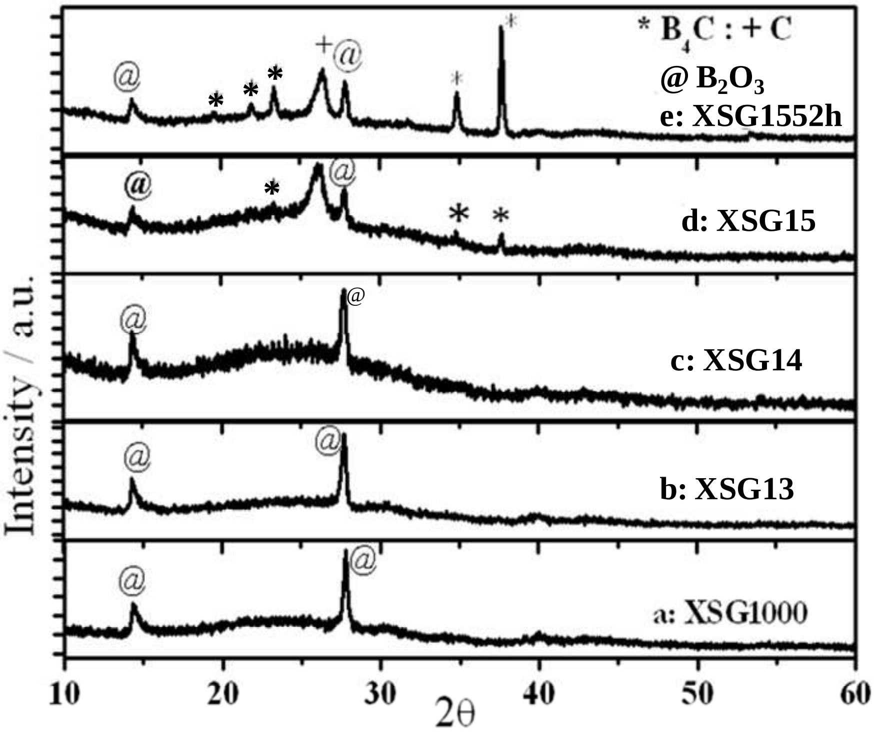

Fig. 4.5 X-ray diffraction patterns of the precursor and heat-treated products

However, the product XSGC0.5 shows the presence of B_4C along with free carbon as the second phase (Fig. 4.6). The absence of any peak pertaining to B_2O_3 in this product indicates the completion of the reaction or due to the evaporation of B_2O_3 from the reaction mixture or both.

The average size of boron carbide crystallites in the sample XSGC0.5 calculated by using the Scherrer formula was found to be 55 nm. A plot for Bcosθ versus 4sinθ corresponding to the diffraction pattern of XSGC0.5 is shown in Fig.4.7. The lattice strain computed from the slope of this plot was found to be rather insignificant (0.012 %) and the crystallite size obtained from the intercept was found to be 52 nm. This value is in good agreement with the X-ray crystallite size calculated from the Scherrer formula.

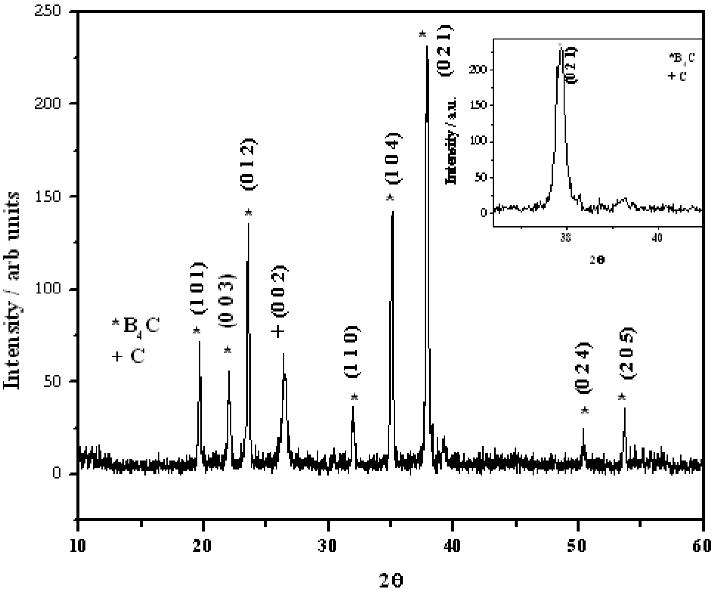

Fig. 4.6 X-ray diffraction pattern of XSGC0.5

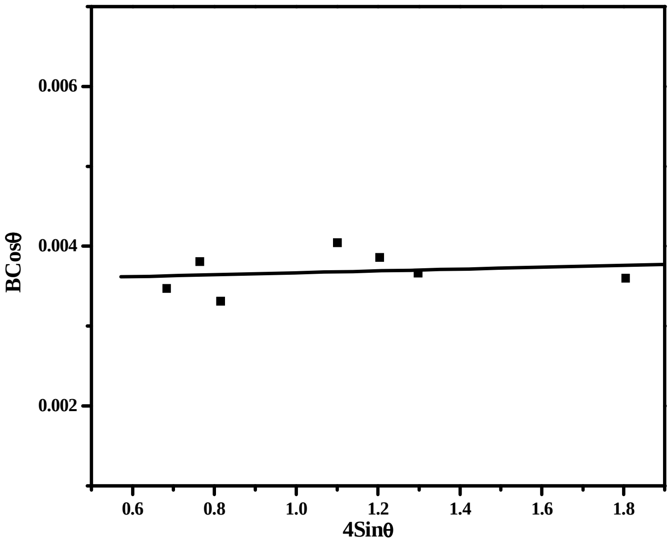

Fig. 4.7 Williamson–Hall plot pertaining to XSGC0.5

4.1.2.4 Microstructure and particle size analysis

Fig. 4.8 reveals the microstructure of XSGC0.5. From this microstructure it is clear that the crystallites of boron carbide formed during the heat treatment agglomerate into irregular fine particles. Selective growth of crystallites of B_4C is also observed.

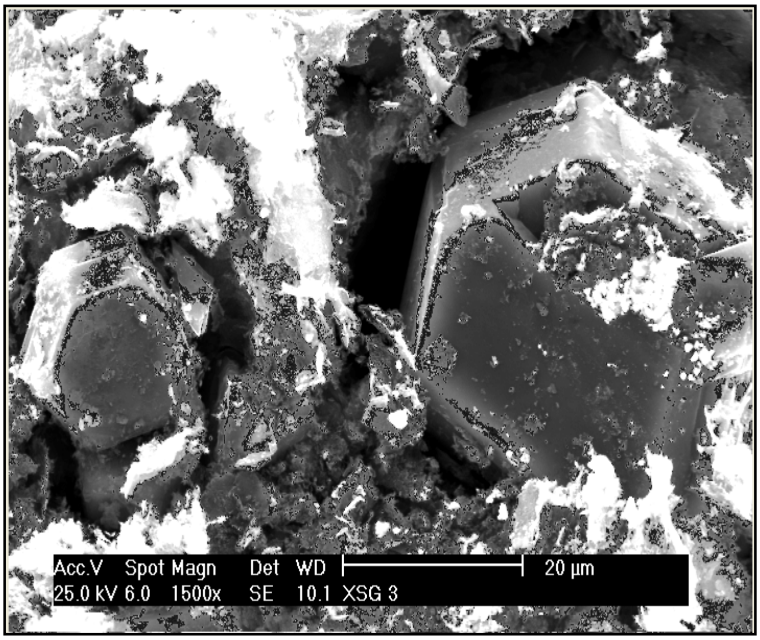

Fig. 4.8 Scanning electron micrograph of XSGC0.5

A typical TEM image of XSGC0.5 is shown in Fig. 4.9 and the SAD (Selected area diffraction) pattern pertaining to an area where boron carbide crystallite was present is shown as the inset in Fig. 4.9. Spotty ring pattern confirms the nanocrystallinity of the randomly oriented boron carbide crystallites while diffraction pattern corresponds to the hexagonal B_4C phase.

The particle size distribution of XSGC0.5 is shown in Fig. 4.10. It is seen that the size distribution of the boron carbide particles is unimodal and falls in the range of 10–100 μm while the product obtained in an earlier study [100] from a citrate gel precursor had a bi-modal distribution.

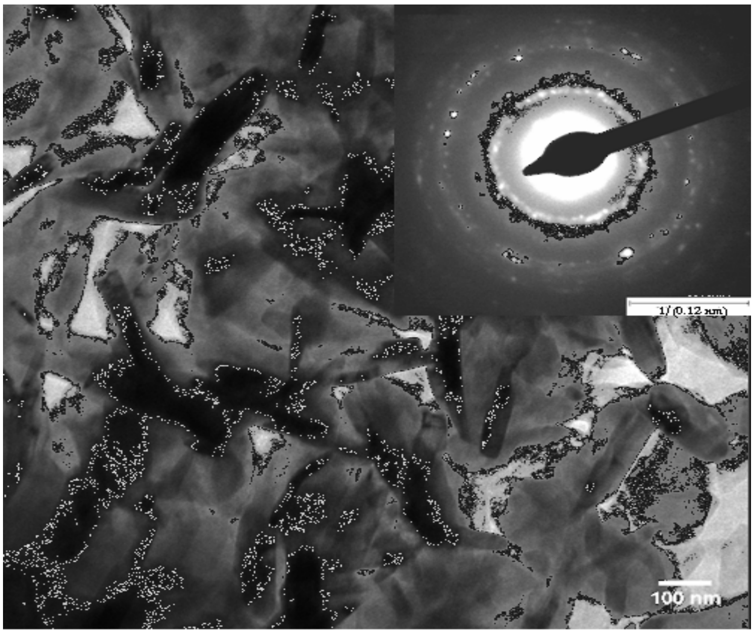

Fig. 4.9 Transmission electron micrograph of XSGC0.5. The inset shows the SAD pattern of nanocrystalline boron carbide

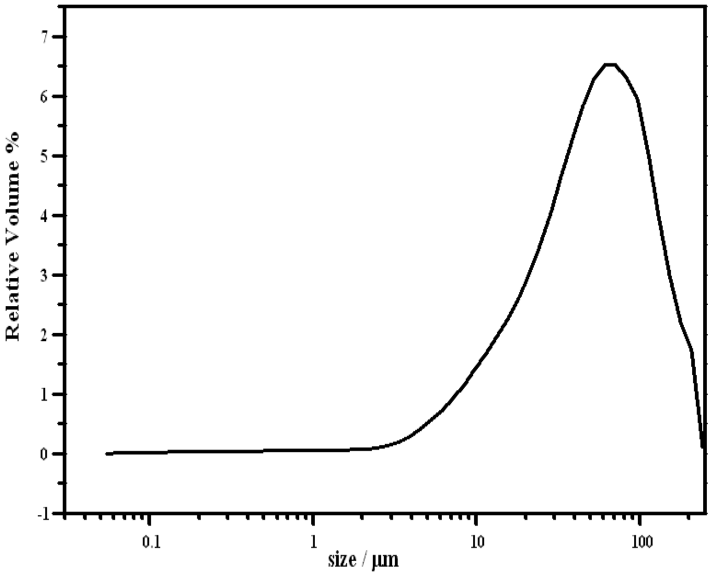

Fig. 4.10 Particle size distribution of XSGC0.5

4.2 Synthesis of boron carbide from boric acid-citric acid xerogel

4.2.1 Experimental

In a typical experiment, 22.5 g of citric acid was taken in a combustion bowl and melted using a silicone oil bath at 423 ± 10 K. To this melt, 11.3 g of boric acid was added slowly in order to obtain a homogeneous gel. Upon heating this gel at 423 ± 10 K, a yellow coloured dry xerogel (XCG) was obtained. This product was placed in a high-density graphite crucible and pyrolyzed using a kanthal wire-wound resistance furnace (vertical) under a flowing stream of UHP argon at 773, 873, 973 and 1073 K for 2 h and the products thus obtained were designated as XCG500, XCG600, XCG700 and XCG800 respectively. Based on the C/B weight ratio, XCG600 was selected for the high temperature pyrolysis. This precursor was compacted into pellets of 16 mm diameter by using a uniaxial hydraulic press. These pellets were placed in a high-density graphite cylinder with lids on both sides (lids having an orifice diameter of 0.5 mm) and heated at 1573, 1673, 1773 and 1823 K for 3h under UHP argon. The resultant products are designated as XCG61300, XCG61400, XCG61500 and XCG61550 respectively. The scheme of preparation is shown in Fig. 4.11.

The xerogel and the precursor (XCG600) were characterized by using Fourier transform infrared spectroscopy. The constituent phases were identified by using X-ray diffraction while their elemental composition was established with the help of chemical assay. The microstruture of boron carbide synthesized in this study was examined with the help of SEM.

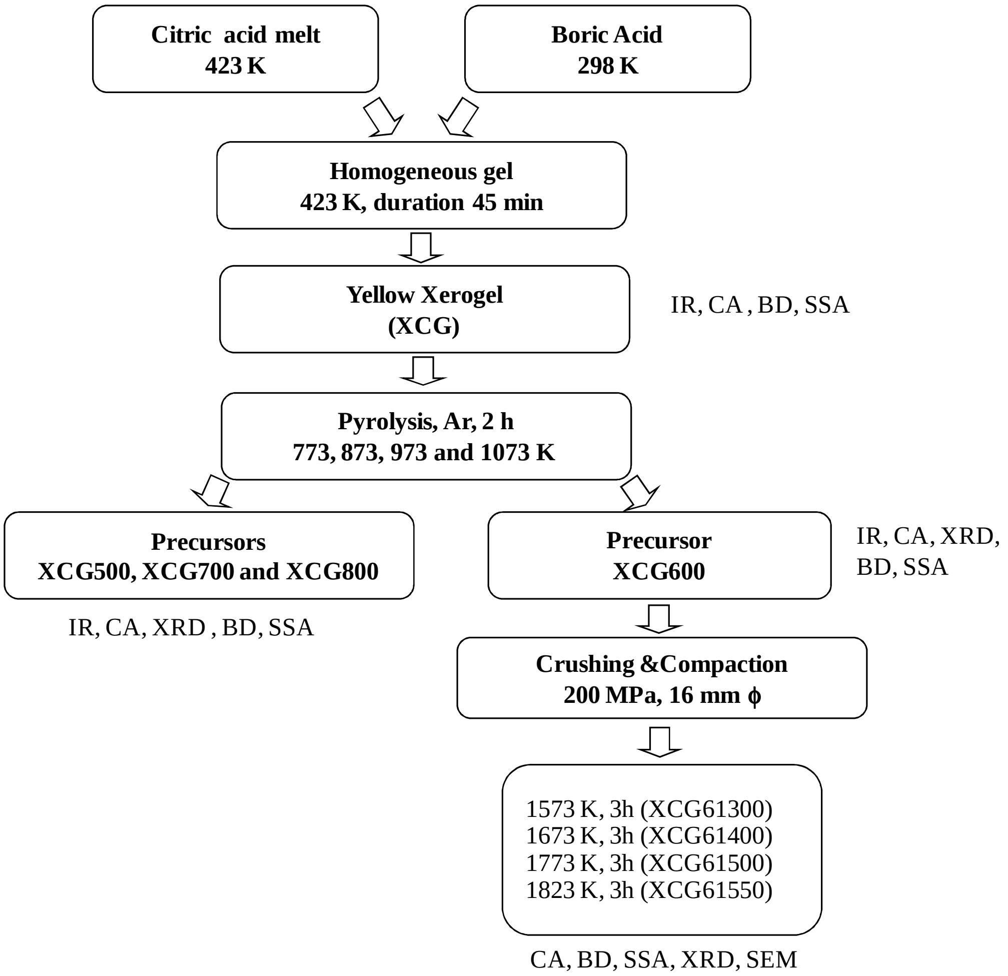

Fig. 4.11 The scheme of preparation of boron carbide from boric acid-citric acid xerogel precursor

4.2.2 Results and discussion

4.2.2.1 IR analysis

Fig. 4.12 shows the FTIR spectra of XCG and XCG600. A complex is formed between H_3BO_3 and citric acid during the gelation as indicated by the band at 1015 cm^{-1} that could be assigned to the B-O-C stretching frequency in the IR spectrum of XCG. The absence of this feature in the IR spectrum of XCG600 suggests the destruction of the complex formed between boric acid and citric acid during pyrolysis. A broad band between 2900 and 3500 cm^{-1} could be assigned to the stretching frequency of O-H pertaining to the moisture absorbed on to the surface of the samples XCG and XCG600. The broad band at 1450 cm^{-1} could be attributed to the B-O stretching frequency and that at 1190 cm^{-1} to the B-O-H stretching. These results show that a complex is formed between boric acid and citric acid during gel formation and is decomposed during the pyrolysis.

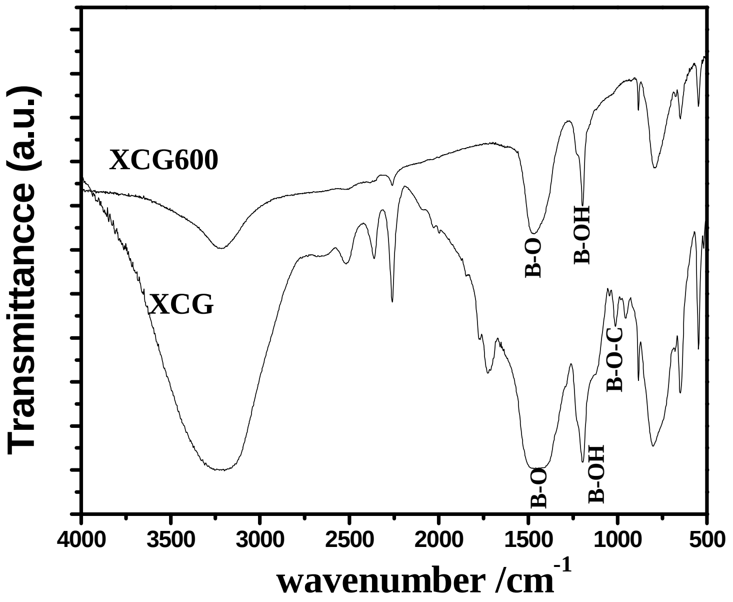

Fig. 4.12 The IR spectra of XCG and XCG600

4.2.2.2 Chemical analysis

The overall reaction between boric acid and citric acid could be presented by Eq. 4.2.

$$12\ H_3BO_3 + 7\ C_6H_8O_7.H_2O \rightarrow 3\ B_4C + 39\ CO + 46\ H_2O \qquad (4.2)$$

Table 4.4 shows the chemical composition of XCG, XCG500, XCG600, XCG700 and XCG800. The C/B weight ratio in the products (XCG, XCG500 and XCG600) are less than that demanded by stoichiometric Eq. 1.2 (Chapter 1) whereas the the products (XCG700 and XCG800) contain C/B weight ratio more than the stoichiometric value. However, the C/B weight ratio in the product XCG600 is very close to the optimum value found in the earlier study on the synthesis of boron carbide from boric acid-sucrose gel precursor (Section 4.1.2.2). This suggests that the optimum temperature of pyrolysis of boric acid-citric acid xerogel is 873 K. The chemical analysis of the product (XCG61550) obtained after heat treatment of XCG600 at 1823 K for 3 h is also shown in Table 4.4. The final product contain about 10.3 wt% free carbon which is slightly lower than that in studies using citric acid as a gel forming agent [99].

Table 4.4 Chemical analysis of XCG, XCG500, XCG600, XCG700, XCG800 and XCG61550

Sample	B (wt%)	C (wt%)	C/B weight ratio	B.D (g/cc)	SSA (m^2g^{-1})	XCS (nm)
XCG	12.2	16.4	1.34	0.22	2.5	
XCG500	15.7	23.3	1.48	0.43	13.5	
XCG600	15.1	26.1	1.72	0.44	21.3	
XCG700	14.5	27.8	1.92	0.35	22.3	
XCG800	14.8	29.7	2.01	0.27	24.1	
XCG61550	71.3	28.2		0.69	33.5	181

SSA: specific surface area, XCS: X-ray crystallite size, B.D: bulk density

However, the yield of boron carbide was found to be only 36% when the precursor XCG600 was heated at 1823 K for 3 h. The yield is much less than that obtained from boric acid-sucrose gel precursor.

4.2.2.3 Phase identification and microstructure analyses

Fig. 4.13 shows the X-Ray diffraction (XRD) patterns of XCG500, XCG600, XCG700 and XCG800. All these patterns show the presence of only cubic boric oxide in the precursors. However, due to amorphous nature of carbon present in these precursors, peaks pertaining to carbon were not seen in the XRD patterns of the precursors. XRD patterns pertaining to XCG61300, XCG61400 and XCG61500 (products obtained when XCG600 heated at 1573, 1673 K and 1773 K for 3 h respectively) are also shown in Fig. 4.13.

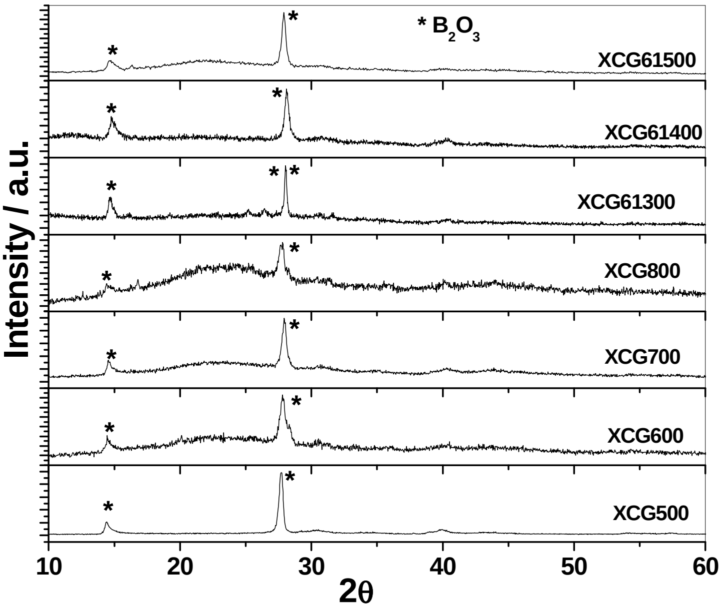

Fig. 4.13 X-ray diffraction pattern of the precursor (XCG500, XCG600, XCG700 and XCG800) and heat-treated products

The absence of peaks pertaining to boron carbide indicates that the formation of boron carbide is not feasible at temperatures at least upto 1773 K. The XRD pattern of the product XCG61550 is shown in Fig. 4.14. This product shows peaks pertaining to boron carbide (JCPDS file No. 35-0798) and carbon (JCPDS file No. 89-7213). The absence of characteristic peaks corresponding to boric oxide indicates the completion of the reaction or the evaporation of boron in the form of its oxides or both. The presence of carbon in these samples indicates the loss of boron in the form of its gaseous oxide species. The average crystallite size calculated from Scherrer formula was found to be 181 nm.

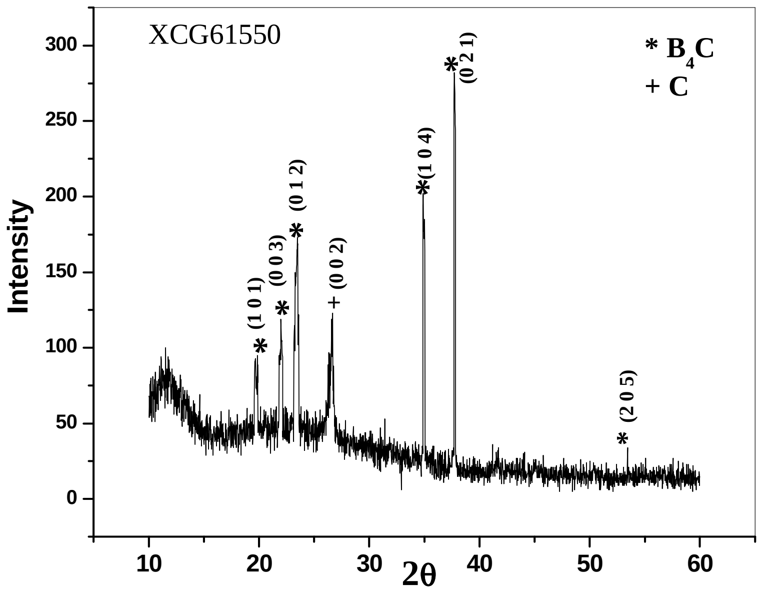

Fig. 4.14 X-ray diffraction pattern of XCG61550

Microstructure of XCG61550 is shown in the Fig. 4.15. The figure shows the agglomeration of nanocrystalline boron carbide particles of different sizes and different shapes

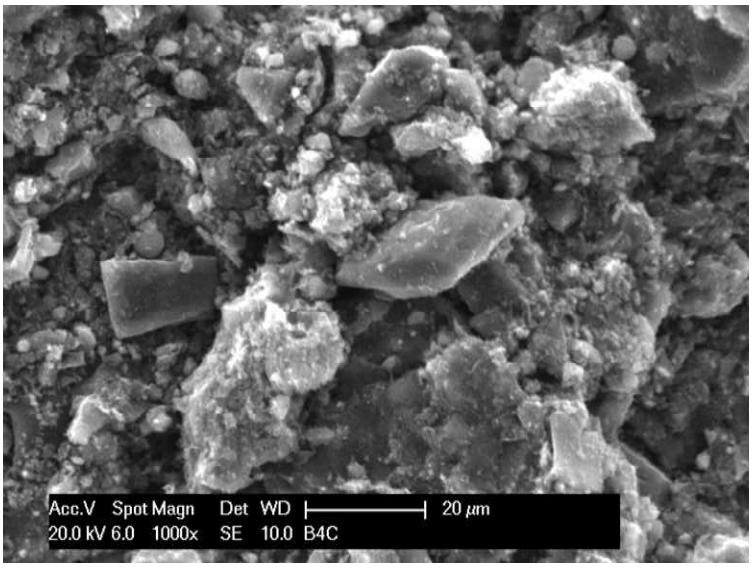

Fig. 4.15 Scanning electron micrograph of XCG61550

4.3 Synthesis of boron carbide from boric oxide-citric acid gel precursor

4.3.1 Experimental

In a typical experiment, 12.6 g of boric oxide and 43.8 g of citric acid were taken in a stainless steel (SS) vessel (Fig. 2.4). This vessel containing the reactants was then placed inside an SS reactor as shown in Fig. 2.4. The residual moisture present in the reaction mixture was removed by vacuum degassing at 393 K for 2 h. Subsequently the reaction mixture was heated in a kanthal wire-wound resistance furnace (vertical) in a stream of UHP argon at 773, 873, 973 and 1073 K for 2 h and the products thus obtained were labelled as BOC500, BOC600, BOC700 and BOC800 respectively. Based on C/B weight ratio, BOC700 was chosen for high temperature pyrolysis. This powder was compacted into pellets of 16 mm diameter and 10 mm height. These pellets were placed in a graphite cylinder with lids (lids having an orifice diameter of 0.5 mm) and heated in a molybdenum wire-wound resistance furnace at 1573, 1673, 1773 and 1823 K for 3 h under a flowing stream of UHP argon. The resultant products are designated as BOC71300, BOC71400, BOC71500 and BOC71550 respectively. The scheme of preparation is shown in the Fig. 4.16.

The constituent phases were identified by using X-ray diffraction while their elemental composition was established with the help of chemical assay. The microstructure of boron carbide synthesized in this study was examined with the help of scanning electron microscopy.

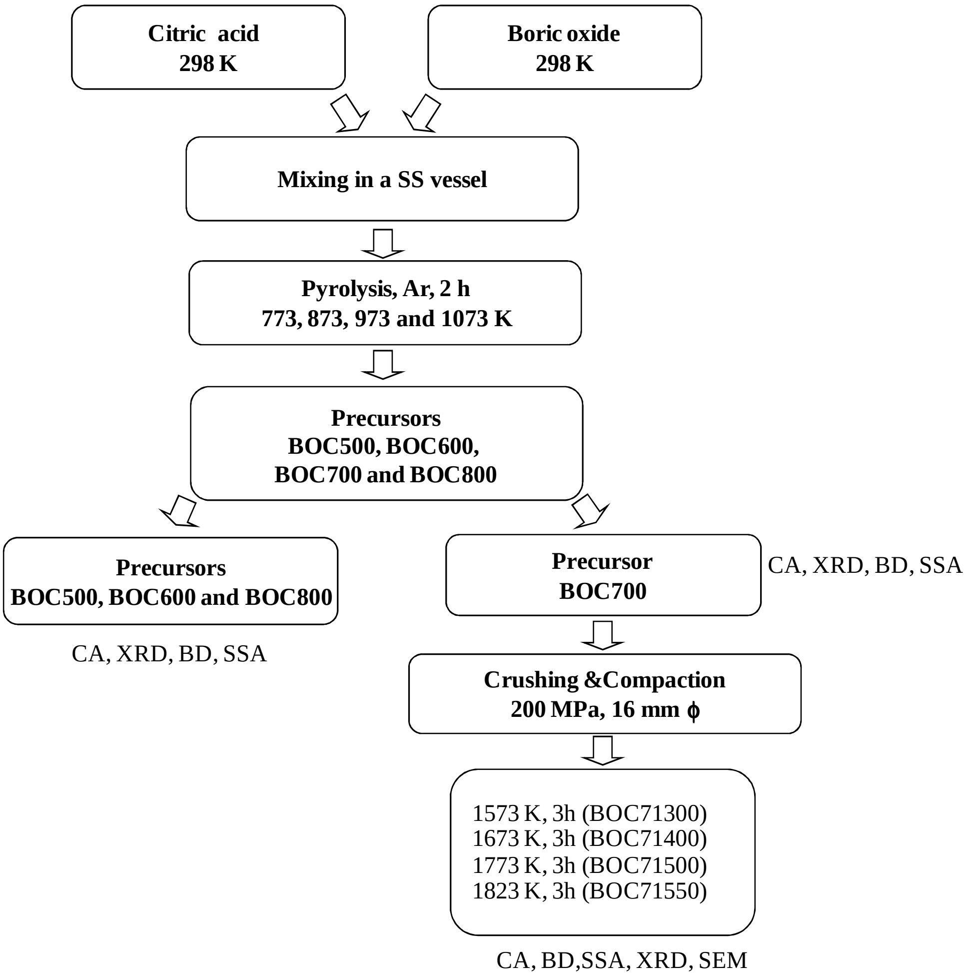

Fig. 4.16 The scheme of preparation of boron carbide from boric oxide-citric acid gel precursor

4.3.2 Results and Discussion

4.3.2.1 Chemical analysis

The overall chemical reaction between boric oxide and citric acid could be represented as:

$$6\ B_2O_3 + 7\ C_6H_8O_7 \rightarrow 3\ B_4C + 39\ CO + 28\ H_2O \qquad (4.3)$$

Table 4.5 shows the chemical composition of BOC500, BOC600, BOC700 and BOC800. The C/B weight ratios of the products BOC500, BOC600 and BOC700 are less than the one demanded by stoichiometric Eq. 1.2 (Chapter 1) whereas the the products BOC800 contain higher than the stoichiometric value. However, the C/B weight ratio in the product BOC700 is very close to the optimum value found in the earlier study on the synthesis of boron carbide from boric acid-sucrose gel precursor (Section 4.1.2). Hence BOC700 is the most suitable precursor for the preparation of boron carbide as it contains the optimum C/B weight ratio. The results of the chemical analysis of the product (BOC71550) obtained after heat treatment of BOC700 at 1823 K for 3 h is also shown in Table 4.5. This product contains about 8.6 wt% free carbon. However, the yield of boron carbide was found to be about 41 %.

4.3.2.2 Phase identification, microstructure and particle size distribution

Fig. 4.17 shows the XRD patterns of BOC500, BOC600, BOC700 and BOC800. All these patterns show the presence of only cubic boric oxide. The XRD patterns of BOC71300, BOC71400 and BOC71500 are also shown in Fig. 4.17. The presence of only cubic boric oxide indicates that boron carbide does not form under these conditions of temperature and time duration. This precursor needed to be heated above 1773 K. The XRD patterns of the product BOC71550 is shown in Fig. 4.18. This shows peaks

Table 4.5 The results of chemical analysis of the BOC500, BOC600, BOC700, BOC800 and BOC71550

Sample	B (wt %)	C (wt %)	C/B weight ratio	B.D (g/cc)	SSA (m^2g^{-1})	XCS (nm)
BOC500	14.1	22.4	1.58	0.34	11.3	
BOC600	14.3	23.8	1.66	0.25	23.6	
BOC700	15.8	27.3	1.73	0.38	21.1	
BOC800	14.5	27.8	1.92	0.46	19.7	
BOC71550	72.9	26.8		0.61	48.2	261

SSA: specific surface area, XCS: X-ray crystallite size, B.D: bulk density

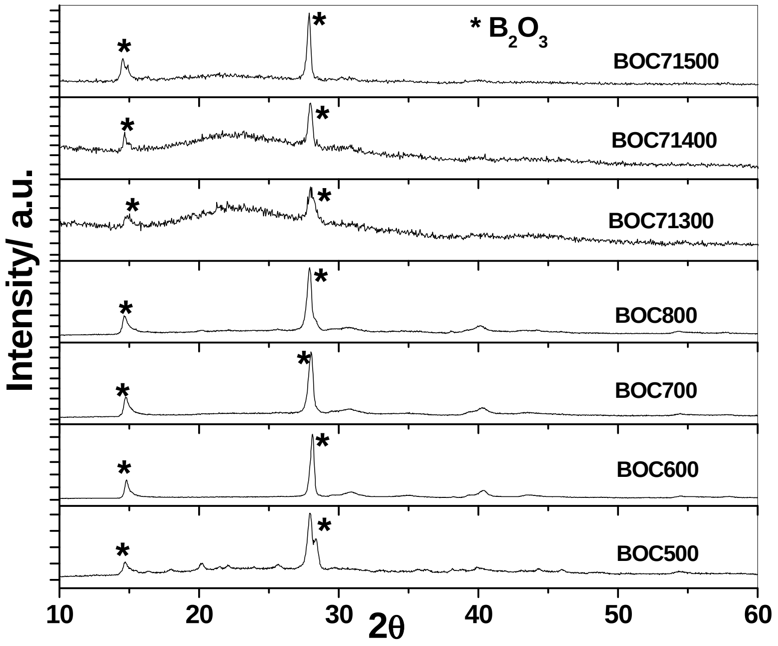

Fig. 4.17 X-ray diffraction pattern of the precursor and heat-treated products

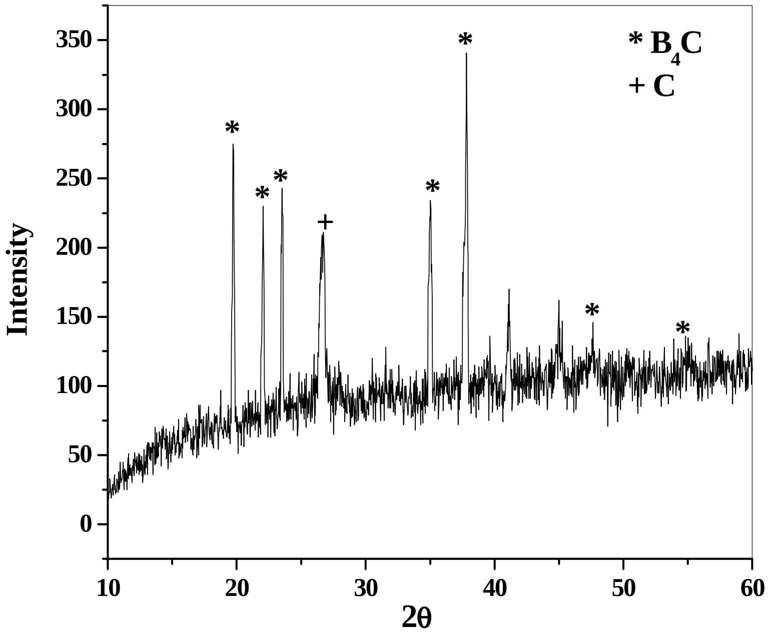

Fig. 4.18 X-ray diffraction pattern of BOC71550

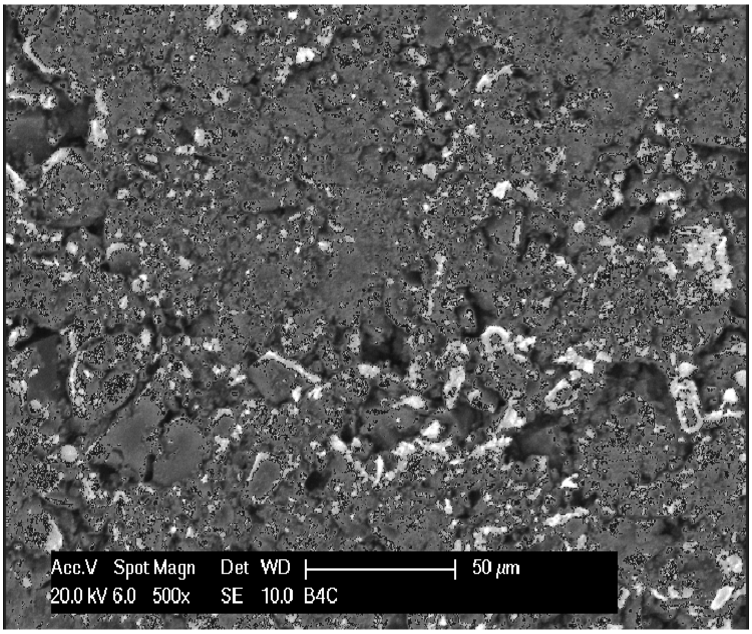

Fig. 4.19 Scanning electron micrograph of BOC71550

pertaining to boron carbide (JCPDS file No. 35-0798) and carbon (JCPDS file No. 89-7213). The absence of characteristic peaks corresponding to boric oxide indicates the completion of the reaction. The average crystallite size calculated from Scherrer formula was found to be 260 nm.

Microstructure of BOC71550 is shown in the Fig. 4.19. It can be seen from the figure that the particles are irregular in size and shapes.

The particle size distribution of BOC71550 is shown in Fig. 4.20. It is seen that the size distribution of the particles (100–500 μm) exhibit a unimodal distribution.

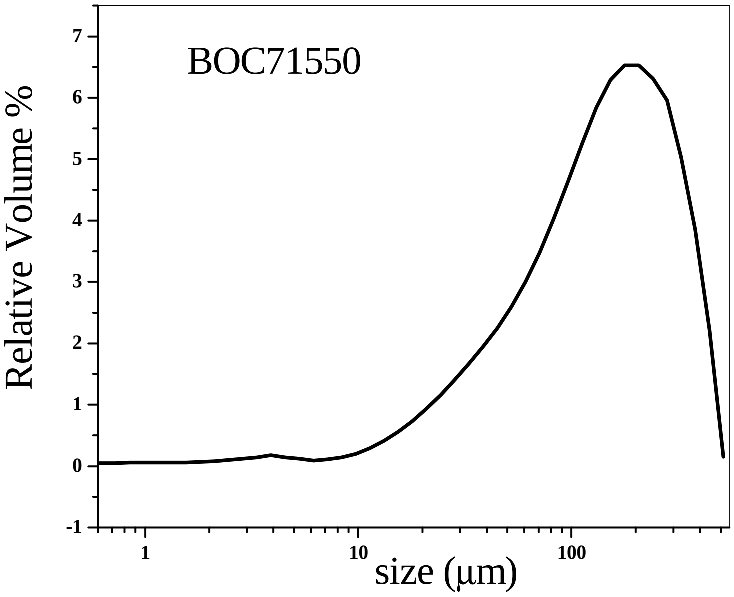

Fig. 4.20 The particle size distribution of BOC71550

4.4 Synthesis of boron carbide from boric oxide-sucrose gel precursor

4.4.1 Experimental

In a typical experiment, a homogeneous mixture of 12.6 g of boric oxide and 18.2 g sucrose was taken in a stainless steel (SS) vessel (Fig. 2.4). This vessel along with the reactants was then placed in an SS reactor (Fig. 2.4). The residual moisture present in the reaction mixture was removed by vacuum degassing at 443 K for 2 h. Subsequently this reaction mixture was heated at 973 K for 2 h using a kanthal wire-wound resistance furnace (vertical) in a stream of UHP argon. A black spongy precursor was formed. This precursor (resultant product is designated as BOS700) was subsequently crushed, ground into fine powder and compacted into pellets of 16 mm diameter and 10 mm height. These pellets were placed in a graphite cylinder with lid (lids having an orifice diameter of 0.5 mm) and heated in a molybdenum wire-wound resistance furnace at 1573, 1673 for 3 h and at 1773 K for 2 and 3 h under flowing UHP argon. The resultant products are designated as BOS713, BOS714, BOS7152h and BOS715 respectively.

In another set of independent experiments the precursors were also prepared by heating a stoichiometric mixture of boric oxide and sucrose at 773, 873 and 1073 K for 2 h (resultant products are designated as BOS500, BOS600, and BOS800 respectively) in order to optimize the temperature of synthesis of the precursor. These precursors (BOS500, BOS600 and BOS800) were also compacted into pellets and heated at 1773 K for 3 h as described above. The resultant products obtained after heat treatment at 1773 K for 3 h are designated as BOS515, BOS615 and BOS815 respectively. The scheme of the synthesis is depicted in Fig. 4.21 as a flow chart.

The constituent phases were identified by using X-ray diffraction while their elemental composition was established with the help of chemical assay. The microstruture of boron carbide synthesized in this study was examined with the help of scanning electron microscopy.

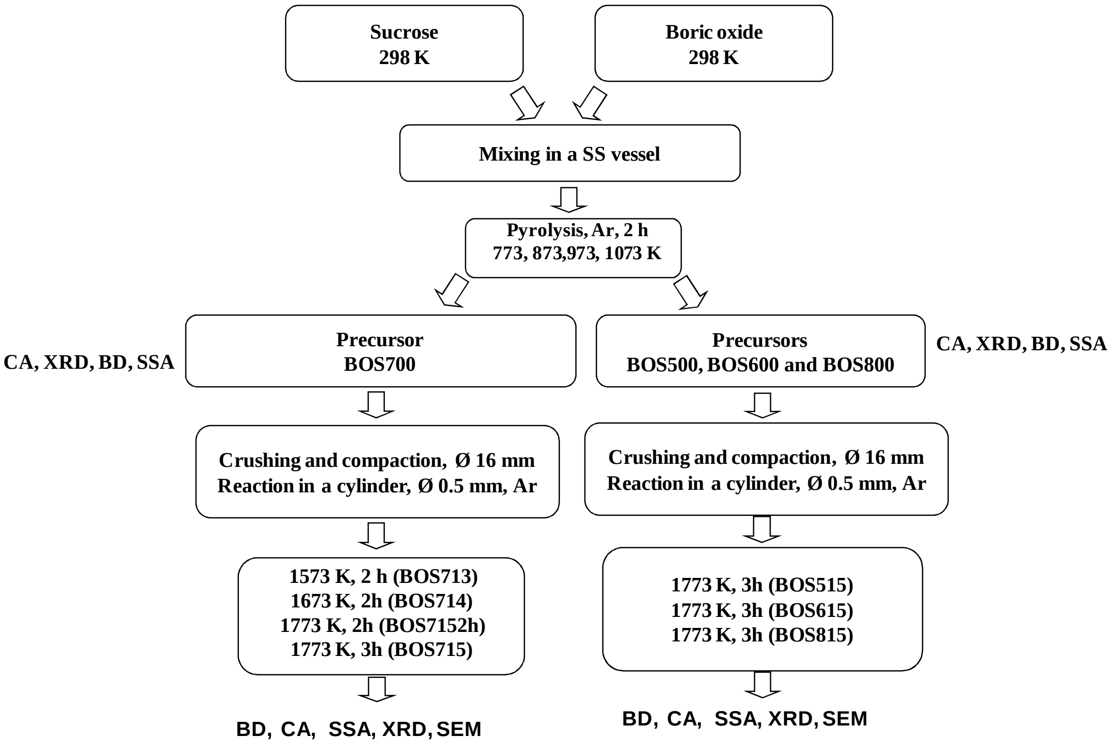

Fig. 4.21 The scheme of preparation of boron carbide from boric oxide-sucrose gel precursor

4.4.2 Results and Discussion

4.4.2.1 Chemical analysis

The overall reaction of boric oxide with sucrose is represented as:

$$24\ B_2O_3 + 7\ C_{12}H_{22}O_{11} \rightarrow 12\ B_4C + 72\ CO + 77\ H_2O \qquad (4.4)$$

Table 4.6 shows typical chemical compositon of various boric oxide-sucrose precursors prepared in this study. Except BOS500, which was brown in colour, all the other precursors were black in colour. It is surmised that this brown colour might be due to incomplete decomposition of sucrose. All the precursors have a value of C/B weight ratio (1.58 for BOS500, 1.68 for BOS600, 1.77 for BOS700 and 1.73 for BOS800) lower than that demanded by Eq. 1.2 (1.9) for the quantitative formation of boron carbide. This lower C/B weight ratio may be due to the loss of boron in the form of its oxides as the vapour pressures of the latter increases with temperature. As discussed in section 4.1.2.2, Yanase et al. [105] suggested the use of reaction mixtures with lower C/B value than the stoichiometric value demanded by Eq. 1.2 (Chapter 1) to synthesize single phase boron carbide. The results of the chemical analyses of BOS515, BOS615, BOS715 and BOS815 are shown in Table 4.7. These results show that the product BOS615 contains minimum free carbon compared to BOS515, BOS715 and BOS815. Hence the optimum temperature for preparation of boric oxide-sucrose precursor in order to obtain boron carbide with minimum free carbon is 873 K. The yield of boron carbide obtained in this study is 61% and the free carbon in the final product BOS615 is found to be about 4 wt%. From this study it is inferred that boron carbide with maximum yield and minimum free carbon content can be prepared from the boric oxide (boron source)-sucrose (carbon source) gel precursor. The bulk density and specific surface area of the prescursor powders and boron carbide powders synthesized in this study are also shown in Table 4.6 and 4.7.

4.4.2.2 Phase identification, microstructure and particle size distribution

Fig. 4.22 shows the XRD patterns of BOS500, BOS600, BOS700 and BOS800. All these patterns show the presence of only cubic boric oxide in the precursors. Peaks pertaining to carbon were not seen in the XRD patterns of the precursors because the carbon present in these precursors is amorphous. The presence of carbon, however, was established by the chemical analysis of these samples. XRD patterns BOS713, BOS714 and BOS7152h are shown in Fig. 4.23. The XRD patterns of BOS713 and BOS714 show the presence of only cubic boric oxide. However, the XRD pattern of BOS7152h shows the presence of a mixture of boron carbide, boric oxide and carbon.

Table 4.6 Results of the chemical analysis of the precursors BOS500, BOS600, BOS700 and BOS800

Sample	Boron (wt %)	Carbon (wt %)	Phases present	Bulk density (g/cc)	Specific surface area (m^2g^{-1})
BOS500	14.9	23.6	B_2O_3 and C	0.22	13.1
BOS600	16.1	27.2	B_2O_3 and C	0.35	26.5
BOS700	16.1	28.5	B_2O_3 and C	0.29	21.3
BOS800	16.2	28.1	B_2O_3 and C	0.32	22.3

Table 4.7 Results of the chemical analysis of BOS515, BOS615, BOS715 and BOS815

Sample/Element	Boron (wt%)	Carbon (wt%)	Phases present	X-ray crystallite size (nm)	Bulk density (g/cc)	Specific surface area (m^2g^{-1})
BOS515	68.4	30.9	B_4C and C	56	0.42	32.2
BOS615	76.2	23.1	B_4C and C	48	0.53	40.1
BOS715	70.5	28.8	B_4C and C	52	0.77	34.3
BOS815	69.1	29.8	B_4C and C	63	0.81	30.9

The presence of boric oxide in this product mixture suggests incompletion of the reaction. The XRD patterns of the BOS515, BOS615, BOS715 and BOS815 are shown in Fig. 4.24. These products show the presence of boron carbide (JCPDS file No. 35-0798) and carbon (JCPDS file No. 89-7213). The absence of boric oxide in these products indicates the completion of the reaction. The presence of carbon residue in these samples indicates the loss of boron in the form of its gaseous oxide species swept in the carrier gas stream. From Fig. 4.24, it is also observed that the intensity of peak corresponding to carbon in the XRD pattern of BOS615 is lower than those of other products (BOS515, BOS715 and BOS815). This indicates that the product BOS615 contains relatively lower free carbon compared to other products. This observation is in agreement with the results obtained by the chemical analysis.

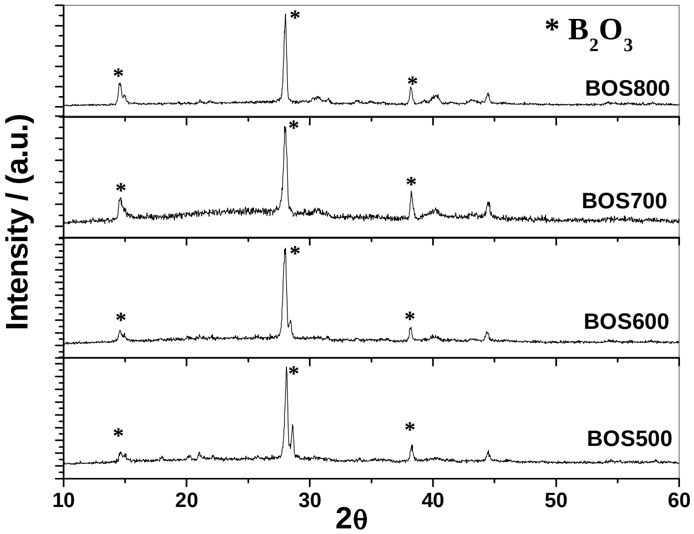

Fig.4.22 X-ray diffraction pattern of the precursors

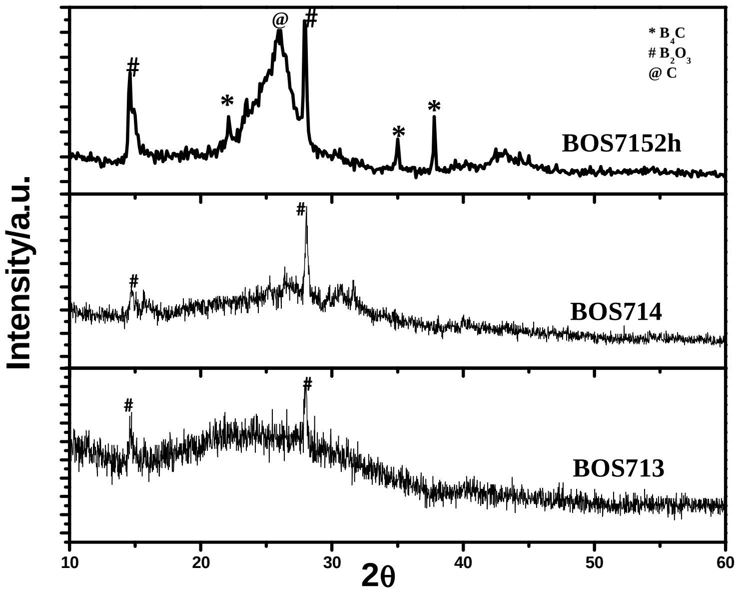

Fig. 4.23 X-ray diffraction patterns of the heat-treated products

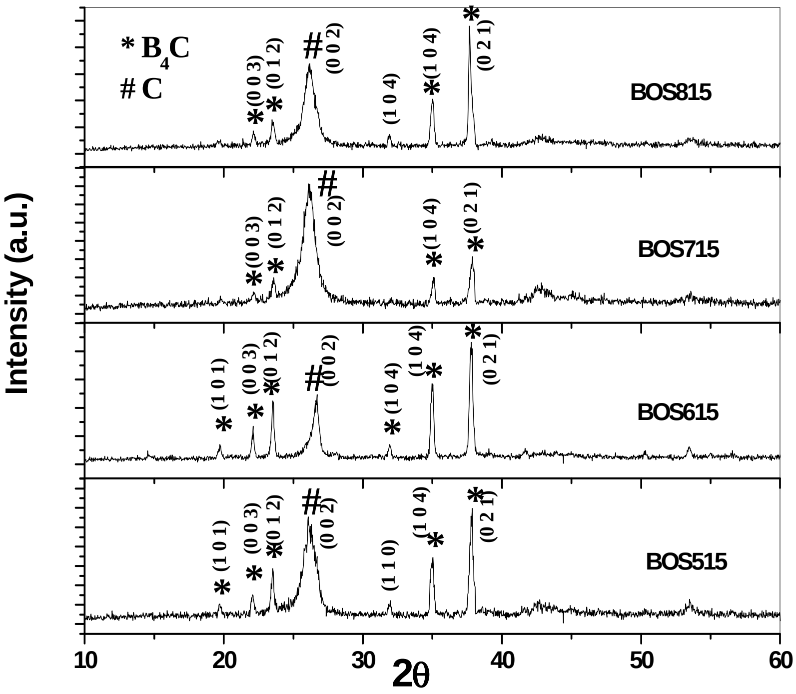

Fig. 4.24 X-ray diffraction patterns of BOS515, BOS615, BOS715 and BOS815

The average size of boron carbide crystallites in the sample BOS615 calculated from the Scherrer formula was found to be 60 nm. Fig. 4.25 shows the Hall Williamson plot pertaining to BOS615. Lattice strain calculated from the slope of this plot is 0.015%. The crystallite size calculated from the intercept of the Hall Williamson's plot is 62 nm. The crystallite size calculated from the Scherrer formula and from the Hall Williamson plot are in good agreement with each other.

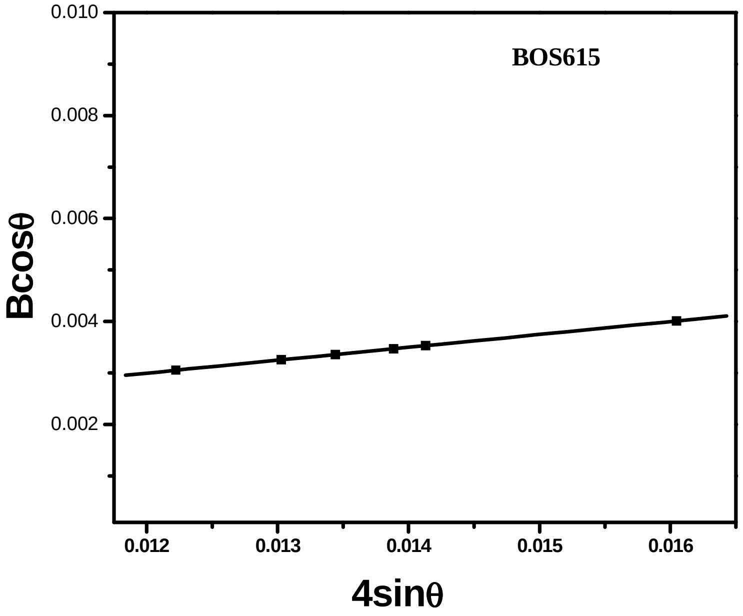

Fig. 4.25 Williamson–Hall plot pertaining to BOS615

Fig. 4.26 shows the microstructure of BOS615. From the microstructure it is evident that the particles of the product BOS615 are irregular in shape and size. In addition, these particles are nanocrystalline agglomerates of boron carbide.

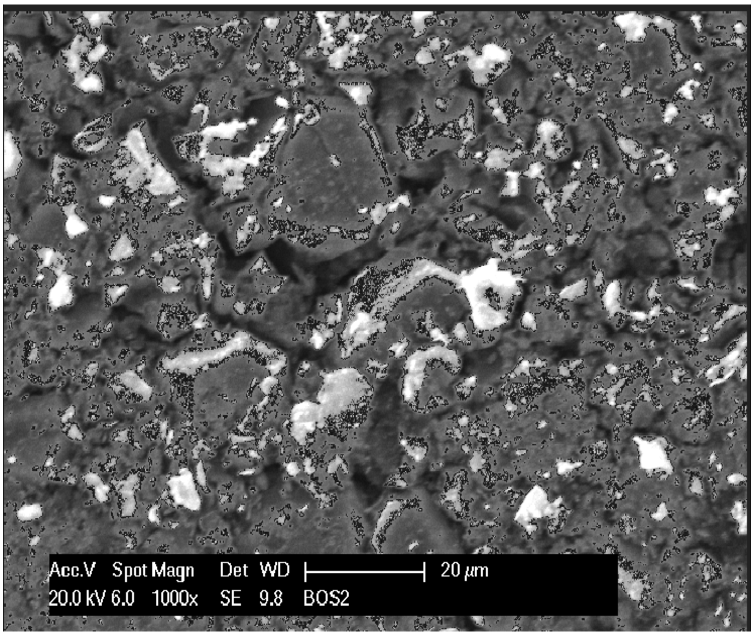

Fig. 4.26 Scanning electron micrograph of BOS615

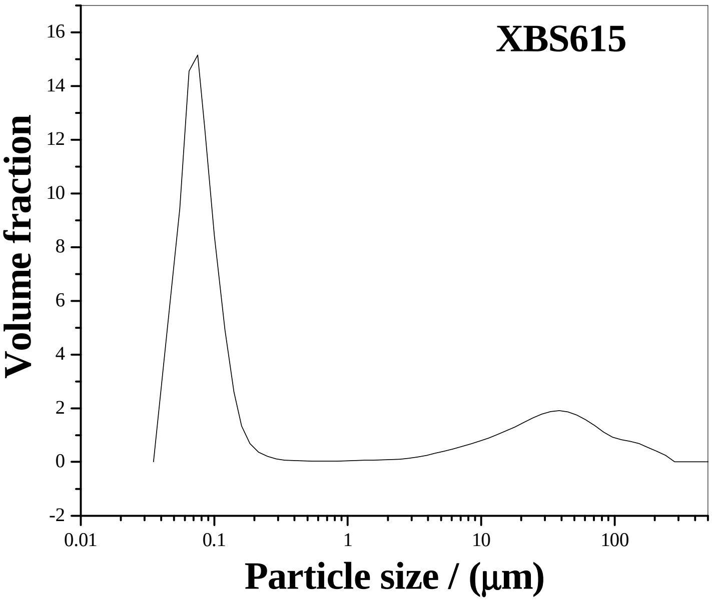

Fig. 4.27 The particle size distribution of BOS615

Particle size distribution of BOS615 is shown in Fig. 4.27. As seen in the plot, the particles exhibit bimodal size distribution with 90 % of the particles (D_{90}) in the size range of 0.02 – 0.2 µm. About 10 % of the powder has particles with size range of 300 to 500 µm. These paricles are much smaller than those synthesized from boric acid-sucrose gel precursor and boric acid-citric acid gel precursors described in earlier sections.

4.5 Summary of studies carried out on the synthesis of nanocrystalline boron carbide

Table 4.8 Summary of studies carried out on the synthesis of nanocrystalline boron carbide

Gel Precursor	% B (wt%)	% C (wt%)	Free carbon (wt%)	Yield (%)	X-ray crystallite size (nm)
Boric acid-Citric acid	71.3	28.2	10.5	36	181
Boric oxide-Citric acid	72.9	26.8	8.5	41	260
Boric acid-Sucrose	75.8	23.9	5.5	48	52
Boric oxide-Sucrose	76.2	23.1	4.1	61	60

Table 4.8 compares the results of the chemical analyses of boron carbide prepared using various gel precursors. This study clearly brings out the fact that the use of sucrose as a gel forming agent has definite advantages over the use of citric acid. Similarly boric oxide was found to be a better boron source compared to boric acid for the synthesis of boron carbide through gel precursor method.

4.6 Conclusions

Alternate energy efficient low temperature methods based on the pyrolysis of suitable gel precursors for the synthesis of boron carbide were developed. Systematic studies were carried out to optimize the process parameters such as composition of the initial reactant mixture and temperature and time for the pyrolysis of the precursors. The precursors and boron carbide prepared from these precursors were characterized by both chemical methods and XRD. The physical properties such as specific surface area, bulk density, and particle size distribution of the precursors as well as the final products measured. The crystallite size of various powders was determined by the X-ray line broadening technique. The microstructure and surface morphology were studied by using scanning electron microscopy and transmission electron microscopy. The performance of boric acid and boric oxide as boron sources and sucrose and citric acid as the carbon source was compared. The studies led to the following conclusions.

1. The products obtained through the gel precursor route were found to be nanocrystalline, free flowing and porous.
2. Yield of boron carbide could be improved by using a specially designed graphite cylinder with lids by minimizing the loss of boron.
3. This study clearly brings out the fact that the use of sucrose as a gel forming agent has definite advantages over the use of citric acid.
4. This study also brings out the fact that the use of boric oxide as a boron source has definite advantages (in improving the yield and lowering the free carbon residue in boron carbide) over the use of boric acid.
5. A novel method for the synthesis of nanocrystalline boron carbide with high yield (~60%) and low free carbon (~4 %) was demonstrated.

Studies on the thermal expansion of nanocrystalline boron carbide

5.0 Introduction

The value of coefficient of thermal expansion (CTE) of materials is an important factor required to address the problems such as thermally induced stresses between dissimilar materials in contact. In this regard, thermal expansion of nuclear fuels, neutron absorbers and clad materials is important in determining their performance in a nuclear reactor [157].

Materials used in nuclear reactors are subjected to high temperatures, steep temperature gradients and intense radiation fields during their lifetime. Measurement of thermal expansion of nuclear materials as a function of temperature is required to assess the dimensional changes during the operation of a nuclear reactor [158]. An important technique used for measuring the lattice thermal expansion is high temperature X-ray diffraction (HT-XRD) technique. The CTE in this case is determined from the lattice parameter values measured at different temperatures. Lattice thermal expansion data are useful supplement to the bulk thermal expansion data, normally measured using dilatometric techniques.

5.1 Thermal expansion of nanocrystalline materials

Nanocrystalline materials are of fundamental scientific interest as their physical properties can differ considerably from those of the corresponding bulk materials [127]. Both theoretical and experimental data on the thermal expansion of various nanocrystalline materials are reported in the literature [159–161]. Theoretical studies show that CTE increases with decrease in crystallite size [159]. Klam et al. [160] and Lu et al. [161] have reported such behaviour for copper and nanocrystalline Ni–P alloys respectively. However, in some cases it was observed to be independent of the crystallite size [159].

5.2 Literature survey on thermal expansion of boron carbide

Information on the high-temperature thermal expansion characteristics of boron carbide is very limited. Thevenot [23] in his review has reported the average CTE of boron carbide to be 4–8×10^{-6} K^{-1} in the temperature range 298–1073 K. Yakel [162] has measured the CTE of boron carbides in the temperature range 285–1213 K by using HT-XRD technique and reported the values to be 5.65×10^{-6} $^{\circ}C^{-1}$ and 5.87 ×10^{-6} $^{\circ}C^{-1}$ for a carbon rich boron carbide phase and a boron rich boron carbide phase respectively. Tsagareishvili et al. [163] also measured the CTE of boron carbide in the temperature range of 298–1213 K by using the HT-XRD technique and reported a value of 5.73 ×10^{-6} K^{-1}. The novel methods based on gel precursor route developed in this study for the synthesis of boron carbide yielded nanocrystalline boron carbide. However, data on the thermal expansion of nanocrystalline boron carbide are not available in the literature.

In the present study, thermal expansion values of both nanocrystalline and microcrystalline boron carbides were measured by HT-XRD technique. The experimentally measured data for the nanocrystalline boron carbide are compared with those obtained for microcrystalline boron carbide.

5.3 Experiment

5.3.1 Sample Preparation

Nanocrystalline boron carbide was prepared from boric acid-sucrose gel precursor. The details of the synthesis are given in Section 4.1 of Chapter 4. Microcrystalline boron carbide was procured from M/s. Boron Carbide Pvt. India Ltd., Mumbai.

5.3.2 Thermal expansion studies

The thermal expansion of boron carbide was measured from 298 to 1773 K by HT-XRD technique. The HT-XRD measurements were performed by using a Philips-X’pert MPD system, equipped with the Buhler’s high vacuum heating stage. Details of the high temperature X-ray diffractometer and measurement conditions are given in Section 2.3.2.5.1 of Chapter 2.

5.4 Results and discussion

5.4.1 X-ray diffraction studies

Fig. 5.1 shows the room temperature (298 K) XRD patterns of the nanocrystalline and microcrystalline boron carbides. It is observed from the XRD patterns that boron carbide crystallizes in a rhombohedral crystal structure. The average crystallite size of boron carbide prepared from boric acid-sucrose gel precursor is 55 nm (designated as N-B_4C) and that of boron carbide prepared by conventional carbothermic reduction is 300 nm (designated as M-B_4C). The room temperature lattice parameters of N-B_4C are a = 0.5602 nm and c = 1.2091 nm and those of M-B_4C are a = 0.5601 nm and c = 1.2091 nm. The diffraction patterns and the lattice parameter values are in good agreement with those reported in JCPDS file No. 35-0798.

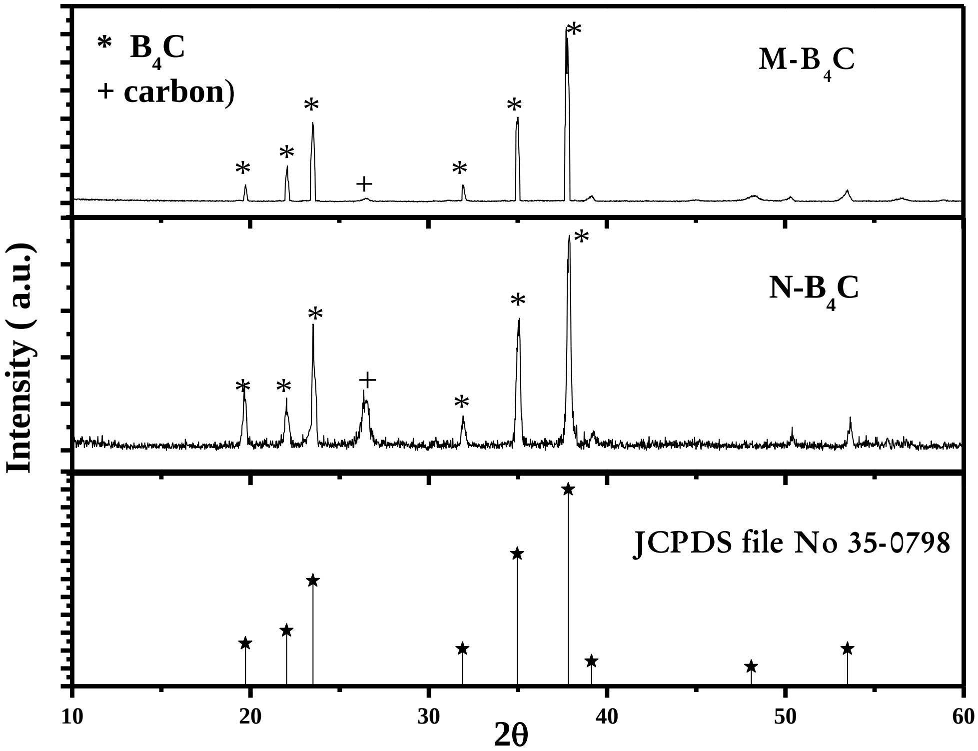

Fig. 5.1 Room temperature XRD patterns of N-B_4C and M-B_4C. JCPDS (35-0798) pattern of boron carbide is included for the purpose of comparison

5.4.2 Thermal expansion studies

Fig. 5.2 shows the variation of lattice parameter, '*a*', of both N-B_4C and M-B_4C as a function of temperature along a axis. Similarly Fig. 5.3 shows the variation of lattice parameter, '*c*', of both N-B_4C and M-B_4C as a function of temperature along c axis. These data are also given in Tables 5.1 and 5.2. For the purpose of calculating thermal expansion, data on the corrected lattice parameter as a function of temperature are fitted to a second-degree polynomial in temperature increment (T-298). It is seen that the lattice parameters increase monotonically with temperature. The relevant fit expressions are given below for both M-B_4C (Eqs. (5.1) and (5.2)) and N-B_4C (Eqs. (5.3) and (5.4)).

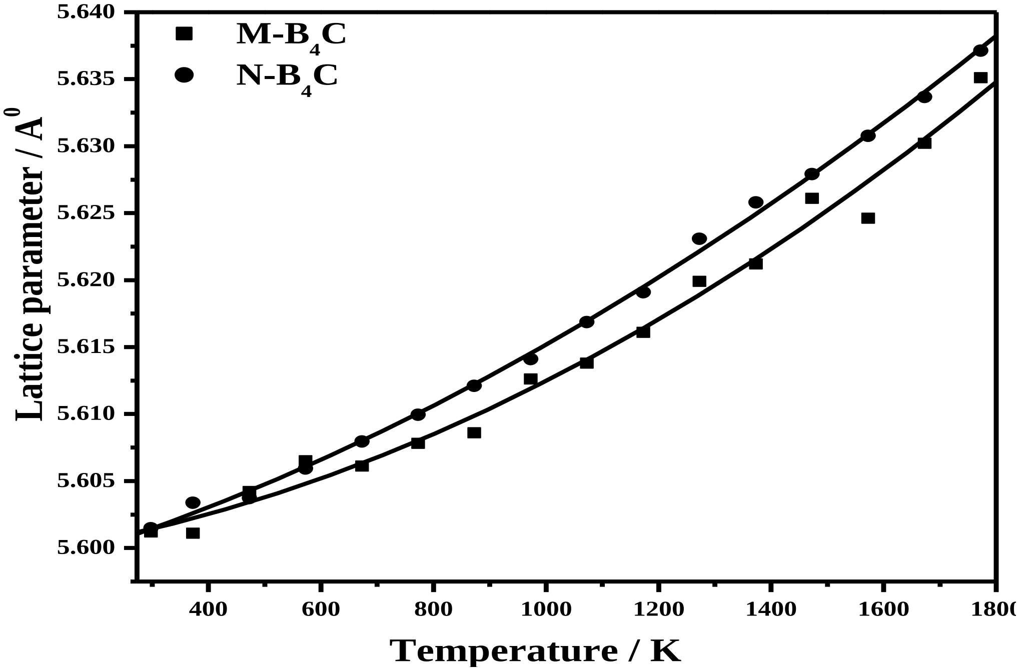

Fig. 5.2 The variation of lattice parameter (*a*) with temperature for both N-B_4C and M-B_4C (polynomial fit is also shown).

For M-B_4C:

a (nm) = $8.0908\times10^{-10}(T-298)^2+5.2418\times10^{-7}(T-298)+0.5599$ (5.1)

c (nm) = $2.7382\times10^{-9}(T-298)^2+1.2719\times10^{-6}(T-298)+1.2085$ (5.2)

For N-B_4C:

a (nm) = $8.5188\times10^{-10}(T-298)^2+6.2606\times10^{-7}(T-298)+0.5600$ (5.3)

c (nm) = $2.9407\times10^{-9}(T-298)^2+1.9671\times10^{-6}(T-298)+1.2083$ (5.4)

where T is in Kelvin.

Table 5.1 The lattice parameter, % thermal expansion as a function of temperature, instantaneous (α_i), mean (α_m), relative (α_r), average (α_{ave}) thermal expansivities for nanocrystalline boron carbide

		α_i	α_r	α_m	% TE	*c*	α_i	α_r	α_m	%TE	α_{ave}
T (K)	*a* (nm)		($10^{-6}K^{-1}$)			(nm)		($10^{-6}K^{-1}$)			($10^{-6}K^{-1}$)
298	0.560262	2.02	2.02	2.02	0.000	1.209147	3.07	3.08	3.08	0.000	2.38
373	0.560352	2.25	2.25	2.25	0.016	1.209443	3.44	3.44	3.44	0.024	2.65
473	0.560487	2.55	2.56	2.56	0.040	1.209888	3.92	3.93	3.93	0.061	3.01
573	0.560638	2.86	2.86	2.86	0.067	1.210393	4.41	4.41	4.42	0.103	3.38
673	0.560807	3.16	3.17	3.16	0.097	1.210956	4.89	4.9	4.9	0.15	3.74
773	0.560993	3.46	3.47	3.47	0.130	1.211578	5.37	5.39	5.39	0.201	4.11
873	0.561196	3.77	3.77	3.77	0.167	1.212258	5.85	5.87	5.88	0.257	4.47
973	0.561416	4.07	4.08	4.08	0.206	1.212998	6.33	6.36	6.36	0.318	4.84
1073	0.561653	4.37	4.38	4.38	0.248	1.213796	6.82	6.85	6.85	0.385	5.20
1173	0.561906	4.67	4.69	4.68	0.294	1.214654	7.29	7.33	7.34	0.455	5.57
1273	0.562177	4.97	4.99	4.99	0.342	1.21557	7.77	7.82	7.82	0.531	5.93
1373	0.562465	5.27	5.30	5.29	0.393	1.216544	8.25	8.31	8.31	0.612	6.30
1473	0.562771	5.57	5.60	5.60	0.448	1.217578	8.72	8.79	8.8	0.697	6.66
1573	0.563093	5.87	5.90	5.90	0.505	1.218671	9.2	9.28	9.28	0.788	7.03
1673	0.563432	6.17	6.21	6.21	0.566	1.219822	9.67	9.76	9.77	0.883	7.39
1773	0.563788	6.47	6.51	6.51	0.629	1.221032	10.14	10.25	10.26	0.983	7.76

Table 5.2 The lattice parameter, % thermal expansion as a function of temperature, instantaneous (α_i), mean (α_m), relative (α_r), average (α_{ave}) thermal expansivities for microcrystalline boron carbide

T (K)	*a* (nm)	α_i	α_r	α_m	% TE	*c* (nm)	α_i	α_r	α_m	%TE	α_{ave} ($10^{-6}K^{-1}$)
			($10^{-6}K^{-1}$)					($10^{-6}K^{-1}$)			
298	0.56014	1.8	1.8	1.8	0.000	1.209122	2.4	2.4	2.4	0.000	2.00
373	0.56022	2.01	2.01	2.01	0.014	1.209355	2.74	2.74	2.74	0.019	2.26
473	0.56034	2.3	2.3	2.3	0.036	1.209714	3.19	3.19	3.19	0.049	2.60
573	0.56048	2.59	2.59	2.59	0.06	1.210128	3.64	3.65	3.65	0.083	2.94
673	0.56063	2.88	2.88	2.88	0.088	1.210596	4.09	4.1	4.1	0.122	3.29
773	0.5608	3.16	3.17	3.17	0.118	1.211119	4.55	4.55	4.55	0.165	3.63
873	0.56098	3.45	3.46	3.46	0.151	1.211697	5	5.01	5.01	0.213	3.97
973	0.56119	3.74	3.75	3.75	0.187	1.21233	5.44	5.46	5.46	0.265	4.32
1073	0.5614	4.02	4.04	4.04	0.226	1.213017	5.89	5.91	5.91	0.322	4.66
1173	0.56164	4.31	4.32	4.32	0.268	1.21376	6.34	6.37	6.36	0.384	5.00
1273	0.56189	4.6	4.61	4.61	0.312	1.214556	6.79	6.82	6.82	0.449	5.35
1373	0.56215	4.88	4.9	4.9	0.36	1.215408	7.23	7.27	7.27	0.52	5.69
1473	0.56244	5.17	5.19	5.19	0.411	1.216315	7.68	7.73	7.72	0.595	6.04
1573	0.56274	5.45	5.48	5.48	0.464	1.217276	8.12	8.18	8.18	0.674	6.38
1673	0.56305	5.74	5.77	5.77	0.52	1.218292	8.56	8.63	8.63	0.758	6.72
1773	0.56338	6.02	6.06	6.06	0.579	1.219363	9.01	9.08	9.08	0.847	7.07

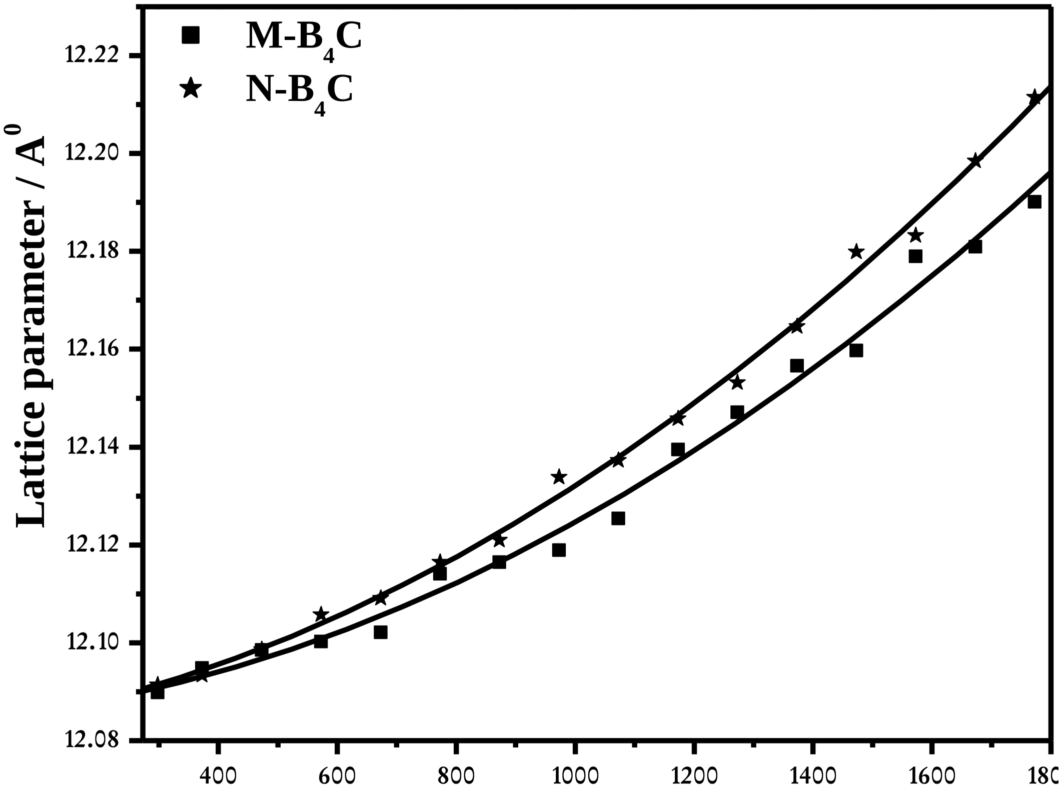

Fig. 5.3 The variation of lattice parameter (c) with temperature for both N-B_4C and M-B_4C (polynomial fit is also shown).

Once the lattice parameter is known as a function of temperature, it is possible to estimate the instantaneous (α_i-instantaneous), mean (α_m-mean), relative (α_r-relative) and average (α_{ave}) CTEs by the following relations:

$$\alpha_i = (1/a_T)(da_T/dT) \quad (5.5)$$

$$\alpha_m = (1/a_{298})\{(a_T - a_{298})/(T - 298)\} \quad (5.6)$$

$$\alpha_r = (1/a_{298})(da_T/dT) \quad (5.7)$$

$$\alpha_{ave} = \frac{[2\alpha_a + \alpha_c]}{3} \quad (5.8)$$

$$\% \text{ Thermal expansion} = 100 \times \{(a_T - a_{298})/a_{298}\} \quad (5.9)$$

In the above expressions (Eqs. 5.5-5.9), a_T represents the lattice parameter at temperature T and a_{298} is the corresponding value at 298 K. The percentage linear thermal expansion values computed using Eq. (5.9) were fitted to a second-degree polynomial in temperature and the expressions are given below.

For M-B_4C:

$$\% \text{ Expansion (a axis)} = 1.442094\times10^{-7}\times T^2+9.406820\times10^{-5}\times T-0.04094628 \quad (5.10)$$

$$\% \text{ Expansion (c axis)} = 2.263169\times10^{-7}\times T^2+1.054712\times10^{-4}\times T-0.05164089 \quad (5.11)$$

For N-B_4C:

$$\% \text{ Expansion (a axis)} = 1.517726\times10^{-7}\times T^2+1.123957\times10^{-4}\times T-0.04712794 \quad (5.12)$$

$$\% \text{ Expansion (c axis)} = 2.433414\times10^{-7}\times T^2+1.626109\times10^{-5}\times T-0.07019606 \quad (5.13)$$

Fig. 5.4 compares the percentage linear thermal expansion obtained for both N-B_4C and M-B_4C along a and c axes. The average CTE (α_{ave}) values from 298 to 1773 K for both M-B_4C and N-B_4C are:

$$\alpha_{ave} = 5.30656\times10^{-15}T^2+3.63777\times10^{-9}\ T + 1.29243\times10^{-6} \quad \text{(for M-B}_4\text{C)} \quad (5.14)$$

$$\alpha_{ave} = 6.02386\times10^{-15}T^2+3.42333\times10^{-9}\ T + 9.79992*10^{-7} \quad \text{(for N-B}_4\text{C)} \quad (5.15)$$

5.4.3 Discussion

It is observed in the present study that the lattice parameters *a* and *c* increase monotonically with temperature. From Figs. 5.2 and 5.3, it is also observed that the lattice parameters of N-B_4C are relatively higher compared to those of M-B_4C along both a and c axes. The average CTE (α_{ave}) of M-B_4C is 5.34×10^{-6} K^{-1} in the temperature range 298-1213 K. This is in reasonable agreement with the value reported in the literature (5.65×10^{-6} K^{-1}) [163]. The average CTE of N-B_4C ($\alpha_{ave} = 7.76\times10^{-6}$ K^{-1}) is marginally higher than that of

M-B_4C ($\alpha_{ave} = 7.07\times10^{-6}\ K^{-1}$) in the temperature range 273–1773 K. This difference is explained as follows.

With decrease in crystallite size, the surface to volume ratio increases. Consequently the number of atoms at the interface or grain boundary increases. According to Kuru et al. [159], atoms at the surface or at grain boundary are not saturated with respect to their state of bonding since their coordination number is less than that for the bulk atoms. In addition, surface atoms are less restricted in their ability to vibrate and they are able to make larger excursions from their equilibrium positions [164]. As a consequence of these atoms at the

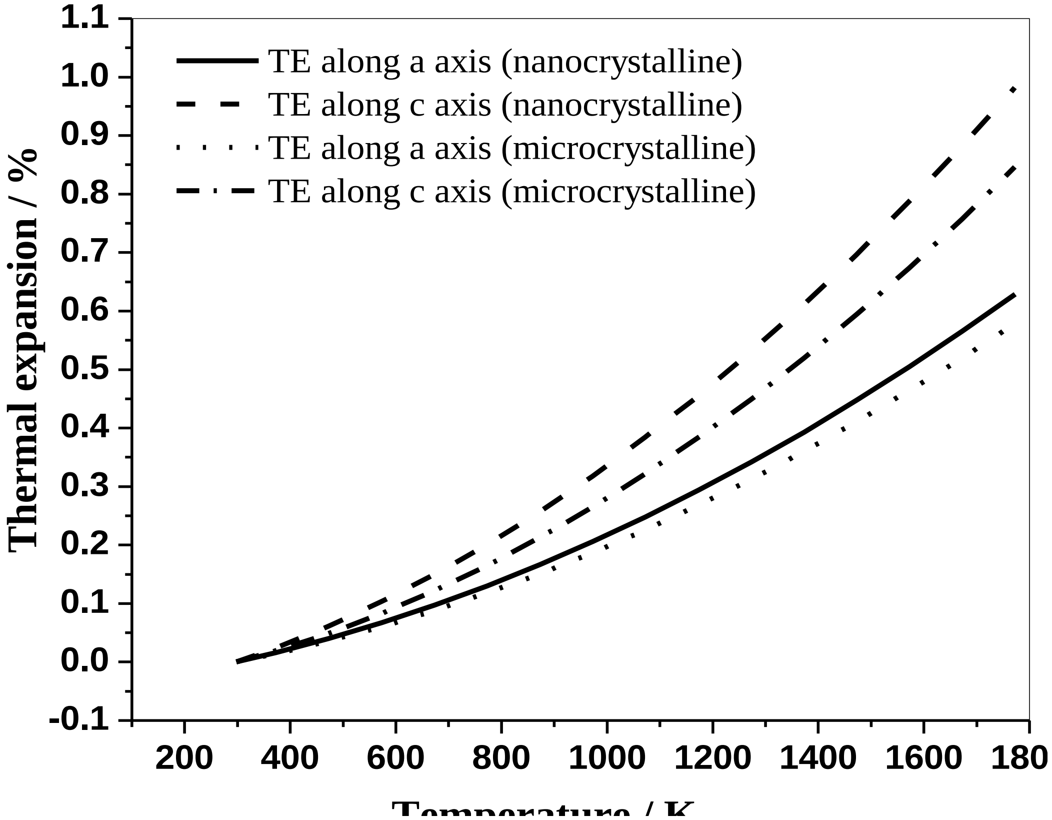

Fig. 5.4 The percentage linear thermal expansion estimated from the lattice parameter of both N-B_4C and M-B_4C along both a and c axis

surface have higher vibrational kinetic energy than the bulk atoms. Sugano et al. [165] prepared gold clusters containing approximately 460 atoms. The electron micrograph of these nanoparticles taken at various times show fluctuation-induced changes in the structure, which supports that the atoms at the surface have higher vibrational kinetic energy than the bulk. This leads to a larger atomic position variation of atoms at the surface than the bulk atoms due to the thermal vibration. Hence, smaller the crystal, larger would be its average thermal expansion coefficient.

The presence of grain boundary can cause an increase in the spacing between atomic planes near the boundary [166]. Barbara et al. [166] studied the influence of the presence of grain boundaries on thermal expansion of nanocrystalline nickel using classical molecular-dynamics simulations with embedded-atom-method potentials and inferred that the presence of grain boundaries cause a slight increase in thermal expansion. This is in agreement with the results of the present study.

5.5 Conclusions

The lattice parameters and CTE of nano crystalline and microcrystalline boron carbides were measured by HT-XRD technique. The average thermal expansion coefficient in the temperature range 298-1773 K for the nanocrystalline and the microcrystalline boron carbide were found to be 7.76×10^{-6} K^{-1} and 7.07×10^{-6} K^{-1} respectively. The results show that the average thermal expansion coefficient of nano crystalline boron carbide is marginally higher than that of microcrystalline boron carbide. A generalized expression was derived from the experimental data in the temperature range between 298 and 1773 K for nanocrystalline and microcrystalline boron carbides.

Development of an alternate method for the digestion of boron carbide for its chemical assay

6.0 Introduction

This chapter discusses the development of an alternate method for the digestion of boron carbide. A simple and fast digestion method was developed for the determination of boron, isotopic ratio of $^{10}B/^{11}B$ and trace elements (Al, Cd, Co, Cr, Cu, Fe, Mg, Mn, Mo, Ni, Pb and Zn) in boron carbide. The boron carbide was digested in an acid mixture using a simple apparatus. The validity and accuracy of the digestion technique developed in this study for the determination of boron, trace elements and isotopic ratio of $^{10}B/^{11}B$ were established by comparing the results of the analysis with those obtained by conventional sodium carbonate fusion method.

6.1 Experimental

6.1.1 Sample preparation

The granules (1-2 mm diameter) of boron carbide were powdered and this powder was graded into different size fractions using a sieve shaker with stack that comprised of 350, 250, 180, 125 and 90 µm stainless steel sieves (M/s. Firtsch GmbH, Germany). These size fractions were collected separately and used in this study.

6.1.2 Digestion of boron carbide

A quartz vessel of 50 mL capacity was designed for the digestion of boron carbide and the details of the quartz vessel are given in Section 2.2.3 of Chapter 2.

In a typical experiment, about 100 mg of boron carbide (particle size < 90 µm) was weighed and taken in the quartz vessel. 2 mL of concentrated sulphuric acid (36 N) was added to this powder, mixed and heated on a hot plate at 473±10 K. To this hot solution, an aliquot of 10 µL of quartz distilled nitric acid was added slowly through the capillary using a pipette. A vigorous reaction took place with the release of brown fumes and the temperature of the solution decreased considerably. Therefore, the solution was heated to raise the temperature to 473 K before the addition of next aliquot of HNO_3. Addition of quartz distilled nitric acid was continued until complete digestion of boron carbide and the solution became clear and colourless. After complete digestion of boron carbide, the vessel was maintained at 473 K for a further duration of 1 h. The total time taken for the entire process was 2 h. The solution was then allowed to cool to room temperature and transferred to a standard 100 mL polypropylene volumetric flask and made upto 100 mL. From this solution, an aliquot of 20 mL was used for the determination of boron by titrating it as a mannitol-boric acid complex using standard potassium hydroxide solution. The details of titration are given in Section 2.3 of Chapter 2.

Digestion experiments were carried out using boron carbide powders with various particle size ranges. In order to ascertain the validity and accuracy of this digestion method for the determination of boron, the same lot of boron carbide samples were digested using conventional sodium carbonate fusion method and the amount of boron in these samples were determined.

6.1.3 Determination of trace elements in boron carbide

6.1.3.1 Preparation of standard solutions containing trace elements

Specpure-grade metals/oxides and certified standard solutions (containing 1 mg / mL) were used for the preparation of stock solution containing Cd, Pb, Co, Mo, Cr, Cu, Ni, Mn, Zn, Fe, Mg and Al. This stock solution was used for the standard addition studies and preparation of calibration standard solutions to calibrate ICP-MS. Calibration standard solutions containing Cd, Pb, Co and Mo ranging from 1 ng to 20 ng / mL, Cr, Cu, Ni and Mn ranging from 5 ng to 100 ng / mL and Zn, Fe, Mg and Al ranging from 100 ng to 1000 ng / mL were prepared from the above stock solution. 0.1 N acidity was maintained for all these solutions.

6.1.3.2 Estimation of trace elements in boron carbide

In order to validate the suitability of the digestion method developed in this study for the determination of trace elements present in boron carbide by ICP-MS method, standard addition method was employed due to non-availability of boron carbide standard reference materials. For this purpose, about 25 mg boron carbide (particle size < 90 µm) sample was weighed and transferred to the quartz vessel. 50 µL of the stock solution was added to the powder and dried at 353 K for 2 h. 1 mL of H_2SO_4 (36 N) was added to it and digested as discussed in Section 6.1.2. The digestion was carried out in duplicate. After complete digestion, the solution was transferred and made up to 10 mL in a polypropylene vial with double distilled water. Similar digestion experiments were carried out with the addition of 100 and 200 µL of stock solutions (in duplicate) to boron carbide.

6.1.3.3 Isotopic analysis of boron in boron carbide

About 10 mg each of natural boron carbide (containing 80 at% ^{11}B and 20 at% ^{10}B) and enriched boron carbide (containing 35 at% ^{11}B and 65 at% ^{10}B) samples were digested independently as described in Section 6.1.2. The solutions were made upto 10 mL in polypropylene vial and used for the analysis of isotopic ratio by using ICP-MS. In order to check the accuracy of the present digestion method coupled with ICP-MS for the analysis of isotopic ratio, both natural boron carbide and enriched boron carbide samples were analyzed by using Thermal Ionization Mass Spectrometry (TIMS) after digesting these samples by conventional sodium carbonate fusion technique.

6.2 Results and discussion

6.2.1 Estimation of boron

Sulphuric acid acts as a medium for the digestion process. The possible reaction of boron carbide with nitric acid is shown below:

$$B_4C + 12\ HNO_3 \rightarrow 4\ H_3BO_3 + CO_x + 12NO_X \quad (6.1)$$

The reaction was found to be endothermic since the temperature of the solution dropped from 473 to around 420 K. Initial experiments were carried out using a quartz vessel with a straight vent tube of 8 mm dia and 100 mm long. However, the estimated value of boron in boron carbide was found to be lower than the actual value. The loss of boron might be due to sudden sputtering of the solution during the addition of nitric acid. In order to avoid this loss, a spiral vent tube was used instead of the straight vent tube. In addition, it was necessary to add nitric acid in small quantities through the capillary tube. Hence the tip of the capillary tube was dipped well inside sulphuric acid to enhance the interaction of nitric acid with boron carbide dispersed in sulphuric acid, facilitating the digestion reaction in a shorter time. As the digestion was carried out using concentrated sulphuric acid, there could be a difference in the nebulization rates of the sample and the standard solutions in the analysis using ICP-MS. In order to eliminate this problem, the digested solution was diluted to bring down the matrix concentration to 1 mg/mL. The final concentration of sulphuric acid in this solution is 0.36 N. This dilution (~100 times) brings the minimum detection limit to ~4 ppm of boron. However, in the case of conventional sodium carbonate fusion method, the dilution is to the extent of ~500 times which causes the detection limit to be around 200 ppm.

The variation of time and quantity of nitric acid required for the digestion of boron carbide with the average particle size is given in Table 6.1 and also shown in Fig. 6.1. When boron carbide powder sample of particle size <90 µm was used, the digestion could be completed within about 20 minutes and the volume of nitric acid consumed was only about 2.4 mL.

The average particle size given in Fig. 6.1 represents the arithmetic mean of the extreme values of the particles in a typical size range assuming unimodal distribution. For example for those particles falling in the size range 90-125 µm, the average size is taken as 107.5 µm. The time and quantity of nitric acid required for the digestion were found to increase with increasing size of boron carbide particles.

Table 6.1 Variation of the digestion time and volume of nitric acid required for the digestion of boron carbide with particle size

Quantity of boron carbide (mg)	Particle size range (µm)	Digestion time (min)	Quantity of nitric acid consumed (mL)
46.5	< 90	20±1	2.4±0.1
40.1	90-125	35±1	2.8±0.2
44.4	125-180	45±2	3.3±0.1
40.1	180-250	65±1	4.1±0.1
39.9	250-350	66±2	4.2±0.3

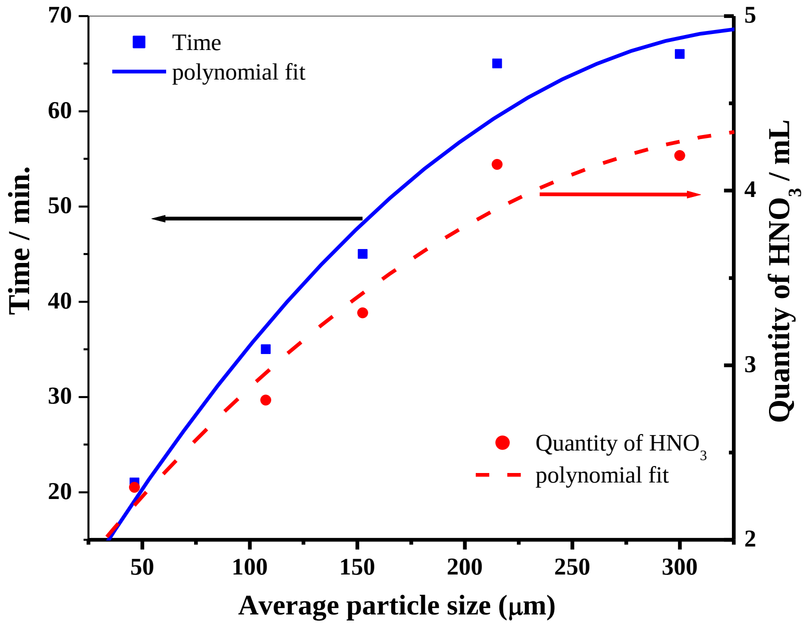

Fig. 6.1 Variation of digestion time and quantity of nitric acid with average particle size

Table 6.2 shows the results of the estimation of boron in boron carbide samples employing the digestion technique developed in this study. The accuracy and precision of the method were obtained from the results of the analyses of ten samples of the same lot of boron carbide having particle size < 90 μm. The results show a precision of 0.4 % (RSD). Table 6.2 also shows the results of the estimation of boron in boron carbide samples employing conventional digestion process (sodium carbonate fusion). The boron carbide samples employed in both the digestion experiments were from the same lot. The results of 6 determinations show a precision of 0.2% (RSD). Comparing the results of the analyses of boron in boron carbide samples employing these two digestion techniques, the accuracy of the present analytical method was found to be 99.8%.

Table 6.2 Results of the analysis of boron in boron carbide

Boron carbide digested by the method developed in this study				Boron carbide digested by conventional sodium carbonate fusion method			
Weight of boron carbide (mg)	% B	Average (% Boron)	Standard Deviation(σ)	Weight of boron carbide (mg)	% B	Average (% Boron)	Standard Deviation(σ)
109.2	78.77	78.9	0.4			79.0	0.2
104.6	79.26						
102.9	79.8			102.1	79.27		
104.4	78.48			105.6	78.98		
104.2	78.51			101.9	78.86		
109.4	78.35			104.6	79.12		
108.5	79.51			103.5	78.95		
104.6	79.30			107.2	79.05		
105.1	78.57						
102.9	79.18						

6.2.2 Determination of trace elements

Standard additions in three different concentrations (with duplicates) were employed for each analyte. The mean recovery and relative standard deviation were calculated from twelve determinations (Table 6.3). The amount of the element added/recovered is expressed in terms of concentration with respect to the mass of boron carbide sample. Good recoveries were obtained for Cr, Co, Cu, Cd, Ni, Fe, Mn, Pb, Zn and Mo. Matrix interference in the analysis of trace elements present in the solutions obtained through the digestion of boron carbide developed in this study by ICP-MS, is minimum when the concentration of boron in these solutions is less than 1 mg/mL. Table 6.4 shows the results of the ICP-MS analysis of trace elements present in boron carbide as impurities. The digestion of boron carbide in quartz vessel has not introduced impurities as can be seen from the blank values given in Table 6.4. Each value given in Table 6.4 is the mean of six determinations. The experimental blank was found to be in the range of 1–10 ng / mL for impurities Cd, Co, Cr, Cu, Mn, Mo, Ni, Pb, Zn and upto 30 ng /mL for Mg Al and Fe. The detection limits (Table 6.4) were calculated as the concentration equivalent to three times the standard deviation obtained with the experimental blank. The detection limits for various elements were found to be in ppb levels except for Fe, Mg and Al. Results of standard additions for the analytes Mg and Al were not consistent due to high blank values. Recoveries for Pb and Cd were quantitative inspite of digestion at 473 K indicating the reliability of this method for the determination of these elements in boron carbide. Table 6.5 compares the limits of detection of the present method with other methods reported in the literature [136, 138, 142, 167].

Table 6.3 Results of the recoveries of trace elements by standard addition method (digestion by the present method)

Elements	Amount added $\mu g\ g^{-1}$	Mean amount recovered $\mu g\ g^{-1}$	Mean Recovery (%)	RSD (%)
Al	50	38		
	100	91	87	18
	200	187		
Cd	2.5	2.36		
	5	4.72	94.5	2.3
	10	9.5		
Co	1.6	1.7		
	3.2	3.15	102.9	4.4
	6.4	6.47		
^{53}Cr	25	26.2		
	50	48.9	97.9	11
	100	92		
Cu	5	4.73		
	10	9.5	95	4
	20	19.1		
^{57}Fe	875	905		
	1750	1790	104	3
	3500	3725		
Mg	50	66		

	100	93	100	15
	200	170		
Mn	5	5.5	102	6.6
	10	9.9		
	20	19.6		
Mo	2.5	2.42	98.5	6.6
	5	5		
	10	9.25		
^{60}Ni	50	51	102	3
	100	102		
	200	207		
Pb	3.5	3.65	100	5.4
	7	7.1		
	14	13.25		
Zn	500	563	109	5.6
	1000	1098		
	2000	2088		

Table 6.4 Results of the analysis of trace elements in boron carbide (digestion of boron carbide by the present method) by ICP-MS

Element	Mean concentration measured (n=6)\µg g^{-1}	Detection limits µg g^{-1}	Blank µg/mL
Al	< 20	-	20
Cd	< 0.1	0.1	0.2
Co	0.84 ± 0.025	0.01	0.012
^{53}Cr	102 ± 3.7	0.04	0.13
Cu	3.2 ± 0.13	0.16	0.4
^{57}Fe	3115 ± 160	25	38
Mg	< 30	30	35
Mn	10.8 ± 0.39	0.07	0.1
Mo	1.34 ± 0.056	0.03	0.03
^{60}Ni	124 ± 6.0	0.18	0.36
Pb	2.9 ± 0.07	0.5	0.04
Zn	590 ± 35	3	6.4

Table 6.5 Comparison of limits of detection for trace metals present in boron carbide determined in the present study with other methods reported in the literature. Limits of detection is given in µg g^{-1}

Element	Present method	Other methods				
		Microwave-assisted acid digestion Neb-ICP-OES [142]	Slurry introduction axial viewed ICP-OES [142]	Total reflection X-ray fluorosence spectrometry [138]	DC-arc OES [136]	SIS-ETV-ICP-OES [167]
Al	-[a]	12	2	-[a]	8.5	0.9
Cd	0.1	-[a]	-[a]	-[a]	-[a]	
Co	0.01	-[a]	-[a]	0.1	-[a]	0.15
Cr	0.04	1	0.2	0.3	9.3	0.25
Cu	0.16	2	0.3	0.1	2.2	0.18
Fe	25	0.6	0.1	0.2	28	0.15
Mg	30	3	0.02	-[a]	0.3	0.002
Mn	0.07	2	0.04	0.3	0.92	0.015
Mo	0.03	-[a]	-[a]	-[a]	-[a]	-[a]
Ni	0.18	10	0.4	0.1	-[a]	2
Pb	0.5	-[a]	-[a]	-[a]	-[a]	-[a]
Zn	3	-[a]	-[a]	-[a]	-[a]	-[a]

-[a] not determined

SlS-ETV-ICP-OES : Slurry Sampling Electrothermal evaporation Inductively Coupled Plasma Optical Emission spectrometry

Neb ICP-OES: Nebulization Inductively Coupled Plasma Optical Emission spectrometry

6.2.3 Determination of $^{10}B/^{11}B$ isotopic ratio

Table 6.6 compares the results of the determination of $^{10}B/^{11}B$ ratio by ICP-MS with those determined by using TIMS. The isotopic ratios of boron present in both natural and enriched boron carbides, determined after digesting the samples by the present method followed by the analysis of the solution by ICP-MS are in good agreement with those obtained through sodium carbonate fusion method followed by the analysis by TIMS. Since the sample size required for the present digestion method is very small, this method can be employed for the determination of isotopic content of boron in irradiated boron carbide (control rod material in nuclear reactors) samples without elaborate experimental arrangements in hot cells. The apparatus can be housed inside a fumehood or glove box for the digestion of irradiated boron carbide.

Table 6.6 $^{10}B/^{11}B$ isotopic ratio in natural as well as enriched boron carbides

Sample	ICP MS (solution obtained employing present digestion method)*	TIMS (solution obtained employing Na_2CO_3 fusion technique)*
Natural boron carbide	0.2490±0.0035	0.2473±0.0009
Isotopically enriched boron carbide	0.661±0.013	0.6596±0.0079

* same lot of boron carbide used for both the digestion techniques

6.3 Conclusions

A simple and fast method was developed for the digestion of boron carbide. This method enables the determination of total boron, isotopic ratio of $^{10}B/^{11}B$ and trace metal impurities present in boron carbide in a shorter period of time compared to conventional techniques. The use of expensive platinum crucibles for digestion is eliminated. The advantages of the present method are the use of a simple apparatus, fast digestion process and small sample size for isotopic analysis. The accurate determination of total boron, isotopic ratio of $^{10}B/^{11}B$ and trace elements in boron carbide powders is also demonstrated.

Summary and Conclusions

Thermodynamic equilibrium calculations were carried out on the system B-O-C using FactSage 6.2 in order to identify the optimum reduction temperature and mole ratio of B_2O_3 to C for the preparation of boron carbide by carbothermic reduction process. Novel and energy efficient methods were developed for the synthesis of nanocrystalline boron carbide, based on gel precursor route. A simple and fast method was developed for the digestion of boron carbide for the determination of boron, isotopic ratio of $^{10}B/^{11}B$ and trace elements (Al, Cd, Co, Cr, Cu, Fe, Mg, Mn, Mo, Ni, Pb and Zn) present in it. Thermal expansion of boron carbide was measured by high temperature X-ray diffraction technique.

7.1 Thermodynamic analysis of carbothermic reduction of boric oxide

Thermodynamic equilibrium calculations were carried out on the system B-O-C using FactSage 6.2 in order to identify the optimum reduction temperature and mole ratio of B_2O_3 to C for the preparation of boron carbide by carbothermic reduction process. The thermodynamic stability region of $B_2O_{3(l)}$, $B_4C_{(s)}$, $B_4C_{(l)}$, $B_{(s)}$, $B_{(l)}$ and $C_{(s)}$ for a mixture of B_2O_3 and C with C to B_2O_3 mole ratio of 0.5 to 1.75 in the temperature range 298-3573 K have been established. Based on these calculations, the optimum reduction temperature and stoichiometry of the reaction mixture were identified.

7.2 Synthesis of nanocrystalline boron carbide from gel precursors

In order to prepare nanocrystalline boron carbide, suitable gel precursors were developed in the present study. Systematic studies were carried out to optimize the process parameters such as stoichiometry of the reactants, pyrolysis temperature etc. The precursors and boron carbide prepared from these precursors were characterized by chemical analysis and X-ray diffraction method. The physical properties such as specific surface area, bulk density and particle size distribution were also measured for the final product. The crystallite size of the powders was determined by the X-ray line broadening technique. The microstructure and surface morphology were studied using scanning electron microscopy and transmission electron microscopy. The performance of boric acid and boric oxide as boron sources and sucrose and citric acid as the carbon sources for the preparation of gel precursors was compared. The studies led to the following conclusions.

1. The products obtained through the gel precursor route were found to be nanocrystalline, free flowing and porous.
2. The yield of boron carbide could be improved by using a specially designed graphite cylinder with lids as the reaction vessel.
3. This study clearly brings out the fact that the use of sucrose as a gel forming agent has definite advantages over the use of citric acid.
4. This study also brings out the fact that the use of boric oxide as a boron source has definite advantages (in improving the yield and lowering the free carbon residue in boron carbide) over the use of boric acid.
5. The yield is maximum (~60%) with minimum carbon content (~4%) when the boric oxide and sucrose were used as boron source and carbon source respectively.

7.3 Studies on the development of a method for the digestion of boron carbide for its chemical assay

A simple and fast digestion method was developed for the determination of boron, isotopic ratio of $^{10}B/^{11}B$ and trace elements (Al, Cd, Co, Cr, Cu, Fe, Mg, Mn, Mo, Ni, Pb and Zn) in boron carbide. Boron carbide was digested using an acid mixture in a simple quartz apparatus. Boron was subsequently determined by the conventional method of titration of mannitol-boric acid complex using the standard potassium hydroxide solution. Trace elements and isotopic ratio of $^{10}B/^{11}B$ were determined by using inductively coupled plasma mass spectrometer. The digestion technique developed in this study was validated by comparing the analytical results with those obtained by conventional “sodium carbonate fusion” method. Comparison of the results of analyses of boron in boron carbide samples employing these two digestion techniques showed the accuracy of the present analytical method to be 99.8%. Good recoveries were obtained for Cr, Co, Cu, Cd, Ni, Fe, Mn, Pb, Zn and Mo. The new digestion technique facilitates relatively fast and accurate determination of total boron, its isotopic content and trace elements present in it. The use of expensive materials such as platinum crucibles is eliminated.

7.4 Studies on thermal expansion of nanocrystalline boron carbide

The thermal expansions of nanocrystalline (N-B_4C) and microcrystalline (M-B_4C) boron carbide were measured over the temperature range 298 to 1773 K by means of high temperature X-ray diffraction technique.

The generalized equations for the lattice parameters (both *a* and *c*) of both nanocrystalline and microcrystalline boron carbides (in nm) as a function of temperature are given below:

For M-B_4C:

$$a(\text{nm}) = 8.0908\times10^{-10}\,(T-298)^2 + 5.2418\times10^{-7}\,(T-298) + 0.5599 \tag{7.1}$$

$$c(\text{nm}) = 2.7382\times10^{-9}\,(T-298)^2 + 1.2719\times10^{-6}\,(T-298) + 1.2085 \tag{7.2}$$

For N-B_4C:

a (nm) = 8.5188×10^{-10} (T-298)^2 +6.2606×10^{-7} (T-298)+0.5600 (7.3)

c(nm) = 2.9407×10^{-9} (T-298)^2 +1.9671×10^{-6} (T-298)+1.2083 (7.4)

The percentage linear thermal expansions were evaluated from the temperature variation of lattice parameter in the temperature range 298 to 1773 K.

The generalized equations for the percentage linear thermal expansions of M-B_4C and N-B_4C are given below:

For M-B_4C:

% Expansion (a axis) = $1.442094\times10^{-7}\times T^2+9.406820\times10^{-5}\times T–0.04094628$ (7.5)

% Expansion (c axis) = $2.263169\times10^{-7}\times T^2+1.054712\times10^{-4}\times T–0.05164089$ (7.6)

For N-B_4C:

% Expansion (a axis) = $1.517726\times10^{-7}\times T^2+1.123957\times10^{-4}\times T–0.04.712794$ (7.7)

% Expansion (c axis) = $2.433414\times10^{-7}\times T^2+1.626109\times10^{-5}\times T–0.07019606$ (7.8)

The generalized equations for the temperature dependence of the coefficient of thermal expansion of both M-B_4C and N-B_4C are given below:

$\alpha_{ave} = 5.30656\times10^{-15}T^2+3.63777\times10^{-9}\ T + 1.29243\times10^{-6}$ (for M-B_4C) (7.9)

$\alpha_{ave}= 6.02386\times10^{-15}T^2+3.42333\times10^{-9}\ T + 9.79992*10^{-7}$ (for N-B_4C) (7.10)

The average thermal expansion coefficients in this temperature range for the nanocrystalline and the microcrystalline boron carbides were found to be 7.76×10^{-6} and 7.06×10^{-6} K^{-1} respectively. The difference observed in the thermal expansion behaviour is probably due to increase in the surface energy of the lattice in the nanocrystalline material.

Scope of future studies

This study has established the feasiblity of synthesis of nanocrystalline boron carbide using citric acid and sucrose as the carbon source and boric acid and boric oxide as the boron source. Systematic studies on sintering of boron carbide powders synthesized in this study using various methods viz., conventional sintering, microwave assisted sintering and spark plasma sintering can be studied to understand the sinterability of these powders.

This study clearly brings out the fact that the use of sucrose (containg 12 carbons) as a gel forming agent has definite advantages over the use of citric acid (containg 6 carbons). It will be of interest to study the feasibility of synthesis of boron carbide using gel forming agents which contain more than 12 carbons such as stearic acid. Studies to explore the feasiblity of synthesis of boron carbide using other boron sources such as borax is another interesting area as its melting point is higher than that of boric oxide and boric acid. This study would give a better understanding of the effect of boron source on the nature and quality of the powders prepared through gel precursors. Systematic studies can be carried out to explore the feasibility of microwave assisted synthesis of boron carbide from the gel precursors. This study may help to improve the yield of boron carbide as it is a bulk and uniform heating method.

It would be intersting to study the synthesis of boron carbide from boric acid/boric oxide and citric acid/sucrose gel precursors in presence of oxidants such as ammonium nitrate.

In the present study, thermal expansions of boron carbides with of two different average crystallite sizes (52 and 300 nm) have been measured. However, systematic studies on the effect of crystallite size on coefficient of thermal expansion could be studied in detail.

In the present study thermodynamic calculations were carried out to understand the carbothermic reduction of boric oxide. It would be of interest to carry out detailed thermodynamic modelling of carbothermic reduction of other boron sources viz., boric acid, borax.

References

[1] R.B. Grover, Subhash Chandra, Scenario for growth of electricity in India, Energ. Policy., 34 (2006) 2834–2847.

[2] M. Tashimo, K. Matsui, Role of nuclear energy in environment, economy, and energy issues of the 21st century-Growing energy demand in Asia and role of nuclear, Prog. Nucl. Energ., 50 (2008) 103-108.

[3] J. Parikh, K. Parikh, India’s energy needs and low carbon options, Energy, 36 (2011) 3650-3658.

[4] Integrated Energy Policy: Report of the Expert Committee, Government of India, Planning Commission, August 2006, New Delhi, India.

[5] S. K. Jain, Inevitability of Nuclear Power in the Asian Region, Energy Procedia., 7 (2011) 5-20.

[6] Anjan Chaki, R.K. Purohit, R. Mamallan, Low grade uranium deposits of India – a bane or boon, Energy Procedia., 7 (2011) 153–157.

[7] Turan Unak, what is the potential use of thorium in the future energy production technology?, Prog. Nucl. Energ., 37 (2000) 137-144.

[8] C. Ganguly, Development of plutonium based advanced LMFBR fuels and thoria based PHWR fuels in India, IAEA-TECDOC-352 (1985)107-127.

[9] C. Ganguly, R.N. Jayaraj, Characterization and quality control of nuclear fuels”, Allied Publishers Pvt. Ltd., New Delhi 2004.

[10] J. G. Coller, G. F. Hewitt, Introudction to Nuclear Power, Hemisphere Publishing Coroporation, USA.

[11] D. D. Sood, Nuclear Materials, Indian Association of Nuclear Chemists and

Allied Scientists, India, 1996, pp. 17-39.

[12] Benjamin M. Ma, Nuclear Reactor Materials and applications, Van Nostrand Reinhold Company Inc, United States of Americas, 1983.

[13] Vijayashree, S. Govindarajan, S.C. Chetal, Design of diverse safety rod and its derive mechanism of PFBR, Proc. of Seminor on Inherent Engineered Safety Aspects of PFBR Design, 30 April, 1996, IGCAR, Kalpakkam.

[14] D. E. Mahagin, R. E. Dahl, Nuclear Applications of Boron and the Borides in V. I.Matkovich. (Ed.). Boron and Refractory Borides. Berlin: Springer-Verlag; 1977.

[15] B. Kopelman, Mateirals for Nuclear Reactors, McGraw-Hill Book Company, Newyork, USA, 1959.

[16] Ioan Ursu, Physics and Technology of Nuclear Materials, Pergamon Press Ltd., England, 1985.

[17] V. R. Babu, R. Veerasamy, S. Patri, S. I. S. Raj, S.C.S.P. K. Krovvidi, S. K. Dash, C. Meikandamurthy, K. K. Rajan, P. Puthiyavinayagam, P. Chellapandi, G. Vaidyanathan, S.C. Chetal, Testing and qualification of Control & Safety Rod and its drive mechanism of Fast Breeder Reactor, Nucl. Eng. Des., 240 (2010) 1728–1738.

[18] V. R. Babu, S. Govindarajan, S.C. Chetal, Design of control & safety rod and its derive mechanism of PFBR, Proc. of seminar on Inherent Engineered Safety Aspects of PFBR Design, 30 April, 1996, IGCAR, Kalpakkam.

[19] C.K. Gupta, Materials in Nuclear energy applications, Vol 2 CRC Press, Inc., Boca Raton, Fluorida, USA 1989

[20] B. Kryger, J. M. Escleine in The nuclear fuel of pressurized water reactors and fast reactors design and behaviour, Edited by Henri Bailly, Denise Menessier, Claude Prunier, Lavoisier Publishing, France, 1999.

[21] M. T. Spohn, Boron carbide, Am. Ceram. Soc. Bull., 72 (1993) 88-89.

[22] S. Ulrich, H. Ehrhardt, J. Schwan, R. Samlenski, R. Brenn, Subplantation effect in magnetron sputtered superhard boron carbide thin films, Diamond Relat. Mater., 7 (1998) 835-838.

[23] F. Thevenot, Boron carbide– a comprehensive review, J. Eur. Ceram. Soc., 6 (1990) 205–225.

[24] R.R. Rigdway, Boron carbide, A new crystalline abrasive and wear-resisting product. Trans. Am. Electrochem. Soc., 66 (1934) 117-33.

[25] A.O. Sezer, J.I. Brand, Chemical vapor deposition of boron carbide, Mater. Sci., Eng. B, 79 (2001) 191-202.

[26] F. Thevenot, A review on boron carbide, Key Eng. Mater., 56-57 (1991) 59-88.

[27] Z. Han, Geyang Li, Jiawan Tian, Mingyuan Gu, Microstructure and mechanical properties of boron carbide thin films, Mater. Lett., 57 (2002) 899-903.

[28] L.G. Jacobsohn, R.K. Schulze, M.E.H. Maia da Costa, M. Nastasi, X-ray photoelectron spectroscopy investigation of boron carbide films deposited by sputtering, Surf. Sci. 572 (2004) 418–424.

[29] S. R. Murthy, Elastic properties of boron carbide, J. Mater. Sci. Lett., 4 (1985) 603–605.

[30] D. Jianxin, Erosion wear of boron carbide ceramic nozzles by abrasive air jets, Mater. Sci. Eng. A, A408 (2005) 227–233.

[31] L.G. Jacobsohn, M. Nastasi, L.L. Daemen, Z. Jenei, P. Asoka-Kumar, Positron annihilation spectroscopy of sputtered boron carbide films, Diamond Relat. Mater., 14 (2005) 201–205.

[32] G. Fanchini, V. Gupta, Adrian B. Mann, Manish Chhowalla, In Situ Monitoring of Structural Changes in Boron Carbide Under Electric Fields, J. Am. Ceram. Soc., 91 (2008) 2666–2669.

[33] S. Thangavel, S.V. Rao, K. Dash, J. Arunachalam, Determination of boron isotope ratios by Zeeman effect background correction-graphite furnace atomic absorption spectrometry, Spectrochim Acta Part B, 61 (2006) 314–318.

[34] K.A. Schwetz, L.S. Sigl, J. Greim, H. Knoch, Wear of boron carbide ceramics by abrasive waterjets, Wear, 181-183 (1995) 148-155.

[35] C. Dominguez, N. Cocuaud, D. Drouan, A. Constant and D. Jacquemain, Investigation on boron carbide oxidation for nuclear reactor safety: experiments in highly oxidizing conditions, J. Nucl. Mater., 374 (2008) 473–481.

[36] C. Brodhag and F. Thevenot, Hot Pressing Of Various Boron Phases, J. Less Comm. Met., 117 (1986) 175–180.

[37] L. Levin, N. Frage, M.P. Dariel, A novel approach for the preparation of B_4C-based cermets, Int. J. Refract. Met. Hard Mater., 18 (2000) 131-135.

[38] S. Lee, J. Mazurowski, G. Ramseyer, P.A. Dowben, Characterization of boron carbide thin films fabricated by plasma enhanced chemical vapor deposition from boranes, J. Appl. Phys., 72 (1992) 4925–4933.

[39] T.K. Roy, C. Subramanian, A.K. Suri, Pressureless sintering of boron carbide, Ceram. Int., 32 (2006) 227–233.

[40] R. Ma, Y. Bando, High purity single crystalline boron carbide nanowires, Chem. Phys. Lett., 364 (2002) 314–317.

[41] M. Beauvy, Stoichiometric limits of carbon-rich boron carbide phases, J. Less Comm. Met., 90 (1983) 169-175.

[42] R.P. Elliott, Contract No. AT (11–1), 578, Project Agreement No. 4, Armour Res. Found., Rep. ARF 220012, 1961

[43] M. Bouchacourt, F. Thevenot, J. Ruste, J. Less Comm. Met., 59 (1978) 139-152.

[44] M. Bouchacourt, F. Thevenot, The melting of boron carbide and the homogeneity range of the boron carbide phase, J. Less Comm. Met., 67 (1979) 327-331.

[45] M. Bouchacourt, F. Thevenot, The properties and structure of the boron carbide phase, J. Less Comm. Met. 82 (1981) 227.

[46] U. Kuhlmann, H. Werheit, On the microstructure of boron Carbide, Solid State Commun., 83 (1992) 849-852.

[47] D. Emin, Structure and single phase reime of boron carbides, Phys. Rev. B 38 (1988) 6041-6055.

[48] I.A. Howard, C.L. Beckel, D. Emin, Bipolarons in boron-rich icosahedra: Effects of carbon substitution, Phys. Rev. B 35 (1987) 9265-9270.

[49] E. Amberger, W. Stumpf, Boron, K.C. Buschbeck, Gmelin Handbook of Inorganic Chemistry, 8th Ed., Springer-Verlag, Berlin, 1981.

[50] A. K. Suri, C. Subramanian, J. K. Sonber, T. S. R. Ch. Murthy, Synthesis and consolidation of boron carbide: a review, Int. Mater. Rev., 55 (2010) 4-40.

[51] A. Lipp, Boron carbide: production properties and application,Technische Rundschau, 1965, 14, 28, 33 and 1966, 7.

[52] D. Jianxin, Erosion wear of boron carbide ceramic nozzles by abrasive air jets, Mater. Sci. Eng. A, 408 (2005) 227–233.

[53] Y. Chen, Y. W. Chung, S. Y. Li, Boron carbide and boron carbonitride thin films as protective coatings in ultra-high density hard disk drives, Surf. Coat. Technol., 200 (2006) 4072–4077.

[54] A. Gatti, R. Cree, J. B. Higgins, E. Feingold, Boron carbide continuous filaments, Technical report. Jul 64–Jun 65, Philadelphia, PA, Missile and Space Div., General electric Co., 1965, available at: http://www.ntis.gov/

[55] K. E. Lee, J. Y. Lee, M. J. Park, J. H. Kim, C. B. Lee, C. O. Kim, Preparation of boron carbide thin films for HDD protecting layer, J. Magn. Magn. Mater., 272–276 (2004) 2197–2199.

[56] P. Dunner, H. J. Heuvel, M. Horle, Absorber materials for control rod systems of fast breeder reactors, J. Nucl. Mater., 124 (1984) 185-194.

[57] R. Jimbou, M. Saidoh, K. Nakamura, M. Akiba, S. Suzuki, Y. Goto, Y. Suzuki, A.Chiba, T. Yamaki, M. Nakagawa, K. Morita, B. Tsuchiya, New composite composed of boron carbide and carbon fiber with high thermal conductivity for first wall, J. Nucl. Mater., 233-237 (1994) 781-786.

[58] S. Lee, J. Mazurowski, Characterization of boron carbide thin films fabricated by plasma enhanced chemical vapour deposition from boranes, J. Appl. Phys., 72 (1992) 4925–4932.

[59] C. Subramanian, T. S. R. Ch. Murthy, A. K. Suri, Synthesis and consolidation

of titanium diboride, Int. J. Refract. Met. Hard Mater., 25 (2007) 345–350.

[60] M. Bouchacoart, F. Thevenot, The correlation between the thermoelectric properties and stoichiometric properties and stoichiometry in boron carbide phase B_4C-$B_{10.5}C$, J. Mater. Sci., 20 (1985) 1237-1247.

[61] G. Goller, C. Toy, A. Tekin and C. K. Gupta, The production of boron carbide by carbothermic reduction, High Temp. Mater. Proc., 15 (1996) 117–122.

[62] S. A. Tucker, H. J. W. Bliss, The Preparation Of Boron carbide in the electric furnace, Z. Anorg. Chem., 5 (1992) 605-608.

[63] F. Schroll, A. Vogt, Electrothermic production of boron carbide, US patent no. 2 163 293, 1939.

[64] J. J. Scott, Arc furnace process for the production of boron carbide, US patent no. 3 161 471, 1964.

[65] R. R. Ridgeway, Methods of making abrasive metal carbides, US patent no. 2 155 682, 1939.

[66] M. P. L. N. Rao, G. S. Gupta, P. Manjunath, S. Kumar, A. K. Suri, N. Krishnamurthy, C. Subramanian, Temperature measurements in the boron carbide manufacturing process – a hot model study, Int. J. Refract. Met. Hard Mater., 27 (2009) 621–628.

[67] M. P. L. N. Rao, G. S. Gupta, P. Manjunath, S. Kumar, A. K.Suri, N. Krishnamurthy, C. Subramanian, Core temperature measurement in carbothermal reduction process, Thermochim. Acta, 482 (2009) 66–71.

[68] C. Subramanian, A. K. Suri, Development of boron based neutron absorber materials, Met. Mater. Process., 16 (2004) 39–52.

[69] A. Alizadeh, E. T. Nassaj, N. Ehsani, H. R. Baharvandi Production of boron carbide powder by carbothermic reduction from boron oxide and petroleum coke or carbon active, Adv. Appl. Ceram., 105 (2006) 291–296.

[70] Yu.N. Tumanov, The synthesis of boron carbide in a high frequency electromagnetic field, J. Less Comm. Met., 67 (1979) 521–529.

[71] A. W. Weimer, W. G. Moore, R. P. Roach, Method for producing uniform, fine boron containing ceramic powders, US patent no. 5 194 234, 1993.

[72] S. Herth, W. J. Joost, R. H. Doremus, R. W. Siegel, New approach to the synthesis of nanocrystalline boron carbide, J. Nanosci. Nanotechn., 6 (2006) 954–959.

[73] R. Ma, Y. Bando, High purity single crystalline boron carbide nanowires, Chem. Phys. Lett., 364 (2002) 314–317.

[74] L. H. Bao, C. Li, Y. Tian, J. F. Tian, C. Hui, X. J. Wang, C. M. Shen and H. J. Gao, Synthesis and photoluminescence property of boron carbide nanowires', Chin. Phys. B, 17B (2008) 4585–4591.

[75] F. F. Xu, Y. Bando, Formation of two-dimensional nanomaterials of boron carbides, J. Phys. Chem. B, 108B (2004) 7651–7655.

[76] A. Aghai, C. Falamaki, B. E. Yekta and M. S. Afarani, Effect of seeding on the synthesis of B_4C by the magnesiothermic reduction route, Ind. Ceram., 22 (2002) 121–125.

[77] E. G. Gray, Process for the production of boron carbide, US patent no. 2 834 651, 1958.

[78] A. Muta and T. Geja, Method for producing boron carbide, US patent no. 3 338

679, 1967.

[79] T. A. Zhang, Z. H. Dou, H. Yang, Q. L. Ding, Preparation of boron carbide by magnesium reducing – SHS, J. North Eastern Univ., 24 (2003) 935–938.

[80] A. K. Khanra, M. M. Godkhindi, Synthesis of boron carbide by self – propagating high temperature synthesis, J. Aust. Ceram.Soc., 41 (2005) 30–35.

[81] F. Deng, H. Y. Xie, L. Wang, Synthesis of submicron B_4C by mechanochemical method, Mater. Lett., 60 (2006) 1771–1773.

[82] J. Guojian, Xu Jiayue, Z. Hanrui, Li Wenlan, Combustion of $Na_2B_4O_7$+Mg+C to synthesis B_4C powders, J Nucl. Mater., 393 (2009) 487–491.

[83] L. L Wang, Z. A. Munir, J. B. Holt, The feasibility of synthesis of B_4C fiber – MgO composites by combustion, Scr. Metall. Mater., 31 (1994) 93–97.

[84] L. J. Berchmans, V. Mani, K. Amalajyothi, Synthesis of boron carbide by calciothermic reduction process, Int. J. Selfpropagat. High Temp. Synth., 18 (2009) 60–63.

[85] G. Goller, C. Toy, A. Tekin, C.K. Gupta, The production of boron carbide by carbothermic reduction, High Temp. Mater. Proc., 15 (1996) 117-122.

[86] A. Jain, S. Anthonysamy, K. Ananthasivan, R. Ranganathan, V. Mittal, S. V. Narsimhan and V. Mittal, Charecterization of electrodeposited elemental boron, Mater. Charact., 59 (2008) 890–900.

[87] Umberto Anselmi-Tamburini, Zuhair A. Munir, Influence of Synthesis Temperature on the Defect Structure of Boron Carbide: Experimental and Modeling Studies, J. Am. Ceram. Soc., 88 (2005) 1382–1387.

[88] E. M. Heian, S. K. Khalsa, T. Yamamoto, M. Ohyanagi, Synthesis of dense,

high-defect-concentration B_4C through mechanical activation and field assisted combustion, J. Am.Ceram. Soc., 87 (2004) 779–783.

[89] K. Yamada, Boron carbide articles formed from an amorphous boron/graphite powder mixture using a shock wave technique, J. Am. Ceram. Soc., 79 (1996) 1113–1116.

[90] J. Wei, B. Jiang, Y. Li, C. Xu, D. Wu, Straight boron carbide nanorods prepared from carbon nanotubes, J. Mater. Chem., 12 (2002) 3121–3124.

[91] S. Chen, D. Z. Wang, J. Y. Huang, Z. F. Ren, Synthesis and characterization of boron carbide nanoparticles, Appl. Phys. A, 79A (2004) 1757–1759.

[92] B. Chang, B. L. Gersten, S. T. Szewczyk, J. W. Adams, Characterization of boron carbide nanoparticles prepared by a solid state thermal reaction, Appl. Phys. A, 86A (2007) 83–87.

[93] A.W. Weimer, W.G. Moore, R.P. Roach, J.E. Hitt, R.S. Dixit, S.E. Pratsinis, Kinetics of carbothermal reduction synthesis of boron carbide, J. Am. Ceram. Soc., 75 (1992) 2509-2514.

[94] G. L. Harris, D. S. Parsons, Method of producing boron carbide from water-alchol solution of carbon source, U S Patent No 3 885 022, 1975.

[95] M. Kakiage, Y. Tominag, I. Yanase, H. Kobayashi, Synthesis of boron carbide powder in relation to composition and structural homogeneity of precursor using condensed boric acid–polyol product, Powder Technology 221 (2012) 257-263.

[96] H.Wada, S. Ito, K. Kuroda, C. Kato, The synthesis of boron nitride and boron carbide by pyrolysis of boric acid/1,2,3-propanetriol condensation product,

Chem. Lett.,14 (1985) 691–692.

[97] H. Wada, K. Kuroda, C. Kato, Preparation of boron nitride and boron carbide by thermal treatment of boric acid-glycerin condensation product as a precursor,Yogyo-Kyokai-Shi 94 (1986) 61–65.

[98] A. Sinha, T. Mahata and B. P. Sharma, Carbothermal route for preparation of boron carbide powder from boric acid-citric acid gel precursor, J. Nucl. Mater., 301 (2002) 165–169.

[99] A.M. Hadian, J.A. Bigdeloo, The effect of time, temperature and composition on boron carbide synthesis by sol–gel method, J Mater. Eng. Perform., 17 (2008) 44–49.

[100] A.K. Khanra, Production of boron carbide powder by carbothermal synthesis of gel material, Bull. Mater. Sci., 30 (2007) 93–96.

[101] Dj. Kosanovic, Lj. Milovaovic, S. Milovanovic, A. Saponjic Low-temperature synthetic route for boron carbide powder from boric acid-citric acid gel precursor, Mater. Sci. Forum., 555 (2007) 255-260.

[102] H. Konno, A. Sudoh, Yoshitaka Aoki, Hiroki Habazaki, Synthesis of C/B_4C composites from Sucrose-boric acid mixed solutions, Mol. Cryst. Liq. Cryst., 386 (2002) 15-20.

[103] A. Sudoh, H. Konno, H. Habazaki, H. Kiyono, Synthesis of boron carbide microcrystals from saccharides and boric acid, Carbon, 45 (2007) 1373–1375.

[104] S. Mondal, A. K. Bhathia, Low temperature synthetic route for boron carbide, J. Euro. Ceram. Soc., 25 (2005) 287-292.

[105] I. Yanase, R. Ogawara, H. Koayashi, Synthesis of boron carbide powder from

polyvinyl borate precursor, Mater. Lett., 63 (2009) 91-93.

[106] G. L. Harris and D. S. Parsons: Method of producing boron carbide from water alcohol solution of carbon source, US patent no. 3 885 022, 1975.

[107] J. Economy and I. Matkowich, Boron carbide fiber production, US patent no. 3 825 469, 1974.

[108] S. Cihangir, C. Ergun, S. Yilmaz and F. C. Sahin, Synthesis of B_4C/SiC composite from sugar based precursor, Diffus. Defect Data A, 283–286A (2008) 268–272.

[109] Masaki Kakiage, Naoki Tahara, Ikuo Yanase, Hidehiko Kobayashi, Low-temperature synthesis of boron carbide powder from condensed boric acid–glycerin product, Mater. Lett., 65 (2011) 1839–1841.

[110] R. G. Bourdio, Process of preparing boron carbide from boron halide and a hydrocarbon, US patent no. 3 334 967, 1967.

[111] R. A. Clifton, Production of boron carbide whiskers, US patent no. 3 525 589, 1970.

[112] E. W. James, Catalyst for growth of boron carbide crystal whiskers, US patent no. 3 423 179, 1969.

[113] J. F. Ditter, F. J. Gerhart and R. E. Williams, Boron carbide, US patent no. 4 017 587, 1977.

[114] I. M. MacKinnon and B. G. Reuben, The synthesis of boron carbide in an RF plasma, J. Electrochem. Soc., 122 (1975) 806–811.

[115] L. Shi, Y. Gu, L. Chen, Y. Qian, Z. Yang, J. Ma, A low temperature synthesis of crystalline B_4C ultrafine powders, Solid State Commun.,128 (2003) 5–7.

[116] Y. Gu, L. Chen, Y. Qian, W. Zhang, J. Ma, Synthesis of nanocrystalline boron carbide via a solvothermal reduction of CCl_4 in the presence of amorphous boron powder, J. Am. Ceram. Soc., 88 (2005) 225–227.

[117] C. Ronning, D. Schwen, S. Eyhusen, U. Vetter, H. Hofsass, Ion beam synthesis of boron carbide thin films, Surf. Coat. Technol., 158–159 (2002) 382–387.

[118] B. M. Todorovic, I. Draganic, D. Vasiljevic-Radovic, N. Romdevic, M. Romccevic, M. Dramicanin, Z. Markovic, Synthesis of amorphous boron carbide by single and multiple charged boron ions bombardment of fullerene thin films, Appl. Surf. Sci., 253 (2007) 4029–4053.

[119] M. Carlsson, F. J. G. Garcia, M. Johnsson, Synthesis and characterization of boron carbide whiskers and thin elongated platelets, J. Cryst. Growth, 236 (2002) 466–476.

[120] R. V. Krishnarao, J. Subrahmanyam, Studies on the formation of whiskers and platelets of B_4C and BN, J. Mater. Sci., 39 (2004) 6263–6269.

[121] R. Ma, Y. Bando, Investigation on the growth of boron carbide nanowires, Chem. Mater., 14 (2002) 4403–4407.

[122] Hong Zeng, Yan-Mei Kan, Guo-Jun Zhang, Synthesis of boron carbide powder from hexagonal boron nitride, Mater. Lett., 64 (2010) 2000–2002.

[123] Ahmet Atasoy, The aluminothermic reduction of boric acid, Int. J. Refract. Met. Hard Mater., 28 (2010) 616–622.

[124] Z.C Tan, L. Wang, Q. Shi, Study of heat capacity enhancement in some nanostructured materials, Pure Appl. Chem., 81 (2009) 1871–1880.

[125] H. Gleiter, Nanocrystalline materials, Prog. Mater. Sci., 33 (1989) 223–315.

[126] C. Suryanarayana, C.C. Koch, Nanocrystalline materials–current research and future directions, Hyperfine Interact., 130 (2000) 5–44.

[127] R. Birringer, Nanocrystalline materials, Mater. Sci. Eng. A-Struct., 117 (1989) 33–43.

[128] G.K. White, Thermal expansion of solids: a review, High Temp. High Press, 18 (1986) 509–516.

[129] H. D. Megaw, Crystal structure, A working Approach, W. B Saunders Publishing Company, Philadelphia, 1973.

[130] R.S. Krishnan, R. Srinivasan, S. Devanarayanan, Thermal Expansion of Crystals, Pergamon Press, Oxford, 1979.

[131] G. Panneerselvam, R. Venkata Krishnan, M.P. Antony, K. Nagarajan, T.Vasudevan, P.R. Vasudeva Rao, Thermophysical measurements on dysprosium and gadolinium titanates, J. Nucl. Mater., 327 (2004) 220–225.

[132] R. Korner, M. Ricken, J. Nolting, I. Riess, Phase transformations in reduced ceria: Determination by thermal expansion measurements, J. Solid State Chem., 78 (1989) 136-147.

[133] K. P. Birch, An Automatic absolute interferometric dilatometer, J. Phy. E. Sci. Instrum, 20 (1987) 1387-1392.

[134] G. Panneerselvam, 2006, Ph. D thesis, Alagappa university, Karaikudi, India

[135] I. E. Campbell, E. M. Sherwood (Eds.), High Temperature Materials and Technology, P 891, John Wiley and Sons, London, 1967.

[136] Tibor Kantor; Jurgen Hassler, Otto Forster, Determination of trace metals in industrial boron carbide by solid sampling optical emission spectrometry.

Optimization of DC arc excitation (current, atmosphere and chemical modifier), Microchim. Acta, 156 (2007) 231–243.

[137] H.J. Heinrich, R. Matschat, Spectro. Chim Acta B, 62 (2007) 807–816.

[138] M.A. Amberger, J.A.C. Broekaert, Direct multielement determination of trace elements in boron carbide powders by total reflection X-ray fluorescence spectrometry and analysis of the powders by ICP atomic emission spectrometry subsequent to sample digestionJ. Anal. At. Spectrom., 24 (2009) 1517–1523.

[139] V. K. Manchanda, M.S. Subramanian, Volumetric Determination of boron in boron carbide, BARC Report no.1017 (1979).

[140] G. H. Jeffery, J. Bassett, J. Mendham, R C. Denney, Text book of quantitative inorganic analysis, John Wiley & Sons, Inc., New York, 4th Edn. 1978, 299-300

[141] Watanabe Mitsuyoshi, Precise determination of boron in boron carbide powder by stepwise pressure alkali/acid decomposition/mannitol titration method, Bunseki Kagaku, 50 (2001) 139-141.

[142] Zheng Wang, Deren Qiu, Guangyi Tao, Pengyuan Yang, J. Anal. At. Spectrom., 24 (2009) 1258–1261.

[143] N. N. Greenwood, A. Earnshaw, Chemistry of elements Ed.2, Butterworth Heinemann, 1997.

[144] A. I. Vogel, A text book of quantitative inorganic analysis including elementary instrumental analysis, 3rd Ed., The English language book society and LongmansGreen & Co. Ltd., New York, 1962.

[145] Y. S. Sayi, K. L. Ramkumar, V. Venugoal, Determination of non metallic impurities in nuclear fuel, IANCAS Bulletin, Vol. VII, No. 3 (2008) 180.

[146] Stephen Brunauer, P. H. Emmett, Edward Teller, Adsorption of Gases in Multimolecular Layers, J. Am. Chem. Soc., 60 (1938) 309-319.

[147] J. Michael Hollas, Modern Spectroscopy, John Wiley & Sons, Ltd, England.

[148] B. D. Cullity, Elements of X-ray diffraction, Addison-Wesley Publishing Company, Inc. USA, 1967.

[149] H. P. Klug, L. E. Alexander. X-ray diffraction procedures for polycrystalline and amorphous materials, Wiley, USA, 1954.

[150] J. I. Goldstein, H Yakowitz, Practical Scanning Electron Microscopy, Plenum Press, New York, 1975.

[151] G. B. Williams, C. B. Carter, Transmission electron microscopy- a text for Materials Science Plenum Press, New York (1996).

[152] T. Allen, Particle size measurement Ed. 2, Champman and Hall, London, 1975.

[153] B. Z. Dacic, V. Jokanovic, B. Jokanovic, M. D. Dramicanin, Thermodynamics of gas phase carbothermic reduction of boron-anhydride. J. Alloys Compd, 413 (2006) 198–205.

[154] C. Bale, P. Chartrand, S. Degterov, G. Eriksson, K. Hack, R. Ben Mahfoud, J. Melancon, A. Pelton, S. Petersen, Factsage thermochemical software and databases, Calphad 26 (2002) 189–228.

[155] C. H. Jung, M. J. Lee, C. J. Kim, Preparation of carbon-free B_4C powder from B_2O_3 by carbothermal reduction process, Mater. Lett., 58 (2004) 609–614.

[156] D. K. Bose, K. U. Nair, C.K. Gupta, Production of high purity boron carbide, High Temp. Mat. Proc., 7 (1986) 133-140

[157] G. Panneerselvam, R. V. Krishnan, M. P. Antony, K. Nagarajan, T. Vasudevan,

P.R. Vasudeva Rao, Thermophysical measurements on dysprosium and gadolinium titanates, J. Nucl. Mater., 327 (2004) 220–225.

[158] Birringer, H. Gleiter, Advances in Materials Science, Encyclopedia of Materials Science and Engineering, Pergamon, Oxford, 1983, Vol I, 339-349.

[159] Y. Kuru, M. Wohlschlogel, U. Welzel, E.J. Mittemeijer, Crystallite size dependence of the coefficient of thermal expansion of metals, Appl. Phys. Lett., 90 (2007) 243113_1-243113_3.

[160] H.J. Klam, H. Hahn, H. Gleiter, The thermal expansion of grain boundaries Acta Metall., 35 (1987) 2101-2104.

[161] K. Lu, M.L. Sui, Thermal expansion behaviors in nanocrystalline materials with a wide grain size range, Acta Metall. Mater., 43 (1995) 3325-3332.

[162] H.L. Yakel, Lattice expansion of two boron carbides between 12-940^{0}C, J. Appl. Cryst., 6 (1973) 471-474.

[163] G.V. Tsaagareishvili, T.G. Nakashidze, J.Sh. Jobava, G.P. Lomidze, D.E. Khulelidze, D.Sh. Tsagaraeishvili, O.A. Tsaagareishvili, Thermal exapansion of boron and boron carbide, J. Less Comm. Met., 117 (1986) 159-161.

[164] Charles P. Poole Jr., Frank J. Owens, Introduction to Nanotechnology,Wiley & Sons. Inc., Hoboken, New Jersey, 2003.

[165] S. Sugano, H. Koizumi, Microcluster Physics, Springer, Berlin, 1988

[166] S. Barbara, L.J. Lewis, I. Swainson, U. Erb, Thermal expansion and hydrogen diffusion in nanocrystalline nickel, Phys. Rev. B 60 (1999) 10107-10113.

[167] M.A.Amberger, J.A.C. Broekaert, Direct multielement determination of trace elements in boron carbide powders by slurry sampling ETV-ICP-OES, J. Anal. At. Spectrom., 25 (2010) 1308-1315.

Publications

Journals

1. Synthesis of nano crystalline boron carbide from boric acid–sucrose gel precursor

   Trinadha Raja Pilladi, K. Ananthasivan, S. Anthonysamy and V. Ganesan

   Journal of material science, 47 (2012) 1710-1718
2. Thermal expansion of nanocrystalline boron carbide

   Trinadha Raja Pilladi, G. Panneerselvam, S. Anthonysamy and V. Ganesan

   Ceramic international, 38(2012) 3723-3728
3. Development of a digestion method for the analysis of boron carbide

   Trinadha Raja Pilladi, R. K. Prabhu and S. Anthonysamy

   Communicated to Current Analytical Chemistry.
4. Thermodynamic analysis of carbothermic reduction of boric oxide

   Trinadha Raja Pilladi, K. Ananthasivan and S. Anthonysamy

   Manuscript under preparation.
5. Synthesis of boron carbide from boric oxide – sucrose gel precursor,

   Trinadha Raja Pilladi, K. Ananthasivan and S. Anthonysamy

   Communicated to Powder Technology.

Conferences:

1. Synthesis of boron carbide

   Trinadha Raja Pilladi, K. Ananthasivan, S. Anthonysamy and V. Ganesan Proceeding of National symposium for Material research scholars (MR09), IIT Bombay, 2009

2. Synthesis of nano crystalline boron carbide from boric acid–sucrose gel precursor

   Trinadha Raja Pilladi, K. Ananthasivan, S. Anthonysamy and V. Ganesan, Proceeding of International Conference on Nanomaterials and Nanotechnology (NANO-2010), Tiruchengode, 2010

3. Synthesis of nano crystalline boron carbide from boric acid–sucrose gel precursor

   Trinadha Raja Pilladi, K. Ananthasivan, S. Anthonysamy and V. Ganesan Chemistry Research Scholars Symposium (CRSM), Kalpakkam, 2011.

4. Thermodynamic analysis of carbothermic reduction of boric oxide

   Trinadha Raja Pilladi, K. Ananthasivan, S. Anthonysamy and V. Ganesan, International Conference in Vistas in Chemistry(ICVC), Kalpakkam, 2011

5. Participated in National symposium on Chemistry for Societal and Environmental Needs, Central Leather Research Industry, Chennai, August 29-31, 2011